

Effective Field Theory calculations of $NN \rightarrow NN\pi$.

Vadim Baru*

*Institut für theoretische Physik II, Fakultät für Physik und Astronomie Ruhr-Universität
Bochum,
44780 Bochum Germany, and
Institute for Theoretical and Experimental Physics, 117218, B. Chermushkinskaya 25, Moscow,
Russia*

Christoph Hanhart†

*Institute for Advanced Simulation, Institute for Nuclear Physics, and Jülich Center for Hadron
Physics,
52425 Jülich, Germany*

Fred Myhrer‡

*Department of Physics and Astronomy, University of South Carolina, Columbia, SC 29208,
USA*

Received (received date)

Revised (revised date)

In this review we present the recent advances for calculations of the reactions $NN \rightarrow NN\pi$ using chiral effective field theory. Discussed are the next-to-next-to leading order loop contributions with nucleon and Delta-isobar for near threshold s-wave pion production. Results of recent experimental pion-production data for energies close to the threshold are analyzed. Several particular applications are discussed: (i) it is shown how the measured charge symmetry violating pion-production reaction can be used to extract the strong-interaction contribution to the proton-neutron mass difference; (ii) the role of $NN \rightarrow NN\pi$ for the extraction of the pion-nucleon scattering lengths from pionic atoms data is illuminated.

*vadimb@tp2.rub.de

†c.hanhart@fz-juelich.de

‡myhrer@sc.edu

1. Introduction

After the first high quality data for the reaction $NN \rightarrow NN\pi$ were published,¹ it became quickly clear that this first hadronic inelastic channel of the NN interaction is far more difficult to handle theoretically than what was initially expected. The best phenomenological model existing at the time² failed to explain the cross section data by factors of 2 and 10 for the reactions $pp \rightarrow d\pi^+$ and $pp \rightarrow pp\pi^0$, respectively. Various attempts were made to identify the phenomenological mechanisms responsible for this discrepancy — the most popular ones were heavy meson exchanges^{3–6} and off-shell πN rescattering.^{7,8} Both mechanisms were successful quantitatively but no consensus on the underlying dynamics was achieved in the literature. In addition, for the neutral channel severe quantitative discrepancies appeared in the description of polarization observables.⁹

All phenomenological approaches have their drawbacks. For example, they do not have a readily identifiable expansion scheme and there is no guiding principle that allows one to judge which diagrams are important and which ones can be neglected. In addition, the requirements of chiral symmetry can easily be violated in phenomenological approaches. On the other hand, a quantitative understanding of the reactions $NN \rightarrow NN\pi$ at threshold is of particular importance. First of all the system is controlled by several scales: the large initial momentum, the small final momenta, the pion mass and the typical hadronic scale $\Lambda_\chi \simeq 1$ GeV. A systematic understanding of such systems is not only of conceptual interest but is an important step towards the development of effective field theories. Secondly, the calculations of πd scattering observables also need accurate input for the pion absorption amplitudes and their corresponding dispersive corrections,^{10,11} in order to reach a precision high enough to extract the isoscalar πN scattering amplitude.^{12,13}

Since low-energy pion interactions are largely dictated by the requirements of chiral symmetry of the strong interaction, chiral perturbation theory (ChPT) is the proper tool to resolve the above mentioned discrepancy. ChPT allows for a systematic, model independent expansion of the amplitudes in terms of momenta and pion masses measured in units of Λ_χ . However, the use of the standard ChPT power counting, which is based on the assumption that all relevant momenta are effectively of the order of the pion mass, was not very successful. The first calculations of $NN \rightarrow NN\pi$ reactions in this framework were done at tree level up to next-to-next-to leading order (N²LO) for both $pp \rightarrow pp\pi^0$ ^{14–16} as well as for $pp \rightarrow d\pi^+$.^{17,18} These early studies revealed, in particular, that the discrepancy between theory and experiment increases for both channels due to a destructive interference between the impulse approximation or leading order (LO) amplitude and the isoscalar rescattering contributions that enter at next-to leading order (NLO) in standard counting. In addition, some loop contributions at N²LO were found in Refs.^{19,20} to be significantly larger than the NLO contribution, revealing a problem regarding the convergence of the standard ChPT approach to the $pp \rightarrow pp\pi^0$ reaction.²¹

Based on the observation that the initial nucleon three-momentum at threshold ($p = |\vec{p}| \simeq \sqrt{m_N m_\pi} \sim 360$ MeV where m_π and m_N denote the pion and nucleon mass, respectively) is significantly larger than the pion mass, Refs.^{14,17} proposed a modification of the chiral counting scheme. The expansion parameter in the new counting scheme is

$$\chi_{\text{MCS}} = p/\Lambda_\chi \simeq \sqrt{m_\pi/m_N} \simeq 0.4, \quad (1)$$

where Λ_χ is here identified with the nucleon mass. In what follows, this power counting will be referred to as the momentum counting scheme (MCS)—it will be discussed in detail in the next section. This scale was first implemented in the actual calculations in Refs.,^{22,23} see Ref.²⁴ for an earlier review article. Ref.²⁴ demonstrated that the order of magnitude differences between the two-pion exchange diagrams of Ref.¹⁹ could easily be understood in the MCS, since the diagrams are of different orders in this new counting scheme as will be shown in Sec. 3. It has been known for years that the strength of the s-wave pion production amplitude in the charged channels $pp \rightarrow d\pi^+$ and $pp \rightarrow pn\pi^+$ is dominated by the leading order (LO) Weinberg-Tomozawa (WT) operator.² However, the cross sections for these two reactions were underestimated by a factor of 2.²⁴ Meanwhile, the application of the MCS to s-wave production in the $pp \rightarrow d\pi^+$ channel at next-to-leading order (NLO)²⁵ revealed quite good agreement with experimental data. In contrast, for s-wave pion production in the neutral channel $pp \rightarrow pp\pi^0$ the situation is completely different. In this channel the large isovector WT rescattering vertex does not contribute while the other mechanisms at LO and NLO are either strongly suppressed or vanish completely.^{14–16,23,26} Therefore, we believe that the experimentally measured $pp \rightarrow pp\pi^0$ reaction is unique in that it directly probes the higher order MCS contributions which in the other channels are masked by the dominant lower order Weinberg–Tomozawa term. This was the motivation for the derivation of the pion s-wave production operator at N²LO in MCS which was performed in Refs.^{26,27} and will be discussed in Sec 3.

Pion production near threshold is also useful for studying isospin violation in, e.g. nucleon-nucleon reactions. Within the standard model there are only two sources of isospin violation, namely the electromagnetic interaction and the mass difference of the two lightest quarks, $m_d - m_u \sim m_u$.^{28,29} In processes where we are able to disentangle these two sources, the observation of isospin violation in hadronic reactions gives a window to quark mass effects^{29,30i}. The mass difference between the neutral and charged pions, which is almost completely due to electromagnetic interactions, is by far the largest isospin-violating effect. This mass difference drives, for example, the spectacular energy dependence of the π^0 -photoproduction amplitude near threshold (see, e.g., the review article³² and references therein). Thus, in order to disentangle the two isospin-violating sources, it is important to use isospin

ⁱ Quark masses themselves are not directly observable and additional information is necessary to assign a scale to these fundamental parameters of the standard model (see e.g.³¹).

violation observables where the pion mass difference does not contribute. An example where the pion mass difference does not enter is charge symmetry breaking (CSB) observables.

Within effective field theory there is a close correlation between the leading CSB pion-nucleon scattering amplitude and the proton–neutron mass difference. Already in 1977 Weinberg predicted a huge effect of up to 30% difference in the $\pi^0 p$ and $\pi^0 n$ scattering lengths due to CSB in $\pi^0 N$ scattering.^{28,33} Since scattering experiments with neutral pions are not feasible,ⁱⁱ Refs.^{35–37} focused instead on NN induced pion-production reactions to study CSB. There have been two successful CSB measurements close to the pion threshold, namely the forward-backward asymmetry in the $pn \rightarrow d\pi^0$ reaction, $A_{fb}(pn \rightarrow d\pi^0)$,³⁸ and the $dd \rightarrow \alpha\pi^0$ reaction cross section,³⁹ see an early review article.⁴⁰ We will concentrate our discussion on the first CSB reaction, see Sec. 7, before we make some remarks regarding the $dd \rightarrow \alpha\pi^0$ reaction. Following the arguments presented in Ref.³⁶ we will show that at leading CSB order within the MCS scheme, only the strong (quark-mass induced) contribution to the proton-neutron mass difference enters the CSB pion-production operator in $pn \rightarrow d\pi^0$. Using data on $A_{fb}(pn \rightarrow d\pi^0)$,³⁸ the strong contribution to the proton-neutron mass difference was extracted in Ref.³⁶ within MCS.

An effective field theory (EFT) is a low energy theory where the short distance physics is characterized by local operators with their corresponding low energy constants (LECs), see Sec. 2.1. In few-nucleon systems these LECs parametrize the short distance two-nucleon correlations not explicitly probed in low-energy reactions. One LEC appearing in $NN \rightarrow NN\pi$ turns out to be important in a variety of other few-nucleon processes at relatively low orders: as was stressed in Ref.,²² the short range physics of the near threshold reactions $NN \rightarrow NN\pi$ is given by a $(NN)^2\pi$ short ranged operator which is closely connected to the short ranged three–nucleon force. The latter is discussed in, e.g., Refs.^{41–44} The strength of this short range two-nucleon operator is given by the LEC d , which can be thought of as the two-nucleon analog of the axial constant g_A . At the same time, this LEC plays a pivotal role in various few-nucleon processes, like in the pp fusion reaction,⁴⁵ $pp \rightarrow de^+\nu_e$, which is the primary process in stellar thermonuclear reactions, and the neutrino deuteron breakup reactions^{46,47} which were experimentally measured at the Sudbury Neutrino Observatory⁴⁸ establishing the total neutrino flux from the sun. In addition, the same short range operator is also of importance in $\gamma d \rightarrow \pi NN$ ^{49,50} and $\pi d \rightarrow \gamma NN$ ^{51,52} as well as in weak reactions like tritium beta decay.^{44,45,52} In these different reactions the operator appears in very different kinematical regimes, ranging from very low energies for both incoming and outgoing NN pairs in weak reactions and proton-deuteron scattering up to relatively high initial energies for the NN induced pion production. In Fig. 1 we illustrate some few-nucleon processes where this short range operator (and the corresponding

ⁱⁱ The $\pi^0 p$ scattering length might be measurable in polarized neutral pion photoproduction at threshold.³⁴

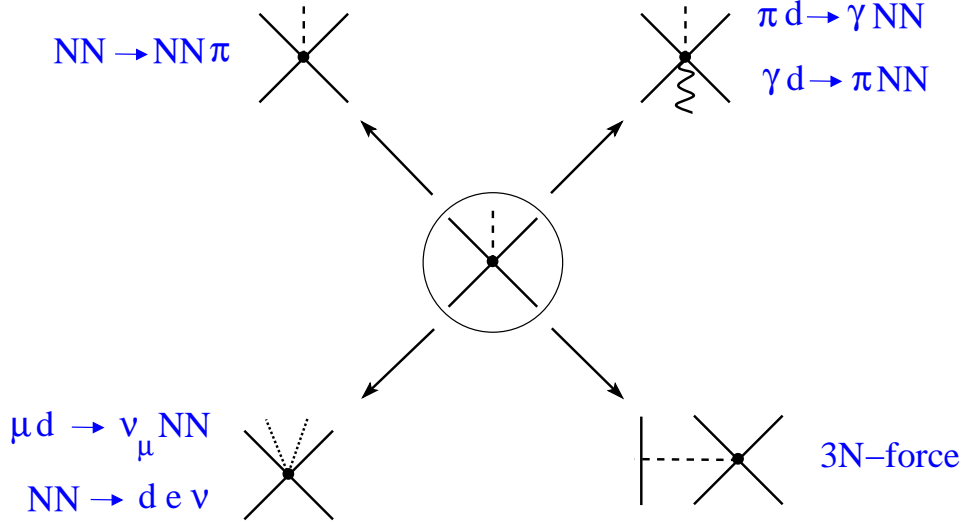


Fig. 1. An illustration of few-nucleon reactions where the LEC d contributes.

LEC d) parametrizes common short distance two-nucleon physics. In Ref.⁴⁵ a first determination of the LEC d from data was done in a technically involved EFT calculation of the tritium β -decay. Ref.⁴⁵ then used this value for d to predict the astrophysical S-factors of the solar nuclear processes. The results of Ref.⁴⁵ for the rate of $pp \rightarrow de^+\nu_e$ were later used by Ref.⁵² to reduce the cutoff dependence in the reaction $\pi^-d \rightarrow \gamma nn$, which was proposed as a tool to extract the nn -scattering length.^{53,54} In a recent work using EFT,⁴⁴ it was shown that both the ${}^3\text{H}$ and ${}^3\text{He}$ binding energies and the tritium β -decay can be described with the same contact term. Although there are good reasons to believe that the use of EFT for the three-nucleon system is reliable, it was realized early on that it is desirable to determine the LEC d within the two-nucleon system, for this provides an independent cross check for the formalism. The strength of this $(NN)^2\pi$ short range operator could be experimentally relatively well determined by the muon capture rate on deuterons, $\mu^-d \rightarrow nn\nu_\mu$, cf. e.g., Refs.⁵⁵⁻⁵⁹ The ongoing measurement of $\mu^-d \rightarrow nn\nu_\mu$ by the MuSun Collaboration at PSI⁵⁶ aims at the determination of the rate with a precision of 1.5 %. Below we will argue that the direct access to the strength of this $(NN)^2\pi$ short ranged operator comes also from the study of the $NN \rightarrow NN\pi$ reactions. Once this LEC is determined the EFT will have predictive power for all the reactions mentioned above.

How the short range operator connects these processes can easily be understood from the general structure of the chiral Lagrangian. The Lagrangian is written in terms of the standard chiral field $U(x)$ which depends non-linearly on the pion field

6 *Vadim Baru, Christoph Hanhart, Fred Myhrer*

π . The LO Lagrangian reads⁶⁰

$$\mathcal{L}_{\pi N}^{(1)} = N^\dagger (i v \cdot D + \hat{g}_A S \cdot u) N + \dots, \quad (2)$$

where the field $N(x)$ denotes the large component of the heavy-nucleon field, \hat{g}_A is the bare axial-vector coupling of the nucleon, $D_\mu N$ is the covariant derivative, $D_\mu N = (\partial_\mu + \Gamma_\mu) N$ with $\Gamma_\mu = [\xi^\dagger, \partial_\mu \xi]/2$ [we here ignore the external electroweak fields which are, however, introduced in Eq. (4)], and $\xi = \sqrt{U(x)}$. Furthermore, $u_\mu \equiv i(\xi^\dagger \partial_\mu \xi - \xi \partial_\mu \xi^\dagger)$, the nucleon's four-velocity vector $v^\mu = (1, \vec{0})$ and the covariant nucleon spin operator⁶⁰ $S^\mu = (0, \vec{\sigma}/2)$. The following two-nucleon interaction Lagrangian, which is part of the Lagrangians to be specified in Sec. 2.1, describes the short-range contact interaction illustrated in Fig. 1.

$$\mathcal{L}_{NN}^{int} = -2d (N^\dagger S \cdot u N) N^\dagger N, \quad (3)$$

where the strength of the short-ranged operator is d , and, including the external electromagnetic fields, we observe how u^μ connects pion production with the external vector V_μ and axial-vector A_μ currents via

$$f_\pi u_\mu = -\tau \partial_\mu \boldsymbol{\pi} - \varepsilon_{3ab} V_\mu \pi_a \tau_b + f_\pi A_\mu + \dots. \quad (4)$$

Here $\boldsymbol{\pi}$ corresponds to the pion field and f_π is the pion decay constant ($f_\pi = 92.4$ MeV). In Eq. (4) we have expanded u^μ in terms of the pion field, which as mentioned appears non-linearly in u^μ , and where the ellipses correspond to higher powers in pion field interaction terms. It is Eq. (4) that highlights the connection of pion production and the weak currents. As follows from Eqs. (3) and (4), the contact operator supplemented by the LEC d is proportional to the pion derivative. Therefore it should contribute to production of p-wave pions in $NN \rightarrow NN\pi$ while connecting to final state S-wave nucleons. There are two reaction channels which fulfil this condition. One corresponds to the case with a spin-triplet S-wave NN final state interaction (FSI) which is realized in the reactions $pp \rightarrow pn\pi^+$ and $pp \rightarrow d\pi^+$. The other channel is the spin-singlet S-wave NN FSI which appears in the reaction $pn \rightarrow pp\pi^-$ as indicated in Table 1. As will be explained in Sec. 5, in order to experimentally ensure that the final two nucleons are in a relative S-wave, one restricts the final relative two-nucleon energy in $NN \rightarrow NN\pi$ to be very small, typically < 3 MeV. Note that this contact term does not contribute to the reaction $pp \rightarrow pp\pi^0$ where a p-wave pion can only be produced in combination with the final NN -pair in a relative P-wave. The initial and final NN partial wave combinations for production of p-wave pions can be read off from Table 1. They are $^1S_0 \rightarrow ^3S_1 p$ [and $^1D_2 \rightarrow ^3S_1 p$] for π^+ production and $^3S_1 \rightarrow ^1S_0 p$ [and $^3D_1 \rightarrow ^1S_0 p$] for π^- production. We will show in Sec. 5 that $NN \rightarrow NN\pi$ p-wave pion production may be an excellent tool in order to extract information about this LEC.

The paper is organized as follows. First, in Sec. 3 we will present the evaluations of the amplitudes for s-wave pion production where some pertinent details of the lengthy loop-evaluations of the NLO and N²LO two-pion-exchange amplitudes will be given. In MCS, the pion p-wave production amplitude is given by tree level

Spin of the NN state	Reaction channel	Partial waves
Spin-triplet S-wave NN FSI	$pp \rightarrow d\pi^+$	${}^3P_1 \rightarrow {}^3S_1s$
	$pp \rightarrow pn\pi^+$	${}^1S_0 \rightarrow {}^3S_1p$
	$pp \rightarrow d\pi^+$	${}^1D_2 \rightarrow {}^3S_1p$
	$pn \rightarrow d\pi^0$	(CSB) ${}^1P_1 \rightarrow {}^3S_1s$
Spin-singlet S-wave NN FSI	$pp \rightarrow pp\pi^0$	${}^3P_0 \rightarrow {}^1S_0s$ $({}^3P_2 - {}^3F_2) \rightarrow {}^1S_0d$
	$pn \rightarrow pp\pi^-$	${}^3P_0 \rightarrow {}^1S_0s$ $({}^3P_2 - {}^3F_2) \rightarrow {}^1S_0d$ $({}^3S_1 - {}^3D_1) \rightarrow {}^1S_0p$

Table 1. Partial waves and reaction channels restricted to the spin-triplet and spin-singlet S-wave NN final state interaction.

diagrams up to N²LO while for pion s-wave production, loop diagrams start to contribute individually already at NLO. The reason for this apparent asymmetry lies in the Goldstone nature of the pion: since pions have to decouple from matter in the chiral limit for vanishing momenta, direct production (where a nucleon emits a pion) in the s-wave can only occur through a nucleon recoil process. However, these NLO loops turn out to cancel completely both for the neutral²³ and charged²⁵ pion production — this cancellation, a necessary requirement of field theoretic consistency, is discussed in detail in Sec. 3. As a by-product of this systematic treatment of nucleon recoil effects in the $\pi N \rightarrow \pi N$ vertex in Ref.,²⁵ the isovector rescattering one-pion exchange amplitude at LO was found to be enhanced by a factor of 4/3 which was sufficient to overcome the apparent discrepancy with the data when the final two nucleons are in the 3S_1 state. The contributions to the pion-production amplitudes from subleading loops were derived in Ref.,²⁶ see also Ref.⁶¹ for an earlier study, and are presented in Sec. 3. Early on it was realized that the Delta-isobar (Δ) should be explicitly included as a dynamical degree of freedom.¹⁴ In the MCS expansion the Delta-nucleon (Δ -N) mass splitting is numerically of the order of p and will contribute to s-wave pion production starting at NLO diagrams. The general argument justifying the inclusion of the Δ resonance was confirmed numerically in phenomenological calculations,^{9,62,63} see also Refs.^{14,17,23,64} where the effect of the Δ in $NN \rightarrow NN\pi$ was studied within chiral effective field theory. We will elaborate on this topic in Sec. 4. As discussed earlier, in Sec. 5 we present one possible determination of the LEC d by comparing the N²LO calculation of Refs.^{22,65} with the measured observables. Finally, we mention that the reactions $NN \rightarrow NN\pi$ provide a direct experimental access to charge symmetry breaking (CSB) operators, which are difficult to study otherwise, — a topic we will present in Sec. 7. In Table 1 we indicate a CSB reaction to be discussed in Sec. 7. In Secs. 8-10 we will discuss several applications of the MCS scheme in $NN \rightarrow NN\pi$ to two-pion production in nucleon-nucleon collisions (Sec. 8), πd scattering at threshold (Sec. 9)

and decays of heavy quarkonia (Sec. 10). The results of the review are summarized in Sec. 11.

2. Formal aspects of the momentum counting scheme

2.1. Lagrangian densities

The heavy baryon ChPT Lagrangian is written as a series in increasing powers of derivatives. The underlying assumption in writing this series is that the higher order Lagrangian terms will only contribute smaller corrections to the dominant amplitudes which are generated by the lowest order Lagrangian terms.

$$\mathcal{L}_{\text{ch}} = \mathcal{L}_{\pi N}^{(1)} + \mathcal{L}_{\pi N}^{(2)} + \mathcal{L}_{\pi\pi}^{(2)} + \mathcal{L}_{\pi N}^{(3)} + \dots, \quad (5)$$

where $\mathcal{L}^{(\bar{p})}$ ($\bar{p} = 1, 2, \dots$) denotes the number of derivatives and/or powers of m_π in the Lagrangian. Note that within the MCS some terms from higher order Lagrangians might get promoted to lower orders — see e.g. the discussion below Eq. (7). The effective chiral Lagrangian to lowest-order (LO) in the πN interaction terms read in σ -gauge^{60,66} when we expand Eq.(2) in powers of the pion field

$$\mathcal{L}_{\pi N}^{(1)} = N^\dagger \left[\frac{1}{4f_\pi^2} \boldsymbol{\tau} \cdot (\dot{\boldsymbol{\pi}} \times \boldsymbol{\pi}) + \frac{\dot{g}_A}{2f_\pi} \boldsymbol{\tau} \cdot \vec{\sigma} \left(\vec{\nabla} \boldsymbol{\pi} + \frac{1}{2f_\pi^2} \boldsymbol{\pi} (\boldsymbol{\pi} \cdot \vec{\nabla} \boldsymbol{\pi}) \right) \right] N + \dots. \quad (6)$$

The ellipses represent further terms which are not relevant for the presentation in this review. The next-higher order πN interaction terms have the form

$$\begin{aligned} \mathcal{L}_{\pi N}^{(2)} = & \frac{1}{8m_N f_\pi^2} \left[iN^\dagger \boldsymbol{\tau} \cdot (\boldsymbol{\pi} \times \vec{\nabla} \boldsymbol{\pi}) \cdot \vec{\nabla} N + h.c. \right] \\ & - \frac{\dot{g}_A}{4m_N f_\pi} \left[iN^\dagger \boldsymbol{\tau} \cdot \left(\dot{\boldsymbol{\pi}} + \frac{1}{2f_\pi^2} \boldsymbol{\pi} (\boldsymbol{\pi} \cdot \dot{\boldsymbol{\pi}}) \right) \vec{\sigma} \cdot \vec{\nabla} N + h.c. \right] \\ & - \frac{\dot{g}_A}{8m_N f_\pi^3} N^\dagger \boldsymbol{\pi} \cdot (\vec{\sigma} \cdot \vec{\nabla}) (\dot{\boldsymbol{\pi}} \times \boldsymbol{\pi}) N \\ & + \frac{1}{f_\pi^2} N^\dagger \left[\left(c_3 + c_2 - \frac{g_A^2}{8m_N} \right) \dot{\boldsymbol{\pi}}^2 - c_3 (\vec{\nabla} \boldsymbol{\pi})^2 - 2c_1 m_\pi^2 \boldsymbol{\pi}^2 \right. \\ & \left. - \frac{1}{2} \left(c_4 + \frac{1}{4m_N} \right) \varepsilon_{ijk} \varepsilon_{abc} \sigma_k \tau_c \partial_i \pi_a \partial_j \pi_b \right] N + \dots. \quad (7) \end{aligned}$$

To be consistent with chiral symmetry the chiral Lagrangian is only allowed to have terms analytic in the quark masses. Since the square of the pion mass depends linearly on the quark masses, only terms of even powers of m_π appear in the hierarchy of the Lagrangian densities Eq. (5).

Note that in MCS some nucleon recoil terms $\propto 1/m_N$ in the Lagrangian will appear at lower order than what is indicated by the Lagrangian order. For example, the WT term leads to a πN rescattering vertex proportional to m_π . Whereas in the standard chiral counting the corresponding WT recoil correction term, the first term in Eq. (7), would be of next order, in MCS this WT recoil correction term is proportional to $\vec{p}^2/m_N \sim m_\pi$, i.e., it is of the same order as the WT vertex

from the lower order Lagrangian Eq. (6). A more complete discussion on this topic will be presented in a separate subsection, Sec. 2.3. We refrain from presenting the complete $\mathcal{L}_{\pi N}^{(3)}$ Lagrangian and refer to the literature.^{60,67,68}

The pion Lagrangian density $\mathcal{L}_{\pi\pi}^{(2)}$, which gives the leading 4π vertex needed for the calculation of the reaction $NN \rightarrow NN\pi$ up to N²LO, reads in the sigma-gauge:

$$\mathcal{L}_{\pi\pi}^{(2)} = \frac{1}{2f_\pi^2} (\boldsymbol{\pi} \cdot \partial^\mu \boldsymbol{\pi}) (\boldsymbol{\pi} \cdot \partial_\mu \boldsymbol{\pi}) - \frac{m_\pi^2}{8f_\pi^2} \boldsymbol{\pi}^4 + \dots, \quad (8)$$

and we will also refer to the following S-wave NN Lagrangian, which specifies the two LECs, C_S and C_T :

$$\mathcal{L}_{NN} = -\frac{1}{2} C_S (N^\dagger N) (N^\dagger N) - \frac{1}{2} C_T (N^\dagger \vec{\sigma} N) \cdot (N^\dagger \vec{\sigma} N). \quad (9)$$

The derivation of the analytical expression for the transition amplitude, $\mathcal{A}_{\text{prod}}$, for pion production in nucleon–nucleon collisions including N²LO contributions will be presented in the next sections. At N²LO new short range operators with the associated LECs describing the short distance processes not probed at energies associated with pion-production threshold have to be introduced. Parity conservation requires the presence of one derivative that acts either on the pion field — leading to a p-wave pion with the final nucleon pairs in an S-wave — or on a nucleon field, leading to a pion s-wave production, as reflected in Table 1. Then, however, there must be an additional pion mass term present for consistency with the Goldstone theorem — this is why in the equations below the pion field appears with a time derivative. One may write following Ref.¹⁴ :

$$\begin{aligned} \mathcal{L}_{NNNN\pi} = & \frac{\tilde{e}_1}{2m_N f_\pi} \left[i \left(N^\dagger (\boldsymbol{\tau} \cdot \dot{\boldsymbol{\pi}}) \vec{\sigma} \cdot \vec{\nabla} N \right) (N^\dagger N) + h.c. \right] \\ & + \frac{\tilde{e}_2}{2m_N f_\pi} \left[i \left(N^\dagger (\boldsymbol{\tau} \cdot \dot{\boldsymbol{\pi}}) \vec{\sigma} \times \vec{\nabla} N \right) \cdot (N^\dagger \vec{\sigma} N) + h.c. \right] \\ & - \frac{d}{f_\pi} \left(N^\dagger \boldsymbol{\tau} \vec{\sigma} \cdot (\vec{\nabla} \boldsymbol{\pi}) N \right) (N^\dagger N) + \dots \end{aligned} \quad (10)$$

where the LECs \tilde{e}_i , $i = 1, 2$, are of order $\mathcal{O}(1/f_\pi^2 m_N)$ and the LEC d is the one in Eq. (3). These LECs will be discussed in more detail in Secs. 3 and 5, respectively. Note that a pion in an s-wave can be produced in channels either with the spin-triplet or spin-singlet NN FSI, as shown in Table 1. As a consequence, the production operator for s-wave pions contains at N²LO only two independent LECs called \tilde{e}_1 and \tilde{e}_2 in Eq.(10). We also emphasize that the effective Lagrangian of Ref.¹⁴ contains other $(NN)^2\pi$ contact operators both for s- and p-wave pions that can be shown to be redundant as a consequence of the Pauli principle.^{22,26,41,45}

2.2. The hybrid approach and the concept of diagram reducibility

It is well known that perturbation theory is insufficient to properly describe two or more nucleons at small relative momenta — a finite sum of diagrams can neither

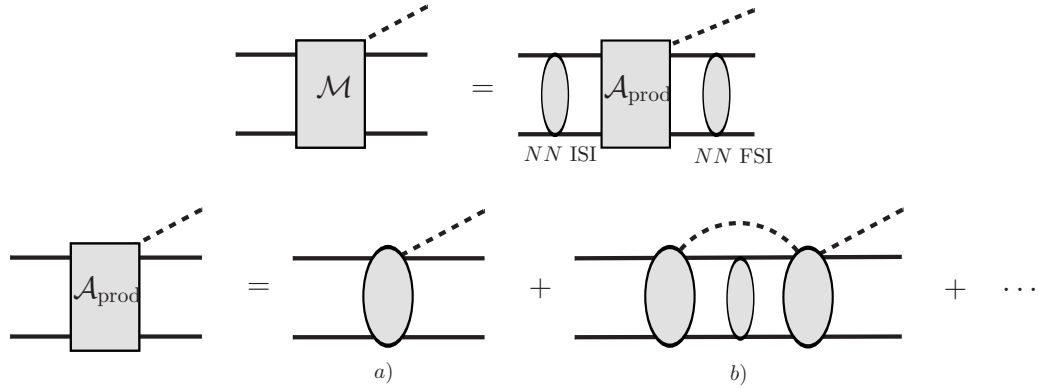


Fig. 2. Graphical illustration of the approach for calculating the amplitude \mathcal{M} for $NN \rightarrow NN\pi$. The initial and final state NN interactions sandwich the $NN \rightarrow NN\pi$ transition amplitude $\mathcal{A}_{\text{prod}}$ evaluated using ChPT.

produce the unnaturally large NN scattering lengths nor bound nucleons in nuclei. In order to adopt the perturbative approach of EFT to few nucleon systems, Weinberg proposed to classify all possible diagrams as reducible or irreducible.^{66,69–71} Those diagrams that have a two nucleon cut are classified as reducible, whereas those which do not are considered irreducible. The latter diagrams make up the NN potential which is to be constructed according to the rules of ChPT. The former diagrams are generated by solving the Schrödinger equation, using the ChPT evaluated NN potential as kernel. This scheme acknowledges the special role played by the two-nucleon cuts.

Furthermore, Weinberg suggested how to calculate few-nucleon systems interacting with an external low-energy probe.⁷² First, one should note that the relevant transition operators of such an external probe will act perturbatively and as such the transition operators can be calculated using ChPT. The transition operators are then convoluted with the non-perturbative nuclear (NN) wave functions. We will apply this scheme to pion production in NN collisions where the reaction amplitude is calculated by sandwiching the perturbative production operator, $\mathcal{A}_{\text{prod}}$, with NN wave functions in the initial and final states, as illustrated graphically in Fig. 2ⁱⁱⁱ. The transition operator, $\mathcal{A}_{\text{prod}}$, in the second line in Fig. 2, consists of all irreducible diagrams which means that no diagrams with a two-nucleon cut is part of the production operator. The $NN \rightarrow NN\pi$ reaction amplitude reads

$$\mathcal{M}(\mathbf{p}, \mathbf{p}', \mathbf{q}) = \int \frac{d^3l}{(2\pi)^3} \frac{d^3l'}{(2\pi)^3} \Psi_{\text{ISI}}(\mathbf{p}, \mathbf{l}) \mathcal{A}_{\text{prod}}(\mathbf{l}, \mathbf{l}', \mathbf{q}) \Psi_{\text{FSI}}(\mathbf{l}', \mathbf{p}') \quad (11)$$

ⁱⁱⁱThe inclusion of diagram a) in Fig. 2 while neglecting diagram b) and others is equivalent to the so-called distorted wave Born approximation (DWBA) traditionally used in phenomenological calculations. As will be discussed in the next section, for the calculation up-to-and-including N²LO in the MCS it suffices to keep only diagram a).

where the NN wave functions in the initial and final states are

$$\Psi_{\text{ISI}}(\mathbf{p}, \mathbf{l}) = (2\pi)^3 \delta(\mathbf{p} - \mathbf{l}) + \frac{\mathcal{M}_{\text{ISI}}(\mathbf{p}, \mathbf{l}, E)}{4m_N^2[l^2/m_N - E - i0]}, \quad (12)$$

$$\Psi_{\text{FSI}}(\mathbf{l}', \mathbf{p}') = (2\pi)^3 \delta(\mathbf{p}' - \mathbf{l}') + \frac{\mathcal{M}_{\text{FSI}}(\mathbf{l}', \mathbf{p}', E')}{4m_N^2[l'^2/m_N - E' - i0]}. \quad (13)$$

Here $\mathcal{A}_{\text{prod}}$ denotes the production operator and \mathcal{M}_{ISI} and \mathcal{M}_{FSI} stand for the NN amplitudes in the initial and final states evaluated at the energies E and E' , respectively. As will be discussed in Sec.4, since pion-production operator acquires important contributions from diagrams with the Δ -resonance degrees of freedom, it is useful to generalize the formalism described to include $N\Delta$ intermediate states. This can be implemented by utilizing NN models which include explicitly NN and $N\Delta$ coupled channels as in, e.g., Ref.⁷³ The generalisation of the above expressions is straightforward, e.g., see Appendices in Refs.^{27,65} for the explicit results.

A potential obstacle for the application of this approach to the $NN \rightarrow NN\pi$ reaction is the large momentum transfer between initial and final nucleons inherent in this reaction already at threshold

$$t \approx -(\mathbf{p} - \mathbf{p}')^2 \approx -m_N m_\pi. \quad (14)$$

As discussed in the introduction, this brings a new scale into the problem compared to standard ChPT. However, the use of the MCS, which will be discussed in detail in the next paragraph, allows one to build a new hierarchy of diagrams, allowing a systematic perturbative calculation of the production operator. Ideally, the NN wave functions should be evaluated within the same framework, i.e ChPT. However, this pion-production process requires an NN initial state interaction (ISI) at an energy which is beyond the applicability of today's NN potentials constructed within chiral EFT. Therefore, for pragmatic reasons, in a hybrid calculation we make use of the modern realistic phenomenological NN potentials⁷³⁻⁷⁵ to generate the initial and final state NN wave functions. These modern NN potential models are successful in reproducing the NN phase shifts, not only at very low energies where the NN amplitude is governed by the scattering length and effective range parameters, but also at relatively high energies around the pion-production threshold. Unlike chiral EFT, however, the short range interactions of the phenomenological NN potentials are parametrized in model-dependent ways. It is therefore important to require that the variations of the reaction amplitude \mathcal{M} for $NN \rightarrow NN\pi$ due to the use of different NN potentials are no larger than the variations expected from the next order MCS contributions to the reaction amplitude.

The intrinsic scheme-dependence inherent in the hybrid approach needs to be quantified. Specifically, the hybrid approach, as illustrated graphically in Fig.2, does not include the so-called stretched diagrams, where parts of the production operator are intimately connected to those from initial (or final) NN interaction via intermediate states in the Time-Ordered Perturbation Theory (TOPT) version of the diagrams. The study of Ref.⁷⁶ revealed that the stretched box contributions,

which do not possess a two-nucleon cut, are numerically suppressed. In addition, corrections due to NN wave function orthonormalization⁷⁷ are ignored in the hybrid formalism. These corrections normally appear at relatively higher orders and are known to cancel leading parts of stretched diagrams in the static limit.^{77,78} Meanwhile, a systematic treatment of these effects is necessary. Such a treatment is, however, only possible if the production operator and NN wave functions are constructed within the same EFT formalism. For some attempts to study the mismatch between the construction of the NN wave functions and the production operator we refer to Ref.⁷⁹ In this review we will not elaborate further on these topics.

2.3. Power Counting

In ChPT the standard expansion parameter is Q/Λ_χ , where Q is identified either with a typical momentum of the process or m_π . The key assumption for convergence of the theory is $Q \ll \Lambda_\chi$. As mentioned earlier, the reaction $NN \rightarrow NN\pi$ at threshold involves momenta of “intermediate range” $p \approx \sqrt{m_\pi m_N}$ larger than m_π but still smaller than the $\Lambda_\chi \sim m_N$. In the MCS we are thus faced with a two-scale expansion. Furthermore, for near threshold pion production, the outgoing two-nucleon pair has a very low relative three-momentum p' . For counting purposes we therefore assign an order m_π to p' , and the expansion parameter is written as:

$$\chi_{\text{MCS}} \simeq \frac{p'}{p} \simeq \frac{m_\pi}{p} \simeq \frac{p}{m_N}. \quad (15)$$

To implement this scheme properly it is necessary to keep explicitly track of momenta and masses in the power counting of the diagrams.

In Fig. 3 we show the hierarchy of the diagrams for s-wave pion production in the MCS up to N²LO. The first two LO diagrams in the first row of Fig. 3 are sometimes called the direct one-nucleon diagrams in the literature, whereas the last two are called the rescattering (WT) diagrams. We will discuss both next. We stress that the one-pion exchange (OPE) and the NN contact term in the direct single-nucleon operator are considered parts of the NN wave function and drawn explicitly only for the purposes of power counting. The estimate of the direct operator gives (in the counting $g_A \sim 1$)

$$\left(g_A \frac{m_\pi}{m_N} \cdot \frac{p}{f_\pi} \right) \cdot \frac{1}{m_\pi} \cdot \frac{1}{f_\pi^2} \sim \frac{1}{f_\pi^3} \frac{p}{m_N} \simeq \frac{1}{f_\pi^3} \chi_{\text{MCS}}, \quad (16)$$

where the expression in the first bracket on the l.h.s corresponds to the recoil πNN vertex given by $\mathcal{L}_{\pi N}^{(2)}$ of Eq. (7), the next term reflects the energy $v \cdot p \sim m_\pi$ of the nucleon propagator, see Sec.2.4 for further details about the treatment of nucleon propagators in MCS. The last term corresponds to the estimate of the OPE or the contact term. Analogously, the estimate of the rescattering operator reads

$$\left(\frac{m_\pi}{f_\pi^2} \right) \cdot \frac{1}{p^2} \cdot \left(g_A \frac{p}{f_\pi} \right) \sim \frac{1}{f_\pi^3} \frac{m_\pi}{p} \simeq \frac{1}{f_\pi^3} \chi_{\text{MCS}}, \quad (17)$$

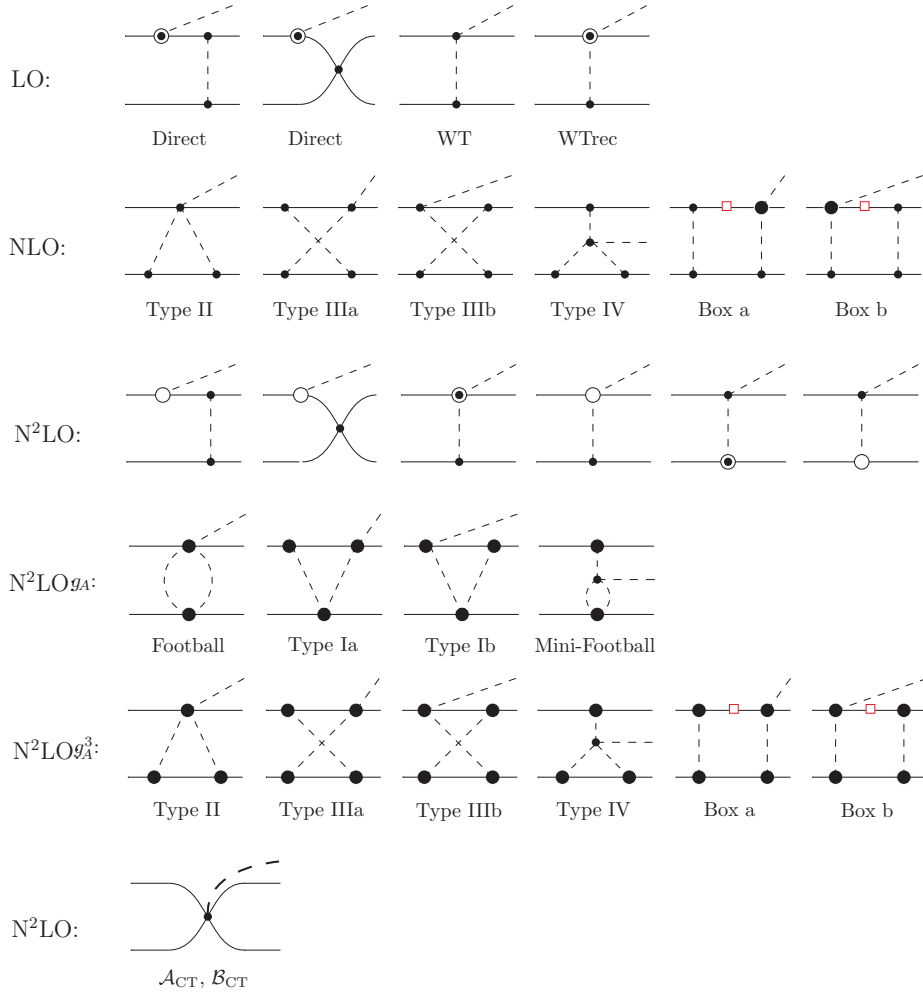


Fig. 3. Complete set of diagrams up to N²LO (in the Δ -less theory) for s-wave pions. Solid (dashed) lines denote nucleons (pions). Solid dots correspond to the leading vertices from $\mathcal{L}_{\pi N}^{(1)}$ and $\mathcal{L}_{\pi\pi}^{(2)}$, \odot stands for the sub-leading vertices from $\mathcal{L}_{\pi N}^{(2)}$ whereas the blob indicates the possibility to have both leading and subleading vertices from $\mathcal{L}_{\pi N}^{(1)}$ and $\mathcal{L}_{\pi N}^{(2)}$, the opaque symbol \circ stands for the vertices $\sim 1/m_N^2$ from $\mathcal{L}_{\pi N}^{(3)}$. The NN contact interaction in the top row is represented by the leading S-wave LECs C_S and C_T from \mathcal{L}_{NN} whereas the contact five-point vertices in the bottom row are given by the LECs \mathcal{A}_{CT} and \mathcal{B}_{CT} . The red square on the nucleon propagator in the box diagrams indicates that the corresponding nucleon propagator cancels with parts of the πN rescattering vertex producing an irreducible contribution from the two box diagrams, see Sec. 3.3 and discussion around Eq. (25) for further details.

where the first term on the l.h.s stands for the Weinberg-Tomozawa vertex given in $\mathcal{L}_{\pi N}^{(1)}$ of Eq. (6), the second term the pion propagator and finally the πNN vertex

of $\mathcal{L}_{\pi N}^{(1)}$, in order. Thus the leading order diagrams are linear in χ_{MCS} for s-wave pion production.

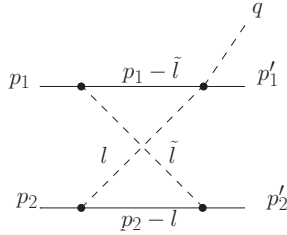


Fig. 4. The kinematics for the example of the loop diagram Type IIIa.

The second row of diagrams in Fig.3 represents the contribution of irreducible pion-nucleon loops at NLO. In order to illustrate the power counting of the loop diagrams in MCS as an example we discuss in detail the power counting for diagram type IIIa in the second row of Fig. 3. First we remind the reader that in heavy baryon ChPT the nucleon four-momentum P^μ is rewritten as $P^\mu = m_N v^\mu + p^\mu$ where the velocity is chosen to be $v^\mu = (1, \vec{0})$. Secondly, for the reaction $NN \rightarrow NN\pi$ close to threshold the initial nucleon, e.g., nucleon no. 1 (see Fig. 4 for the notation) has four-momentum $p_1^\mu = (m_\pi/2, \vec{p})$, meaning $v \cdot p_1 \sim m_\pi$. Analogously, the momentum $p_2^\mu = (m_\pi/2, -\vec{p})$. It is also important for the following discussion to note that the loop diagrams in the second row of Fig. 3 all have a large “external” momentum of order p in the propagators and that all vertices are given by the lowest order Lagrangian in Eq. (6). Furthermore, a consistent power counting of loop-diagrams requires the inclusion of the integral measure $l^4/(4\pi)^2$ where all components of the loop four-momentum l is of order p , i.e. $v \cdot l \sim |\vec{l}| \sim p$ for irreducible diagrams, while for reducible diagrams that explicitly contain an NN cut, the zeroth component $v \cdot l$ is to be counted of order m_π , as discussed in the next subsection. In addition to this integral measure, in the loop-diagram IIIa one has to account for two pion propagators ($\sim 1/(p^2)^2$), two nucleon propagators ($\sim 1/(v \cdot l)^2 \sim 1/p^2$), three πNN vertices ($\sim (p/f_\pi)^3$, and one πN rescattering vertex ($\sim v \cdot l/f_\pi^2 \sim p/f_\pi^2$). Combining all these factors and using $4\pi f_\pi \sim m_N$, one obtains the order estimate for this diagram as follows

$$\frac{p^4}{(4\pi)^2} \cdot \frac{1}{(p^2)^2} \cdot \frac{1}{p^2} \cdot \left(\frac{p}{f_\pi}\right)^3 \cdot \frac{p}{f_\pi^2} \sim \frac{1}{f_\pi^3} \frac{p^2}{m_N^2} \simeq \frac{1}{f_\pi^3} \chi_{\text{MCS}}^2. \quad (18)$$

This counting order estimate of diagram IIIa should be compared with the counting of the leading order diagrams for the $NN \rightarrow NN\pi$ reaction vertex in Fig. 3 estimated above. Thus we find that diagram type IIIa in Fig. 3 indeed contributes at NLO.

At this point the reader should note a peculiar feature of the MCS counting. The

order estimate of a loop diagram in MCS implies that this diagram also contributes at all higher orders in MCS. For example, diagram IIIa is estimated above to be of order NLO but, unlike standard chiral counting, this diagram also contributes at N²LO and higher MCS orders. The reason for this behaviour lies in the two scale expansion employed there, since the evaluation of the loop diagrams typically reveals expressions like $m_\pi \log(1 + m_\pi/p)$. In a theory where p is of order m_π the given term contributes to a single order only. However, in the MCS $m_\pi/p \sim \chi_{\text{MCS}}$, and thus a Taylor expansion of the logarithm becomes necessary. We will return to this discussion in Sec. 2.4.

At N²LO, there are several contributing tree-level diagrams which are topologically similar to those at LO but with sub-leading vertices from $\mathcal{L}_{\pi N}^{(2)}$ and even $\mathcal{L}_{\pi N}^{(3)}$. These diagrams are shown in the third row in Fig. 3. In addition, one needs to account for the pion-nucleon loops which, at this order, can be combined in two series of amplitudes, one proportional to g_A^3 with a topology like the NLO pion-nucleon loop diagrams and one proportional to g_A . These diagrams are given in rows four and five in Fig. 3. To the order we are working, it suffices to include the sub-leading vertex from $\mathcal{L}_{\pi N}^{(2)}$ only once (but we have to consider all possible permutations of this sub-leading vertex) in these loops while retaining the other vertices at leading order, see Ref.²⁷ for further details. Also at N²LO for s-wave pions there are two $(NN)^2\pi$ contact operators \mathcal{A}_{CT} and \mathcal{B}_{CT} which represent contributions to the channels with the spin-singlet (${}^3P_0 \rightarrow {}^1S_0s$) and the spin-triplet (${}^3P_1 \rightarrow {}^3S_1s$) NN FSI, in accordance with the notation of Table 1. The LECs \mathcal{A}_{CT} and \mathcal{B}_{CT} , shown in the last row of Fig.3 can be expressed in terms of linear combinations of the LECs \tilde{e}_1 and \tilde{e}_2 in the Lagrangian (10) to be used in Sec. 3.6.

Finally, we note that the diagram b) in Fig 2, which is also a part of the production operator, starts to contribute at N³LO, that is one order higher than considered in the present study. This type of operators contains the three-body πNN cut, the contribution of which is strongly suppressed near pion production threshold.

2.4. The heavy nucleon propagator in MCS

A major difference between standard chiral counting (see e.g. Ref.⁶⁰) and MCS²⁴ is associated with the different treatments of the heavy nucleon propagator. In heavy baryon ChPT (HBChPT) the nucleon momentum P^μ is written as $P^\mu = m_N v^\mu + p^\mu$, and it is assumed that $|p^\mu| \ll m_N$. In terms of p_μ the Feynman propagator for the heavy nucleon is expressed as

$$S_N(p) = i \frac{\not{P} + m_N}{P^2 - m_N^2 + i0} = \frac{i}{v \cdot p + \frac{p^2}{2m_N} + i0} \left(\frac{1 + \gamma_0}{2} + \frac{\gamma_0 p_0}{2m_N} - \frac{\vec{\gamma} \cdot \vec{p}}{2m_N} \right), \quad (19)$$

where we introduced $v^\mu = (1, 0, 0, 0)$. In the standard HBChPT scheme, the free heavy-nucleon Lagrangian is chosen in such a manner that the heavy-nucleon prop-

agator is given by

$$S_N(p) = \frac{i}{v \cdot p + i0} . \quad (20)$$

The difference between the propagators in Eqs. (19) and (20), which scales as $(p/m_N)^n$ with $n = 1, 2, \dots$, is treated as perturbative recoil corrections in standard HBChPT, and is included in $\mathcal{L}_{\pi N}^{(2)}$ and higher-order Lagrangians in Ref.,⁶⁰ cf. e.g. $1/m_N$ terms in the last two rows in Eq. (7). On the other hand, in some cases the use of Eq. (20) is not justified and one should utilize Eq. (19). One example where a careful treatment of the nucleon propagator in Eq. (19) is required is the two-pion-exchange contribution to NN scattering discussed by Weinberg in Ref.⁷⁰ In this case the second iteration of OPE results in the box diagram with an NN intermediate state which is reducible. A naive evaluation of this diagram with the standard HB propagator Eq. (20) would yield the pinch singularity. To properly account for the two-body singularity (NN cut) one should therefore keep the nucleon kinetic energy in the denominator of Eq. (19) unexpanded, i.e. this HB propagator for both intermediate nucleons deviates from the strict HBChPT formulation and becomes

$$S_N(p) = \frac{i}{v \cdot p - \frac{\vec{p}^2}{2m_N} + i0} , \quad (21)$$

while the residual terms in Eq. (19) are treated as perturbations in the Lagrangian. Only then the p_0 - integration leads to a proper two-nucleon propagator that in particular shows a strong infrared enhancement calling for a re-summation in, e.g., a Schrödinger equation — this is why they are called reducible. In contrast, in NN scattering diagrams which do not possess the two-nucleon cut (e.g. in the crossed boxes) the standard HBChPT expansion of the nucleon propagator is justified, i.e. $v \cdot p \sim |\vec{p}|$.

The treatment of the nucleon propagator in pion production is actually quite similar to NN interaction.^{25,61,80} The calculation of NN reducible diagrams for energies near the pion production threshold requires a non-perturbative treatment of nucleon recoils as given by Eq. (21), which means that zeroth components of 4-momenta are counted as $v \cdot p \sim \vec{p}^2/(2m_N) \sim m_\pi$. Meanwhile, to evaluate irreducible loop contributions in MCS it suffices to use Eq.(20) for the propagator structure while keeping $1/m_N$ (and higher-order) corrections perturbatively. Since there is no NN cut, in the latter case $v \cdot p \sim |\vec{p}| \sim \sqrt{m_\pi m_N} \gg \vec{p}^2/(2m_N)$ since the energy scale is introduced into the diagrams from the pion propagators (cf. Appendix E of Ref.²⁴).

It might be also instructive to discuss the special case of the pion emission from a single nucleon characteristic for the production process, see the first direct diagram in Fig.3 where the OPE is part of the NN FSI. Although this diagram contains an NN intermediate state, it can not go on shell since a massive pion can not be produced by a free nucleon. Therefore, naively one is tempted to expand

the nucleon propagator using standard HBChPT, as it was done in Ref.²¹ Based on this expansion it was argued that the heavy baryon scheme should not be used for pion production. We are now in a position to answer the critical comments in Ref.²¹ regarding the non-convergence of the heavy nucleon propagator. The expansion of the nucleon propagator in the first diagram of Fig. 3 would read, following Ref.²¹

$$S_N(p_1 - q) = \frac{1}{v \cdot (p_1 - q) - \vec{p}_1^2/(2m_N)} = -\frac{2}{m_\pi} \sum_{n=0}^{\infty} \left(-\frac{\vec{p}_1^2}{m_N m_\pi} \right)^n,$$

where on the r.h.s. $v \cdot p_1 = m_\pi/2$ and $v \cdot q = m_\pi$ was used at threshold ($\vec{q} = 0$) and the $1/m_N$ terms were treated as correction. Clearly this series does not converge, since $\vec{p}_1^2 \simeq m_N m_\pi$. However, had Ref.²¹ employed the on-shell condition for the external nucleon, $v \cdot p_1 \simeq \vec{p}_1^2/2m_N$, the propagator would have taken the correct expression $-1/m_\pi$ right from the start. Thus, when applied properly, the heavy baryon prescription can be used for pion-production reactions.⁸⁰

3. s-wave pion production at threshold

3.1. Operator amplitudes from tree-level diagrams up to N^2LO :

The LO tree-level diagrams were discussed in Sec. 2.3 which includes the LO rescattering diagram containing the isovector Weinberg-Tomozawa vertex and its recoil contribution given by $\mathcal{L}_{\pi N}^{(1)}$ and $\mathcal{L}_{\pi N}^{(2)}$, respectively. The same two Lagrangians, Eqs. (6) and (7), will contribute to N^2LO tree-level rescattering diagrams with the same topology as the LO rescattering diagram in Fig. 3. In the MCS the LO diagrams are the direct diagrams and the rescattering diagrams, labelled "Direct" and "WT" in Fig. 3.

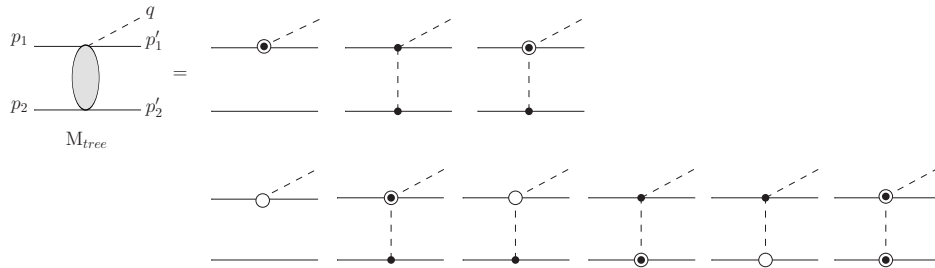


Fig. 5. The single nucleon and the rescattering diagrams which contribute to s-wave pion production up to N^2LO , are given. The meaning of the symbols is the same as in Fig. 3. The diagrams in the first row on the r.h.s appear at LO, the diagrams in the second row give the N^2LO contributions. The last diagrams in the first and second rows involve the WT recoil correction, whereas the second diagram in the second row involves rescattering vertices proportional to the c_i . In the hybrid approach the first diagrams in each row, the single nucleon diagrams, will contribute to $\mathcal{A}_{\text{prod}}$ in Eq. (11) when convoluted with initial and final NN wave functions as discussed in the text.

18 *Vadim Baru, Christoph Hanhart, Fred Myhrer*

The rescattering operator at LO reads ^{iv}:

$$iM_{\text{rescat}}^{\text{LO}} = iM_{\text{WT}}^{\text{LO}} + iM_{\text{WT}}^{\text{recoil}} = \frac{g_A}{2f_\pi^3} \frac{v \cdot q}{k_2^2 - m_\pi^2 + i0} (S_2 \cdot k_2) \tau_\times^a, \quad (22)$$

where the superscript a ($a=1,2,3$) here and in what follows refers to the isospin quantum number of the outgoing pion field, and where the antisymmetric [symmetric] isospin operator is $\tau_\times^a = i(\boldsymbol{\tau}_1 \times \boldsymbol{\tau}_2)^a$ [$\tau_+^a = (\boldsymbol{\tau}_1 + \boldsymbol{\tau}_2)^a$]. The momenta are defined in Fig.5, and we define $k_2 = p_2 - p'_2$.

The rescattering operator at N²LO includes the $1/m_N$ corrections due to the vertices given by $\mathcal{L}_{\pi N}^{(2)}$ and also the corrections $\propto 1/m_N^2$ from $\mathcal{L}_{\pi N}^{(3)}$. We call these amplitude operators $M_{\text{rescat1}}^{\text{N}^2\text{LO}}$ and $M_{\text{rescat2}}^{\text{N}^2\text{LO}}$, respectively. The explicit expressions are:

$$iM_{\text{rescat1}}^{\text{N}^2\text{LO}} = \frac{g_A}{f_\pi^3} \frac{(S_2 \cdot k_2) \tau_2^a}{k_2^2 - m_\pi^2 + i0} \left[4c_1 m_\pi^2 - v \cdot q v \cdot k_2 \left(2c_2 + 2c_3 - \frac{g_A^2}{4m_N} \right) \right] - \frac{g_A}{f_\pi^3} \frac{(v \cdot q) \tau_\times^a}{k_2^2 - m_\pi^2 + i0} \frac{S_2 \cdot (p_2 + p'_2)}{4m_N} (v \cdot k_2) + (1 \leftrightarrow 2), \quad (23)$$

$$iM_{\text{rescat2}}^{\text{N}^2\text{LO}} = \frac{g_A}{f_\pi^3} \frac{v \cdot q}{k_2^2 - m_\pi^2 + i0} \left\{ -\tau_2^a (S_2 \cdot k_2) \frac{k_2 \cdot (p_1 + p'_1)}{m_N^2} \left(m_N c_2 - \frac{g_A^2}{16} \right) + \tau_\times^a (S_2 \cdot k_2) \left[\frac{\vec{p}_1^2 + \vec{p}'_1^2}{16m_N^2} + \frac{1 + g_A^2 + 8m_N c_4}{8m_N^2} \left([S_1 \cdot k_2, S_1 \cdot (p_1 + p'_1)] + \frac{k_2^2}{2} \right) \right] - \frac{\tau_\times^a}{8m_N^2} [(S_2 \cdot p'_2) p_2^2 - (S_2 \cdot p_2) p_2'^2] \right\} + (1 \leftrightarrow 2), \quad (24)$$

The first two terms in the curly bracket in Eq. (24) are due to recoil corrections to the $\pi\pi NN$ vertices from $\mathcal{L}_{\pi N}^{(3)}$ while the last one stands for the analogous correction to the πNN vertex at the same order. Both amplitudes $M_{\text{rescat1}}^{\text{N}^2\text{LO}}$ and $M_{\text{rescat2}}^{\text{N}^2\text{LO}}$ contribute to the isoscalar and isovector part of the production amplitude $\mathcal{A}_{\text{prod}}$ in Eq. (11).

In addition to the rescattering operators, one has to account for the contributions to the transition operator amplitude $\mathcal{A}_{\text{prod}}$ from the pion emission from a single nucleon, the so-called direct diagrams which are shown in the first and third rows of Fig.3. Note that in the hybrid approach the OPE or the NN contact term in these direct diagrams, which appear together with the πNN vertex for the outgoing pion in Fig.3, will be considered as part of the final (or initial) NN wave function as discussed in Sec. 2.2. In Fig. 5 the OPE and the NN contact term are therefore not shown in the direct diagrams. The explicit expressions for these diagrams are derived in Ref.²⁷ In Sec. 3.2 we will discuss the influence of these direct diagrams in more details.

The LO and N²LO operator amplitudes generated by the diagrams in Fig.5 contribute to the N²LO s-wave pion-production operator $\mathcal{A}_{\text{prod}}$ from pion-nucleon

^{iv} At this order it suffices to replace \hat{g}_A by its physical value g_A . The renormalization corrections to \hat{g}_A will be discussed in Sec. 4.5.

diagrams. We postpone the discussion of the s-wave pion-production operator until the end of Sec. 4, where the Δ degrees of freedom will be added to this operator.

3.2. *A discussion of the tree-level diagrams up to N²LO*

The LO diagrams, which contain only pion and nucleon degrees of freedom that contribute to the reaction $NN \rightarrow NN\pi$ for s-wave pions, are shown in the first line of Fig. 3. Traditionally, the direct diagrams have been evaluated numerically by including the pion propagator in the distorted NN wave functions, i.e. only the single nucleon pion-production vertex gives the transition operator. Numerically, in the traditional distorted wave Born approximation approach, the direct diagram appears to be significantly smaller than the estimate based on our naive MCS's dimensional analysis. The suppression of the direct diagram in Fig. 3 comes from two sources: first, there is the momentum mismatch between the initial and final distorted nucleon wave functions²⁴ — see also Refs.^{79,81} for more detailed discussions. Secondly, there are accidental cancellations from the final state interaction present in both channels, $pp \rightarrow pp\pi^0$ and $pp \rightarrow d\pi^+$, that are not accounted for in the power counting. Specifically, the NN phase shift in the final NN 1S_0 partial wave relevant for $pp \rightarrow pp\pi^0$ crosses zero at an energy close to the pion-production threshold.^{82,83} All realistic NN scattering potentials that reproduce this feature show in the half-off-shell amplitude at low energies a zero at off-shell momenta of a similar magnitude. The exact position of the zero varies between different models, such that the direct production amplitude turns out to be quite model dependent. The suppression mechanism of the direct term for the reaction $pp \rightarrow d\pi^+$ comes from a strong cancellation between the deuteron S-wave and D-wave components. Thus, it is not surprising that numerically the direct diagrams in both channels are about an order of magnitude smaller than the LO rescattering amplitudes which are consistent with the dimensional analysis in the MCS. Since this LO rescattering contribution is forbidden by selection rules for $pp \rightarrow pp\pi^0$ while allowed for $pp \rightarrow d\pi^+$, one gains an immediate theoretical understanding why it is a lot more difficult to reproduce the measured cross section for the former reaction.

3.3. *Two-pion exchange diagrams at NLO*

The observation that the LO contributions to the pion s-wave reaction $pp \rightarrow pp\pi^0$ are highly suppressed^{14–16} makes this particular reaction an ideal probe of the higher order contributions, which give smaller corrections to most $NN \rightarrow NN\pi$ reaction amplitudes. Among the next order terms illustrated in Fig. 3, two-pion exchange loop diagrams were evaluated^{19,20} within standard ChPT and some two-pion exchange diagram contributions were found to be very large compared to the tree-level contributions. However, for the channel $pp \rightarrow pp\pi^0$ the sum of NLO diagrams type II^v, III and IV in Fig. 3 is zero due to a cancellation between individual

^v The amplitude for diagram type II in Fig. 3 as given in Ref.¹⁹ has the wrong sign.

20 *Vadim Baru, Christoph Hanhart, Fred Myhrer*

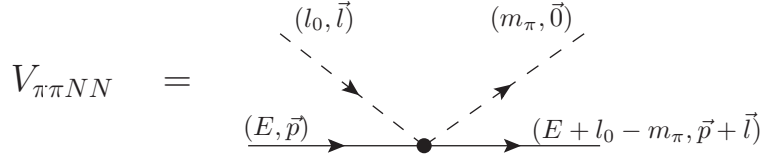


Fig. 6. The πN rescattering vertex: definition of kinematic variables as used in Eq. (25) where, e.g., $v \cdot l = l_0$.

diagrams,²³ where diagrams Box a and b in Fig. 3 are absent since the WT vertex does not contribute to this channel. Some aspects of these diagrams and this cancellation was further discussed in, e.g., Refs.^{61,84} The cancellation among the diagrams for $pp \rightarrow pp\pi^0$ was confirmed in Ref.²⁶ Meanwhile, the sum of diagrams II – IV gives a finite answer for the channel $pp \rightarrow d\pi^+$, as was noted in Ref.²³ Since the net contribution of these operators depends linearly on the NN relative momentum, a large sensitivity of the observables to the short-distance NN wave functions was found in Ref.⁸⁵ This linear NN momentum sensitivity to short-distance NN forces at NLO, $\mathcal{O}(m_\pi/m_N)$, is troubling since chiral symmetry requires interactions to be proportional to an even power of the pion mass, m_π . Specifically, at NLO there is no five-point contact interactions that could absorb this linear momentum behaviour of the loop operators. This puzzle was resolved in Ref.,²⁵ where it was demonstrated that for the deuteron channel there is an additional contribution at NLO, namely the box diagrams in Fig. 3, due to the time-dependence of the Weinberg–Tomozawa pion-nucleon vertex. The cancellation of the NLO loop diagrams found in Ref.²⁵ reinforces the importance of applying ChPT to the $NN \rightarrow NN\pi$ reactions.

To demonstrate that the irreducible parts of the box diagrams in Fig. 3 contribute to the NLO amplitude, we write the expression for the WT πN rescattering vertex, $V_{\pi NN}$, in the notation of Fig. 6, where one pion is the outgoing pion of four-momentum $(m_\pi, \vec{0})$ and the other pion is part of the loop with four-momentum l :

$$\begin{aligned}
 V_{\pi NN} &= l_0 + m_\pi - \frac{\vec{l} \cdot (2\vec{p} + \vec{l})}{2m_N} \\
 &= 2m_\pi + \left(l_0 - m_\pi + E - \frac{(\vec{l} + \vec{p})^2}{2m_N} + i0 \right) - \left(E - \frac{\vec{p}^2}{2m_N} + i0 \right). \quad (25)
 \end{aligned}$$

We keep the leading WT vertex and its nucleon recoil correction, which are of the same order in the MCS, as explained below Eq. (7). For simplicity, we omit the isospin dependence of the vertex. The first term in the last line is the WT-vertex for kinematics with the on-shell incoming and outgoing nucleons, the second term the inverse of the outgoing nucleon propagator while the third one is the inverse of the incoming nucleon propagator; compare the nucleon propagator expression in Eq. (21). Note that for on-shell incoming and outgoing nucleons (as in diagram

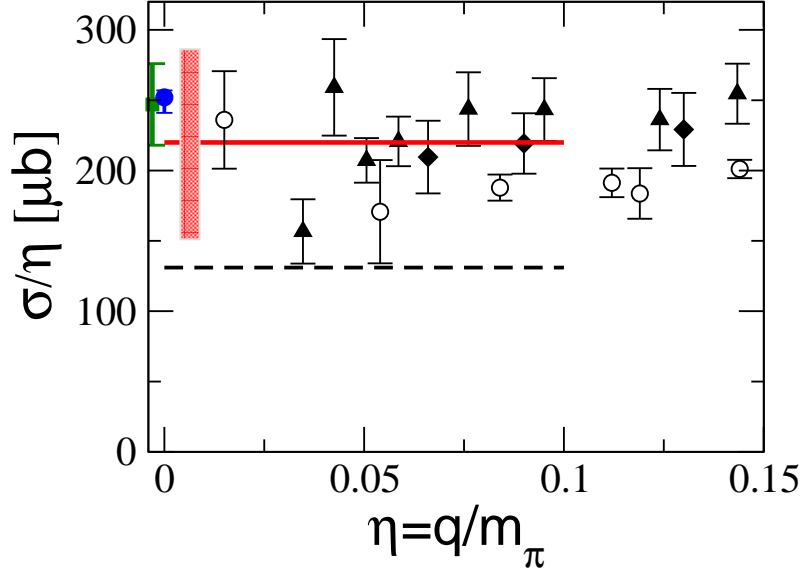


Fig. 7. Comparison of the results of Ref.²⁵ with experimental data for total cross section in $NN \rightarrow d\pi$. The data sets are from Refs.^{86–90} The dashed line corresponds to the model of Koltun and Reitan.² The solid red curve represents the results for s -wave pion-production at threshold, i.e. the coefficient α in Eq.(26), as given in Ref.²⁵ The filled red rectangular box indicates the theoretical uncertainty of the NLO calculation.

WT in Fig. 3), the expressions in brackets in Eq. (25) vanish, and the $\pi N \rightarrow \pi N$ transition vertex takes its on-shell value $2m_\pi$ (even if the incoming pion is off-shell). This is in contrast to standard phenomenological treatments, e.g., Ref.,² where l_0 in the first line of (25) is identified with $m_\pi/2$, the energy transfer in the on-shell kinematics for $NN \rightarrow NN\pi$, but the recoil terms in Eq. (25) are not considered. However, as argued earlier $\vec{p}^2/m_N \approx m_\pi$ so that the recoil terms are to be kept in the vertices and also in the nucleon propagator as discussed in Sec. 2.4. The MCS is designed to properly keep track of these recoil terms. A second consequence of Eq. (25) is that only the first term gives a reducible diagram. The second and third terms in Eq. (25), however, lead to irreducible contributions, since one of the nucleon propagators is cancelled by parts of the adjacent WT πN rescattering vertex expression. These irreducible contributions are illustrated by red squares on the nucleon propagators in the two box diagrams of Fig. 3. It was shown explicitly in Ref.²⁵ that these induced irreducible contributions cancel exactly the finite remainder of the NLO loop diagrams (II – IV) in the $pp \rightarrow d\pi^+$ channel. As a consequence, there are no contributions at NLO for both π^0 and π^+ s -wave production from two initial nucleons.

3.4. Total cross section in $NN \rightarrow d\pi$ at threshold up to NLO

In this subsection we briefly discuss the status of the description to NLO of threshold pion-production data when the final two nucleons are in the spin-triplet (${}^3S_1 - {}^3D_1$) channel. The total cross section in the reaction $NN \rightarrow d\pi$ close to threshold is historically written in the form

$$\sigma = \alpha\eta + \beta\eta^3 + \dots, \quad (26)$$

where the dimensionless variable η is defined in the center-of-mass system as the pion momentum in units of the pion mass, $\eta = |\vec{q}|/m_\pi$ and ellipses stand for the terms of higher order in η . In Fig. 7 we compare the chiral EFT evaluation of α by Ref.²⁵ with experimental data. Note that the green square and the blue circle correspond to the most recent measurements^{89,90} of the coefficient α in Eq. (26), see also Sec. 9. The value for α in Refs.^{89,90} was extracted from the high-precision lifetime measurement of the π^-d atom at PSI. The dashed curve in Fig. 7 corresponds to the calculation of Ref.,² in which the nucleon recoil corrections to the Weinberg-Tomozawa operator were neglected. As pointed out in the Introduction and discussed earlier in this section, the important observation of Ref.²⁵ was that the nucleon recoil corrections $\propto 1/m_N$ contribute in MCS at lower order than what is indicated naively by the order of the Lagrangian. Including the WT recoil correction, labelled “WTrec” in Fig. 3, in Eq.(22) enhances the WT operator by a factor of 4/3. This enhancement resulted in an increase of the cross section by about the missing factor 2 already at LO. Furthermore, as was shown in Ref.²⁵ and discussed in detail in the previous subsection, all loops at NLO cancel. Given the expansion parameter in the MCS, the theoretical uncertainty for α is about $2\chi_{\text{MCS}}$ at NLO, as shown by the filled rectangular box in Fig. 7.

3.5. Two-pion exchange diagrams to N²LO

At N²LO there are new loop diagrams contributing to the $NN \rightarrow NN\pi$ s-wave pion reaction amplitude. The N²LO two-pion exchange diagrams shown in Fig. 3 have been evaluated in Ref.²⁶ One finds that also at this order a similar cancellation pattern appears as discussed in the previous subsection for the NLO contributions. However, at N²LO the cancellation is not complete and leaves us with a non-zero result, which originates from diagrams proportional to g_A of type I and the one called “mini-football”, see the fourth row of diagrams in Fig. 3, and from diagrams proportional to g_A^3 of type III and IV in the fifth row of diagrams in Fig. 3. The other loop diagrams give no net contribution to the amplitude for s-wave pion production.

There are some fundamental reasons why at least some of these cancellations are to be expected. The Goldstone boson nature of the pion requires the pion to decouple from the nucleon field as its four-momentum components become zero in the chiral limit. This chiral symmetry requirement is exemplified by the Lagrangian densities in the so-called sigma gauge given in Eqs. (6), (7) and (8). Another aspect

of ChPT, which forces us to consider classes of diagrams, is that it is the U matrix which enters in the interactions, and the U matrix depends non-linearly on the pion field. The chiral matrix-field $U(x)$ is an $SU(2)$ matrix that has standard chiral transformation properties, see e.g. Ref.⁶⁰ There are several equivalent ways one can define the pion field content of the matrix-field U . The U matrix can be written in terms of the pion field a la Weinberg,⁷⁰ on an exponential form used in, e.g.,⁹¹ or as in Ref.⁶⁰'s sigma-gauge form which is chosen in this review. This $U(x)$ field is expanded in terms of $[\vec{\pi}(x)/f_\pi]$ in order to generate the Lagrangian expression in, e.g., Eq. (6). The different ways to categorize U in terms of the pion field have consequences for interaction terms involving three or more pions, e.g., the last term in Eq. (6). Even the nucleon fields have a certain arbitrariness since we can change $N(x)$ to $N'(x)$ as long as this transformation is consistent with chiral symmetry, see e.g., Ref.⁹² This arbitrariness of defining the fields in the Lagrangian forces one to consider not individual diagrams, but classes of diagrams, and at a given order only the sum of the diagrams is independent of the definitions of the fields in the Lagrangian.

It should be remarked that similar to what occurs in HBChPT, the cancellation of the sum of diagrams for $NN \rightarrow NN\pi$ is also found using Gasser *et al.*⁹³'s covariant formulation of ChPT as shown by Filin.⁹⁴ The pattern of cancellations in this case is even more elegant than in HBChPT, where to see the same cancellations one needs to keep track of all $1/m_N$ terms in the expansion. Specifically, several not obvious cancellations among the N²LO two-pion exchange diagrams in Fig. 3 were observed within the MCS formulation of HBChPT in Ref.²⁶ First, all recoil terms in the vertices ($\propto 1/(2m_N)$) cancel at N²LO, and since the NLO amplitude is zero, as discussed in Sec. 3.3, the nucleon recoil terms in the heavy nucleon propagator, Eq. (21), also do not contribute at N²LO. Secondly, none of the low-energy-constants (LECs), c_i , $i = 1, \dots, 4$ of Eq. (7) contribute in the loop diagrams at N²LO to the s-wave pion-production amplitude. This means none of the interactions in $\mathcal{L}_{\pi N}^{(2)}$ of Eq. (7) contribute to the amplitude from the pion loop diagrams in Fig. 3 at this order. Finally, as a surprise, the result in Ref.²⁶ shows that the isoscalar s-wave amplitude, which gives the s-wave $pp \rightarrow pp\pi^0$ cross section, receives contributions at N²LO only from the two cross-box diagrams, diagrams Type III, in the fifth row of Fig. 3. In particular this implies that earlier phenomenological studies,³⁻⁸ neither of which include the crossed box diagrams, did not include the appropriate long-range physics as we will discuss in the final section.

The evaluations of the two-pion exchange N²LO loop diagrams in Fig. 3 result

24 *Vadim Baru, Christoph Hanhart, Fred Myhrer*

in the following s-wave pion-production operator:²⁶

$$\begin{aligned}
 iM^{N^2\text{LO}} = & \frac{g_A}{f_\pi^5} (v \cdot q) \tau_\times^a (S_1 + S_2) \cdot k_1 \left[\frac{1}{6} I_{\pi\pi}(k_1^2) - \frac{1}{18} \frac{1}{(4\pi)^2} \right] + \\
 & + \frac{g_A^3}{f_\pi^5} (v \cdot q) \left\{ \tau_+^a i \varepsilon^{\alpha\mu\nu\beta} v_\alpha k_{1\mu} S_{1\nu} S_{2\beta} [-2I_{\pi\pi}(k_1^2)] \right. \\
 & \left. + \tau_\times^a (S_1 + S_2) \cdot k_1 \left[-\frac{19}{24} I_{\pi\pi}(k_1^2) + \frac{5}{9} \frac{1}{(4\pi)^2} \right] \right\}, \quad (27)
 \end{aligned}$$

where in the center-of-mass system $\vec{p}_1 = -\vec{p}_2 = \vec{p}$, $k_1 = p_1 - p'_1 = -k_2 + q$, and the approximate relation $k_1^2 \simeq k_2^2$ is used (higher-order terms being ignored). The symmetric combination of the two nucleon spins $S_1 + S_2$ are combined with the isovector operator τ_\times^a , whereas the antisymmetric two nucleon spin operator goes with τ_+^a . Note that $M^{N^2\text{LO}}$ is proportional to the outgoing pion energy $v \cdot q \simeq m_\pi$ as expected. The integral expression for $I_{\pi\pi}(k_1)$, which contains two pion propagators and is UV divergent, is given in the appendix. As will be discussed in the next subsection, the UV divergence has to be regularized, however, the finite long-range $N^2\text{LO}$ loop amplitude behavior of Eq. (27), is renormalization scheme independent.

3.6. Regularization and renormalization of loop diagrams

The form of the threshold operator with s-wave pions and two nucleons in a final S-state is

$$M = \tau_+ (\vec{\sigma}_1 \times \vec{\sigma}_2) \cdot \vec{p} \mathcal{A} - i \tau_\times (\vec{\sigma}_1 + \vec{\sigma}_2) \cdot \vec{p} \mathcal{B} \quad (28)$$

The contributions of the loops to the amplitudes \mathcal{A} and \mathcal{B} in Eq. (28) are separated into singular and finite parts, where the singular parts are given by the UV divergences appearing in the integral, $I_{\pi\pi}(k_1^2)$, in Eq. (27).

$$\begin{aligned}
 \mathcal{A} &= \frac{m_\pi}{(4\pi f_\pi)^2 f_\pi^3} (\tilde{\mathcal{A}}_{\text{singular}} + \tilde{\mathcal{A}}_{\text{finite}}), \\
 \mathcal{B} &= \frac{m_\pi}{(4\pi f_\pi)^2 f_\pi^3} (\tilde{\mathcal{B}}_{\text{singular}} + \tilde{\mathcal{B}}_{\text{finite}}). \quad (29)
 \end{aligned}$$

The UV divergences are absorbed into LECs accompanying the $NNNN\pi$ amplitudes \mathcal{A}_{CT} and \mathcal{B}_{CT} , given in the last row in Fig.3. By renormalization, the singular parts of the loop amplitudes are eliminated and we are left with the renormalized finite LECs, $\mathcal{A}_{\text{CT}}^r$ and $\mathcal{B}_{\text{CT}}^r$, which will be added to the finite parts of the loop amplitudes. Based on the renormalization scheme of Ref.,²⁶ the finite parts of the pion-nucleon loops are

$$\begin{aligned}
 \tilde{\mathcal{A}}_{\text{finite}}(\mu) &= -\frac{g_A^3}{2} \left[1 - \log \left(\frac{m_\pi^2}{\mu^2} \right) - 2F_1 \left(\frac{-\vec{p}^2}{m_\pi^2} \right) \right], \quad (30) \\
 \tilde{\mathcal{B}}_{\text{finite}}(\mu) &= -\frac{g_A}{6} \left[-\frac{1}{2} \left(\frac{19}{4} g_A^2 - 1 \right) \left(1 - \log \left(\frac{m_\pi^2}{\mu^2} \right) - 2F_1 \left(\frac{-\vec{p}^2}{m_\pi^2} \right) \right) + \frac{5}{3} g_A^2 - \frac{1}{6} \right],
 \end{aligned}$$

where μ is the scale and the function F_1 is defined in the appendix, Eq. (A.3). In general, as discussed in Ref.²⁶ the finite parts of the loops $\tilde{\mathcal{A}}_{\text{finite}}$ and $\tilde{\mathcal{B}}_{\text{finite}}$ can be further decomposed into the *short*- and *long*-range parts. The former one is just a (renormalization scheme dependent) constant to which all terms in Eq. (30) except F_1 contribute. On the other hand, the long-range part of the loops is scheme-independent. By expanding the function $F_1(-\vec{p}^2/m_\pi^2)$, Eq. (A.3), which includes the only long-range piece in Eq. (30), in the kinematical regime relevant for pion production, i.e. $(\vec{p}^2/m_\pi^2) \gg 1$, one obtains up-to-and-including terms at N²LO

$$\begin{aligned}\tilde{\mathcal{A}}_{\text{finite}}^{\text{long}} &= -\frac{g_A^3}{2} \log\left(\frac{m_\pi^2}{\vec{p}^2}\right) + \mathcal{O}\left(\frac{m_\pi^2}{\vec{p}^2}\right), \\ \tilde{\mathcal{B}}_{\text{finite}}^{\text{long}} &= \frac{g_A}{12} \left(\frac{19}{4}g_A^2 - 1\right) \log\left(\frac{m_\pi^2}{\vec{p}^2}\right) + \mathcal{O}\left(\frac{m_\pi^2}{\vec{p}^2}\right).\end{aligned}\quad (31)$$

A numerical evaluation of these terms using $g_A = 1.27$ gives $\tilde{\mathcal{A}}_{\text{finite}}^{\text{long}} = 2.2$ and $\tilde{\mathcal{B}}_{\text{finite}}^{\text{long}} = -1.5$. In Ref.²⁶ these numbers were compared with those from the most important phenomenological contributions which were proposed in Refs.³⁻⁶ in order to resolve the discrepancy between phenomenological calculations and experimental data. Using the resonance saturation mechanism, shown to be applicable for the two-nucleon system in Ref.⁹⁵ and proposed for pion-production in NN collisions in Refs.³⁻⁶ to estimate the LECs \tilde{e}_1 and \tilde{e}_2 in Eq. (10), the values for the two finite renormalized $NNNN\pi$ amplitudes $\tilde{\mathcal{A}}_{\text{CT}}^r$ and $\tilde{\mathcal{B}}_{\text{CT}}^r$ are obtained: $\tilde{\mathcal{A}}_{\text{CT}}^r \simeq 2$ and $\tilde{\mathcal{B}}_{\text{CT}}^r \simeq 1$ in the same units. Based on this, it was concluded in²⁶ that the scheme-independent long-range contributions of pion-nucleon loops are comparable in size with the contribution needed to bring theory in agreement with experiment. Hence, the importance of the long-range N²LO pion loop effects, not included in the previous studies, raises serious doubts on the physics interpretation behind the phenomenologically successful models of Refs.³⁻⁶

In the standard ChPT counting scheme the tree-level diagrams will usually be renormalized by including nucleon self-energy pion-loop diagrams as well as vertex loops. However, when we only consider the pion and nucleons fields in the MCS, the loop diagrams which contribute to the renormalization of, e.g., the nucleon mass m_N and the axial coupling constant g_A , do not involve a loop momentum of order $p \sim \sqrt{m_\pi m_N}$. Consequently, these diagrams, driven by a loop momentum $\propto m_\pi$, contribute in the MCS at order N⁴LO which is beyond the level considered. To illustrate the MCS counting of such loop diagrams, we concentrate on the LO rescattering diagram in Fig. 3, which in our naive MCS counting is of order $\sqrt{m_\pi/m_N}$. Consider now pion loops in this diagram at a vertex or on a nucleon line. In standard ChPT counting these pion loops would require a renormalization of the vertex and the nucleon mass. However, these pion loops contain only “small” loop momenta $l \sim m_\pi$, i.e. the loops do not contain any external momenta of order $p \sim \sqrt{m_\pi m_N}$. Therefore, these type of loop diagrams will increase the MCS order by a factor $(m_\pi/m_N)^2$ as shown in, e.g. Ref.,²⁴ Table 11. In other words, at N²LO, we only have to consider the loop diagrams which have already been discussed. We

will return to these considerations in Sec. 4.5 where we include the Δ -resonance in the loops.

4. Delta-resonance induced contributions to s-wave pion production

In the energy region of the pion-production threshold the Δ -resonance is not heavy enough to be parametrized just by πN LECs. In fact, the Δ should be explicitly included in the loops as virtual nucleon excitations in order for the effective theory to properly describe the physics in this energy region. Whereas the mass difference $\delta = m_\Delta - m_N$ is non-zero even in the chiral limit of the theory (when $m_\pi \rightarrow 0$), the physical value of δ , $\delta \approx 300$ MeV, is numerically very close to the “small” scale in the MCS, i.e. the momentum scale $p \sim \sqrt{m_\pi m_N}$. This observation prompted Hanhart and Kaiser²³ to argue that, as a practical consistency in MCS, δ should be counted as p . In this section we will outline the operator structure due to the inclusion of explicit Δ degrees of freedom for the $NN \rightarrow NN\pi$ reaction.

The LECs, c_2 , c_3 and c_4 , which are determined from pion-nucleon data, have to be re-evaluated when the Δ is explicitly included. Consequently, one obtains the LECs in which the Δ contribution is subtracted. These residual LECs enter the calculation of the pion-production operator derived in Sec. 3.1, see Eqs.(23) and (24). When the Δ -field is explicitly included in the Lagrangian, the parameter $\delta \sim p$ will appear in loops containing the Δ propagator and the resulting loop four-momentum will naturally be of the order of p , i.e., these loop diagrams will then contribute at NLO and N²LO in the MCS.

In the MCS with a Δ explicitly included, loop diagrams with topologies different from those discussed in previous sections have to be considered. Some of these additional loop diagrams containing a Δ propagator will renormalize LO diagram vertices as well as the nucleon wave function. This is in contrast to the loop diagrams with only nucleon and pion propagators, which contribute to renormalization of the vertices at N⁴LO only, as argued in Ref.²⁶ This is a higher order contribution and is not considered any further. These considerations will be explained in detail in the next subsections, where we also will outline the regularization of the UV-divergence of this effective field theory containing explicit Δ degrees of freedom.

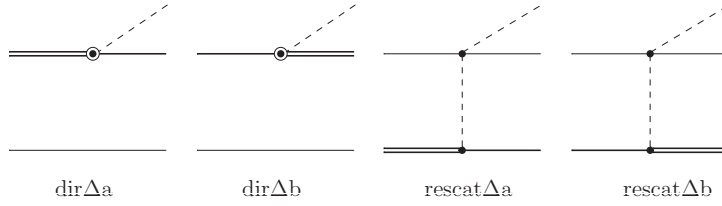


Fig. 8. Single baryon and rescattering diagrams with Δ contributions which appear as building blocks in the construction of the pion-production amplitude. In the last two rescattering diagrams only the on-shell part of the πN vertex ($2m_\pi$) from Eq. (25) should be included.

4.1. The Lagrangian with Δ interactions

The effective Δ Lagrangian^{96,97} written in the sigma-gauge is the basis for the evaluation of the operator contributions

$$\begin{aligned}
 \mathcal{L}_{\pi N \Delta} = & -\Psi_\Delta^\dagger (i v \cdot \partial - \delta) \Psi_\Delta + \frac{g_1}{f_\pi} \Psi_\Delta^\dagger \mathbb{S}^{\dagger \mu} S^\beta \mathbb{S}_\mu T_i \boldsymbol{\tau} \cdot \partial_\beta \boldsymbol{\pi} T_i \Psi_\Delta \\
 & - \frac{1}{4f_\pi^2} \Psi_\Delta^\dagger \left[(\dot{\boldsymbol{\pi}} \times \boldsymbol{\pi}) \cdot T_i^\dagger \boldsymbol{\tau} T_i + 2i \left((\mathbf{T}^\dagger \cdot \boldsymbol{\pi})(\mathbf{T} \cdot \dot{\boldsymbol{\pi}}) - (\mathbf{T}^\dagger \cdot \dot{\boldsymbol{\pi}})(\mathbf{T} \cdot \boldsymbol{\pi}) \right) \right] \Psi_\Delta \\
 & - \frac{h_A}{2f_\pi} \left[N^\dagger \mathbf{T} \cdot \left(\partial^\mu \boldsymbol{\pi} + \frac{1}{2f_\pi^2} \boldsymbol{\pi} (\boldsymbol{\pi} \cdot \partial^\mu \boldsymbol{\pi}) \right) \mathbb{S}_\mu \Psi_\Delta + h.c. \right] \\
 & + \frac{h_A}{2m_N f_\pi} \left[i N^\dagger \mathbf{T} \cdot \dot{\boldsymbol{\pi}} \mathbb{S} \cdot \partial \Psi_\Delta + h.c. \right] + \dots, \tag{32}
 \end{aligned}$$

Here g_1 is the $\pi\Delta\Delta$ coupling constant, h_A is the leading $\pi N\Delta$ coupling constant and \mathbb{S} and \mathbf{T} are the spin and isospin transition matrices, normalized such that

$$\mathbb{S}_\mu \mathbb{S}_\nu^\dagger = g_{\mu\nu} - v_\mu v_\nu - \frac{4}{1-d} S_\mu S_\nu, \quad T_i T_j^\dagger = \frac{1}{3} (2\delta_{ij} - i\epsilon_{ijk} \tau_k), \quad i, j = 1, 2, 3.$$

The value for the $\pi\Delta\Delta$ coupling constant $g_1 = 9/5g_A$ is obtained in the large N_c limit.⁹⁸ An estimate of the $\pi N\Delta$ coupling constant $h_A = 2g_{\pi N\Delta} = 3g_A/\sqrt{2} = 2.7$ is derived from large N_c arguments,⁹⁹ whereas a dispersion-theory analysis gives $h_A = 2.1$.¹⁰⁰

4.2. Tree-level diagrams with Δ -resonance

Since the NN and $N\Delta$ states are coupled in the NN models^{73,74} which will be used in the hybrid approach to evaluate the initial and final state NN wave functions in $NN \rightarrow NN\pi$, the full pion-production amplitude also obtains contributions from the building blocks containing $N\Delta$ states as shown in Fig. 8. In full analogy to the single nucleon direct diagrams in Fig. 3 and as discussed in Sec. 3.1, the single baryon diagrams shown in Fig. 8 do not contribute to the on-shell pion-production operator but are relevant only when convolved with an $NN - N\Delta$ amplitude either in the initial or in the final state. The explicit expressions for the Δ contributions

to the pion-production operator from the diagrams in Fig.8 are

$$\begin{aligned}
 iM_{\text{Dir}\Delta\text{a}} &= -\frac{g_{\pi N\Delta}}{m_N f_\pi} T_1^a v \cdot q (\mathbb{S}_1 \cdot p_1) \delta(\vec{p}_2 - \vec{p}'_2), \\
 iM_{\text{Dir}\Delta\text{b}} &= -\frac{g_{\pi N\Delta}}{m_N f_\pi} T_1^{\dagger a} v \cdot q (\mathbb{S}_1^\dagger \cdot p'_1) \delta(\vec{p}_2 - \vec{p}'_2), \\
 iM_{\text{Rescat}\Delta\text{a}} &= \frac{g_{\pi N\Delta}}{2f_\pi^3} v \cdot q i \epsilon^{bac} \tau_1^c T_2^b \frac{1}{k_2^2 - m_\pi^2 + i0} (\mathbb{S}_2 \cdot k_2), \\
 iM_{\text{Rescat}\Delta\text{b}} &= \frac{g_{\pi N\Delta}}{2f_\pi^3} v \cdot q i \epsilon^{bac} \tau_1^c T_2^{\dagger b} \frac{1}{k_2^2 - m_\pi^2 + i0} (\mathbb{S}_2^\dagger \cdot k_2), \tag{33}
 \end{aligned}$$

These tree-level pion-production amplitudes with a $N\Delta$ initial or final state can not by definition contribute to the $NN \rightarrow NN\pi$ irreducible production operator. However, the amplitudes in Eq. (33) give nonzero contributions to the full pion-production amplitude when they are inserted as building blocks into those of FSI and ISI diagrams that have $N\Delta$ as an intermediate state as mentioned in Sec. 2.2. The DWBA convolution results in the NLO and N²LO contributions to $NN \rightarrow NN\pi$ from the direct and rescattering diagrams in Fig. 8, respectively. This DWBA-approach was used by Ref.⁶⁴ in the evaluation of these operators for the reaction $pp \rightarrow d\pi^+$.

4.3. Role of the tree-level diagrams with Δ resonance

The effect of the tree-level Δ operators has been studied in the literature using both the phenomenological framework and EFT with quite contradictory conclusions. In a phenomenological study⁶ it was shown that the inclusion of the Δ isobar leads to an enhancement of the total cross section in $pp \rightarrow d\pi^+$ by almost a factor of 3 mainly due to the influence of diagrams "rescat Δ a and b" in Fig.8. This enhancement found in Ref.⁶ was not confirmed in a model calculation by Ref.⁶³ Furthermore, an EFT evaluation¹⁷ of the direct tree-level diagrams found results which differ from the findings of Refs.^{6,63} We notice, however, that the static Δ propagator was used in Ref.¹⁷ which led to the large model dependence of the results. A similar problem with the use of the static Δ propagator in πd scattering was investigated in Ref.¹¹ with the result that the recoil in the Δ propagator is needed in the $N\Delta$ intermediate states to obtain scheme independent results. To illustrate the difficulties with the evaluation of the diagrams in Fig. 8 we focus on the πN rescattering diagrams with the Δ , diagrams "rescat Δ a and b" in the figure. These rescattering diagrams contain the energy dependent WT vertex, and thus the method developed in the previous section, see Eq. (25), can be applied. In particular, the πN rescattering vertices in diagrams "rescat Δ a and b" convoluted with NN wave functions can be divided into two parts: the first one is an on-shell πN rescattering vertex ($\propto 2m_\pi$) and the second one cancels the nucleon propagators adjacent to this vertex yielding irreducible loop diagrams (cf. diagrams Δ Box a and b in Fig. 10). Refs.^{23,27} showed that these irreducible contributions take part in a cancellation with other loop diagrams, as will be discussed in the next subsection. Thus, the only contribution

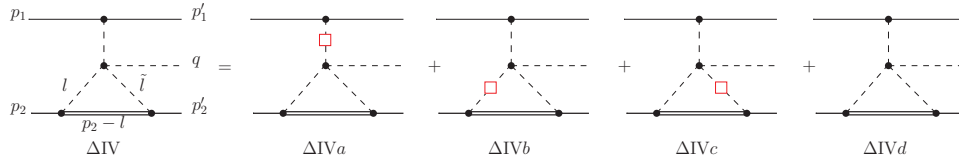


Fig. 9. An example of the loop diagrams with the explicit Δ . Double lines denote the Δ propagator, remaining notation is as in Fig. 3. The red squares on the pion propagators indicate that for each diagram, the pion propagator cancels parts of the four-pion vertex expression, as explained in the text.

of the tree-level diagrams up to N²LO originates from the direct pion production and the rescattering process with the on-shell πN rescattering vertex, shown in Fig. 8. The hybrid EFT calculation of Ref.⁶⁴ where the Δ propagator was treated similar to the nucleon one (see Sec.2.4), revealed that each of these diagrams yields about 10-15% corrections to the transition amplitude discussed in Sec.3.4 but they enter with opposite signs. While the direct diagrams increase the cross section in line with the finding of Ref.⁶³ the rescattering diagrams lead to a reduction by almost the same amount. This significant cancellation between different diagrams resulted in a very small net contribution from the tree-level diagrams in Fig. 8 to $pp \rightarrow d\pi^+$ (see Fig. 7). The calculation in Ref.⁶³ was done with the CCF⁷³ and the Hannover¹⁰¹ coupled-channel NN models, and the pattern of cancellation was the same for both models although the individual contributions were slightly different.

4.4. Loop diagrams with Δ propagators

In order to illustrate the power counting of the loop diagrams with Δ in MCS we, as an example, discuss in detail the power counting for diagram type ΔIV in Fig. 9. First, note that the four-pion vertex of the leftmost diagram in Fig. 9 can be rewritten as a linear combination of the three pion propagators adjacent to this vertex plus a residual vertex term^{vi} (see, e.g., appendix A.4 in Ref.²⁶). This results in a separation of diagram ΔIV in four parts: for the diagrams ΔIV a-c the pion propagator cancels corresponding parts of the four-pion vertex, as indicated by the red square in Fig. 9, while diagram ΔIV d appears as the residual part in this separation. To estimate the magnitudes of the amplitudes of these diagrams, we first remind the reader that for the reaction $NN \rightarrow NN\pi$ close to threshold the initial nucleons have four-momentum $p_1^\mu = (m_\pi/2, \vec{p})$ and $p_2^\mu = (m_\pi/2, -\vec{p})$ with $p = |\vec{p}| \approx \sqrt{m_\pi m_N}$ (see Fig. 9 for the notation). Secondly, we note that the loop diagrams with the explicit Δ all involve the Δ - N mass difference $\delta \sim p$ in the Δ propagator. The power counting for the loop diagrams also requires the inclusion of the integral measure $l^4/(4\pi)^2$ where all components of the loop four-momentum

^{vi} While the first three terms depend explicitly on the parameterisation (or “gauge”) of the pion field, the residual term is pion-gauge independent.⁸⁰

l are of order $\delta \sim p$, i.e. $v \cdot l \sim |\vec{l}| \sim p$. In addition to this integral measure, in the diagrams $\Delta\text{IVa-c}$ one has to account for one Δ propagator ($\sim 1/(v \cdot l) \sim 1/p$), three pion propagators ($\sim 1/(p^2)^3$), the 4π vertex ($\sim p^2/f_\pi^2$) and two $\pi N\Delta$ and one πNN vertices ($\sim (p/f_\pi)^3$). Combining all these factors and using $4\pi f_\pi \sim m_N$, one obtains the order estimate for this diagram as follows

$$\frac{p^4}{(4\pi)^2} \frac{1}{p} \frac{1}{(p^2)^3} \frac{p^2}{f_\pi^2} \left(\frac{p}{f_\pi}\right)^3 \sim \frac{1}{f_\pi^3} \frac{p^2}{m_N^2} \simeq \frac{1}{f_\pi^3} \chi_{\text{MCS}}^2. \quad (34)$$

These dimensional arguments give the above order estimate of diagrams $\Delta\text{IVa-c}$ and should be compared with the estimate of a LO rescattering diagram for the $NN \rightarrow NN\pi$ reaction given by Eq. (17). We find that the diagrams $\Delta\text{IVa-c}$ in Fig. 9 start to contribute at NLO. Meanwhile, the pion-gauge independent diagram ΔIVd starts to contribute at N²LO only. The reason is that the residual pion-gauge independent four- π vertex is suppressed compared to the leading four- π vertex contributions. Notice that the N²LO expression for diagram ΔIV contains more terms than the corresponding pure pion-nucleon diagram IV. As explained in Appendix A.4 in Ref.²⁶ the contributions similar to type ΔIVb and ΔIVc are strongly suppressed in the pion-nucleon case.

Fig. 10 shows the loop diagrams involving Δ which contribute to s-wave pion production up to N²LO. In the first row of Fig. 10, we have the two-pion exchange diagrams with topologies completely analogous to the pion-nucleon g_A^3 -graphs in the second row in Fig. 3. The two-pion exchange diagrams in the first row of Fig. 10 start individually to contribute at NLO. However, these NLO diagrams cancel completely in the sum for the same reason as do the NLO pion-nucleon ones in Fig. 3. In fact, it is relatively straightforward to show that, on the operator level, this cancellation of the NLO level diagrams is independent of whether we have a nucleon or a Δ propagator on the lower baryon line in Figs. 3 and 10. Consequently, in MCS there are no contributions from these two-pion exchange diagrams at NLO. Moreover, the N²LO contributions of the diagrams in the first row in Fig. 10 also show cancellations analogous to the purely pion-nucleon case as shown in Ref.²⁷ It should be mentioned that the diagrams in the first row of Fig. 10 also obtain corrections from higher-order vertices $\propto 1/m_N$ and c_i (Delta-subtracted) from $\mathcal{L}_{\pi N}^{(2)}$. Those corrections, however, again cancel completely at N²LO in a full analogy to the cancellations among the corresponding pion-nucleon loop contributions, see Ref.²⁶ and the discussion in Sec.3.5. As shown in Ref.,²⁷ the sum of the N²LO diagrams in the first row of Fig. 10 receives contributions only from diagrams ΔIIIa and ΔIIIb , where the Weinberg-Tomozawa πN vertices are on-shell, and from the pion-gauge independent ΔIVd shown in Fig.9.

In addition, there are several new loop diagrams containing Δ propagators where one effectively has a pion being exchanged between the two nucleons, see diagrams $\Delta\text{V}-\Delta\text{XI}$ in Fig. 10. Surprisingly, diagrams $\Delta\text{V}-\Delta\text{IX}$ in rows two and three undergo significant cancellations as detailed in Ref.,²⁷ and only the part of the diagram ΔV , that is proportional to the on-shell $\pi\Delta - \pi\Delta$ vertex (equal to $2m_\pi$), remains. The

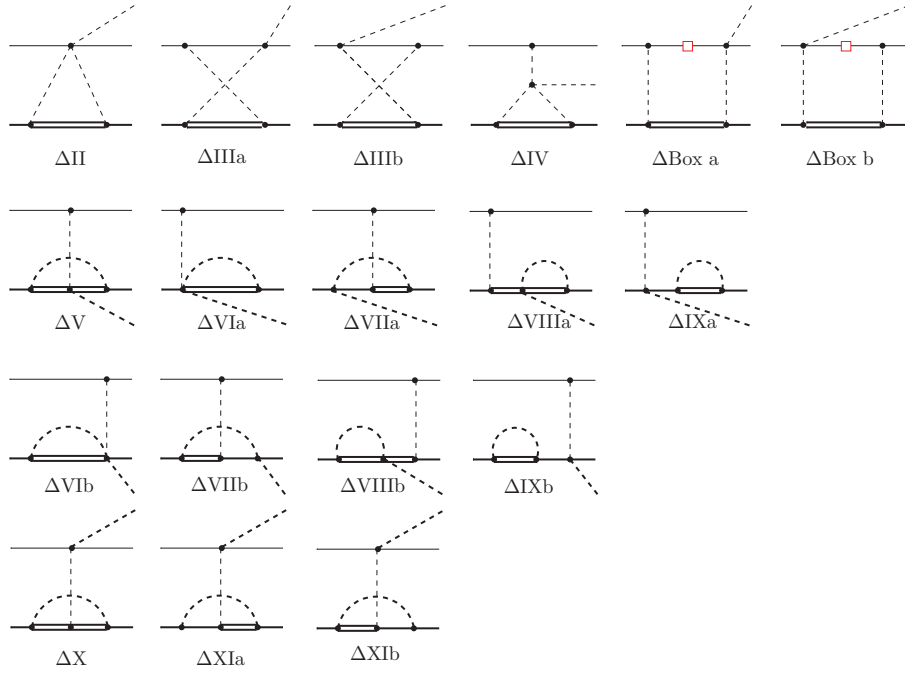


Fig. 10. Loop diagrams with the Δ degree of freedom contributing to s-wave pion production up to N^2LO . Double lines denote the Δ propagator, remaining notation is as in Fig. 3. Again, the red square on the nucleon propagator in the two box diagrams indicates that the corresponding nucleon propagator cancels parts of the Weinberg–Tomozawa πN rescattering vertex leading to an irreducible contribution of the box diagrams as discussed in Sec. 3.1.

three one-pion-exchange Δ loop diagrams in the last row of Fig. 10, which have to be taken into account at N^2LO , contribute only to the renormalization of g_A at N^2LO , see the next subsection where we will discuss the renormalization of these Δ loops and give the N^2LO transition amplitude operator as obtained in Ref.²⁷

4.5. Regularization of UV singularities and renormalization

The loop diagrams with explicit Δ are UV-divergent at N^2LO . Contrary to the pion-nucleon case discussed in Sec. 3.6, these Δ loop diagrams require that the couplings and masses appearing in the Lagrangian are renormalized. In particular, up to N^2LO in the MCS there are two relevant renormalization corrections: one involves the πN coupling constant g_A and the other the nucleon wave function renormalization factor Z_N . These renormalization corrections of order $\delta^2/\Lambda_\chi^2 \sim \chi_{MCS}^2$ were evaluated in Ref.^{67,68,102} for πN scattering with explicit Δ in the loop using dimensional regularization. These results were confirmed in Ref.²⁷ In order to calculate the production operator up to NLO it suffices to use $Z_N = 1$ and $\hat{g}_A = g_A$. However, in a theory with explicit Δ degrees of freedom, renormalization corrections to the tree-

level diagrams at LO in Fig. 3 generate N²LO contributions. At N²LO, the nucleon fields (N) in the Lagrangian must be renormalized, i.e., $N \rightarrow N\sqrt{Z}$, and, similarly, for the axial constant $\dot{g}_A \rightarrow g_A$ (i.e., \dot{g}_A deviates from the physical value), due to the loop corrections with explicit Δ . The explicit evaluations of the diagrams in Fig. 10 reveal that the contributions of diagrams ΔX and ΔXI reproduce the N²LO correction to the tree-level rescattering diagram in Fig. 3 due to renormalization of \dot{g}_A and Z_N , meaning that at N²LO there is no genuine contributions of diagrams ΔX and ΔXI in MCS.

As outlined in Ref.²⁷ the N²LO contribution from Z_N to the WT vertex is included in the rescattering operator together with the residual contributions of the diagrams ΔIII , ΔIV and ΔV and gives non-vanishing correction at N²LO. The individual non-vanishing contributions of the Δ loop diagrams in Fig. 10 are expressed in terms of four scalar integrals, $J_{\pi\Delta}$, $I_{\pi\pi}$, $J_{\pi\pi\Delta}$, and $J_{\pi\pi N\Delta}$, which are defined in the appendix. The two integrals $J_{\pi\Delta}$ and $I_{\pi\pi}$ contain UV singularities from the Δ loop diagrams which as shown in Ref.²⁷ are absorbed by the $(NN)^2\pi$ five-point contact terms.

Before we present the final contribution for s-wave pion production from Δ loop diagrams, there is one issue which deserves attention. In a theory containing a “heavy” resonance Δ , it is not sufficient to require just the regularization of the UV divergent terms with the corresponding LECs. The integrals $J_{\pi\Delta}$ and $I_{\pi\pi}$, which are multiplied by the factor δ^2/k_1^2 , pose an additional problem as discussed in Ref.²⁷ Such polynomial behavior would give divergences if the Δ resonance was infinitely heavy, i.e., if $\delta \rightarrow \infty$. Therefore, to find the most natural finite values of the renormalized LECs, the explicit decoupling renormalization scheme was introduced.^{102,103} In such a scheme, the finite parts of LECs are chosen such that the renormalized contribution from diagrams with Δ loops vanish in the limit $\delta \rightarrow \infty$. Ref.²⁷ showed that the following combinations of loop integrals (up-to-and-including N²LO in MCS) do vanish when $\delta \rightarrow \infty$:

$$k_1^2 J_{\pi\pi N\Delta}, \quad (35)$$

$$\left(I_{\pi\pi} + \frac{1}{2} \frac{J_{\pi\Delta}}{\delta} + \Delta J_{\pi\pi\Delta} + \frac{2}{(4\pi)^2} \right), \quad (36)$$

$$\frac{\delta^2}{k_1^2} \left(I_{\pi\pi} + \frac{1}{2} \frac{J_{\pi\Delta}}{\delta} + \Delta J_{\pi\pi\Delta} + \frac{2}{(4\pi)^2} \right) - \frac{1}{12} \left(I_{\pi\pi} + \frac{1}{2} \frac{J_{\pi\Delta}}{\delta} + \frac{1}{3} \frac{2}{(4\pi)^2} \right). \quad (37)$$

Further, Ref.²⁷ found that the combination of the two integrals $J_{\pi\Delta}$ and $I_{\pi\pi}$ in Eqs. (35)-(37), $I_{\pi\pi} + \frac{1}{2\delta} J_{\pi\Delta}$, cancels the UV divergences of the individual integrals, as shown in Eq.(A.11) in the Appendix, which means that the expressions in Eqs. (35)-(37) are all UV finite and vanish when $\delta \rightarrow \infty$.

The fully renormalized, finite N²LO Δ loops contribution to the s-wave pion

production amplitude derived in Ref.²⁷ is

$$\begin{aligned}
 iM_{\Delta\text{-loops}}^{\text{N}^2\text{LO}} &= \frac{g_A g_{\pi N \Delta}^2}{f_\pi^5} v \cdot q \tau_+^a (i\varepsilon^{\alpha\mu\nu\beta} v_\alpha k_{1\mu} S_{1\nu} S_{2\beta}) \\
 &\times \left\{ \frac{2}{9} \left(I_{\pi\pi} + \frac{1}{2} \frac{J_{\pi\Delta}}{\delta} + \Delta J_{\pi\pi\Delta} + \frac{2}{(4\pi)^2} \right) + \frac{1}{18} k_1^2 J_{\pi\pi N\Delta} \right\} \\
 &+ \frac{g_A g_{\pi N \Delta}^2}{f_\pi^5} v \cdot q \tau_\times (S_1 + S_2) \cdot k_1 \\
 &\times \left\{ \frac{5}{9} \left(I_{\pi\pi} + \frac{1}{2} \frac{J_{\pi\Delta}}{\delta} + \Delta J_{\pi\pi\Delta} + \frac{2}{(4\pi)^2} \right) + \frac{1}{18} k_1^2 J_{\pi\pi N\Delta} \right. \\
 &\left. + \frac{8}{9} \frac{\delta^2}{k_1^2} \left(I_{\pi\pi} + \frac{1}{2} \frac{J_{\pi\Delta}}{\delta} + \Delta J_{\pi\pi\Delta} + \frac{2}{(4\pi)^2} \right) - \frac{2}{27} \left(I_{\pi\pi} + \frac{1}{2} \frac{J_{\pi\Delta}}{\delta} + \frac{1}{3} \frac{2}{(4\pi)^2} \right) \right\}. \tag{38}
 \end{aligned}$$

This expression should be added to the finite s-wave transition operators presented in Sec. 3.6.

4.6. Comparison of the Δ and pion-nucleon loop contributions

In Sec. 3.6 (see also discussion in Ref.²⁶) we argued that the long-range scheme-independent part of the pion-nucleon loops at N²LO is sizable and could resolve the problem with the description of pion production data in the neutral channel, $pp \rightarrow pp\pi^0$. The question to be answered in this subsection is what happens when we add the long-ranged Δ contribution. First, note that the spin-isospin structure of the Δ -loops in Eq. (38) is exactly the same as for the pion-nucleon case in Eq. (27), as required by the threshold decomposition of the pion-production amplitude, Eq.(28). Meanwhile, the dimensionless integrals are different and the coefficients in front of the spin-isospin operators also differ. Ref.²⁷ compared the resultant amplitudes from the nucleon and Δ loop diagrams for NN relative distances relevant for pion production, i.e. for $r \sim 1/p \simeq 1/\sqrt{m_\pi m_N}$. In Ref.²⁷ the long-range scheme-independent contributions of the Δ -loop expressions are separated from the short-range ones by making a Fourier transformation of the expressions in Eqs. (27) and (38). Specifically, Ref.²⁷ Fourier transformed the integral combinations in the curly brackets in Eq. (38) (multiplied by $g_A g_{\pi N \Delta}^2$) corresponding to τ_+ (final NN spin-singlet) and τ_\times (final NN spin-triplet) channels. Ref.²⁷ compared the resulting Fourier transformed Δ loop amplitudes with the Fourier transformed amplitudes of the corresponding pion-nucleon contribution given in Eq. (27), namely $-2g_A^3 I_{\pi\pi}$ and $(-19/24g_A^3 + 1/6g_A) I_{\pi\pi}$. It was found that in the spin-singlet NN channel, the long-range part of the Δ contribution constitutes less than 20% compared to the pion-nucleon loop amplitude, whereas in the spin-triplet NN channel the Δ -loop contribution to the s-wave pion-production amplitude is almost of the same magnitude (roughly 60%). The conclusion of Ref.²⁷ is as follows: the importance of the pion-nucleon loops in explaining $pp \rightarrow pp\pi^0$ appears to be only slightly modified by the Δ loop contributions and the N²LO loop contributions are significant,

whereas for the final spin-triplet NN channel the net N²LO amplitude from the nucleon and Δ loop diagrams is considerably reduced in importance compared to the spin-singlet channel. The pattern that emerged from the N²LO loop diagrams is therefore exactly what is necessary to quantitatively describe the data on both $pp \rightarrow pp\pi^0$ and $pp \rightarrow d\pi^+$ near threshold. For the former reaction there persists a huge discrepancy between data and the chiral perturbation theory calculation to NLO, while the latter already at NLO describes the experimental data quite well.²⁵ As discussed, for the $pp \rightarrow pp\pi^0$ reaction the LO diagrams are suppressed both kinematically as well as dynamically,²⁴ the net N²LO loop diagram results presented provide a dynamical understanding of why it was so much harder to understand phenomenologically the $pp \rightarrow pp\pi^0$ reaction compared to the other channels.

5. p-wave pion production

In this section we will first present evidence that for pion p-wave production the perturbative series, which is ordered according to the MCS, converges as expected. Then we will focus on a specific feature of chiral symmetry which connects the $NN \rightarrow NN\pi$ reactions to different reactions at low energies as discussed in the introduction, Sec. 1. In other words, we will discuss how the reaction $NN \rightarrow NN\pi$ can be used to pin down the $(NN)^2\pi$ LEC, d , which plays an important role connecting many very different few-nucleon reactions as illustrated in Fig. 1. As follows from Eqs. (3)-(4) the contact operator associated with the LEC d is proportional to the pion derivative. Therefore, it should contribute to the production of p-wave pions in $NN \rightarrow NN\pi$ while connecting S-wave nucleons. This implies that for all partial waves where there are NN P-waves in the final state, the chiral perturbation theory calculation is parameter free up to N²LO.

In contrast to pion s-wave production, the p-wave pion-production operator up to N²LO in MCS consists of tree level graphs only, shown in Fig. 11. In particular, the only operator at LO corresponds to the direct emission of a pion from one of the nucleons. The estimate for this operator based on the naive dimensional analysis outlined in Sec. 2.3 gives $|\vec{q}|/(f_\pi^3 m_\pi)$, where \vec{q} is the pion three-momentum. The pion can also be produced through the de-excitation of a Δ resonance. However, since the Δ propagator contains the mass-difference $\delta \sim p$, it is suppressed by one order of χ_{MCS} as compared to the nucleon one, and the corresponding diagram starts to contribute at NLO. To this order the production operator does not involve any free parameters. All N²LO diagrams in the MCS have tree-level topologies and include pion rescattering operators with $\pi\pi NN$ vertices from $\mathcal{L}_{\pi N}^{(1)}$ of Eq. (6) and $\mathcal{L}_{\pi N}^{(2)}$ of Eq. (7), and recoil correction to the πNN vertex at LO, and finally the contact operator with the associated LEC d , all shown in Fig. 11.

In order to demonstrate the rate of convergence of the series defined within the MCS, we will concentrate on the evaluation of the spin cross section ${}^3\sigma_1$ for $pp \rightarrow pp\pi^0$. This observable is a linear combination of the reactions total cross section and the double polarization observables $\Delta\sigma_T$ and $\Delta\sigma_L$ tailored such that

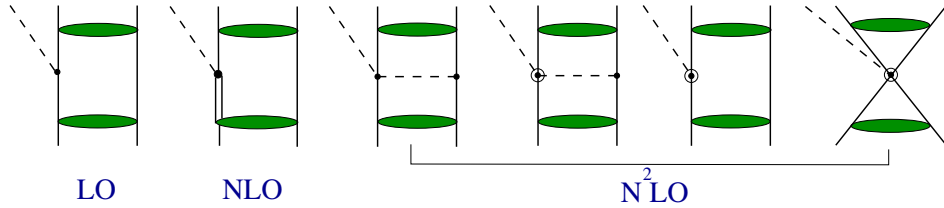


Fig. 11. Diagrams that contribute to p-wave pion production up to N^2LO in the MCS where the shaded ovals indicate initial and final NN state interactions.

only the pp spin 1 with spin projection +1 in the initial state contributes. The measurement and detailed discussion of this observable can be found in Ref.¹⁰⁴ The spin-1 cross section ${}^3\sigma_1(pp \rightarrow pp\pi^0)$ appears to provide a test of the convergence of the theory up to N^2LO . The reason is that the unknown contact term d does not contribute to ${}^3\sigma_1(pp \rightarrow pp\pi^0)$ as pointed out in Ref.^{22,24} since, due to selection rules, a p-wave pion can only be produced in combination with the final NN -pair in at least a P-wave. The lowest final state partial waves contributing in the final state are pp P-waves together with pion p-waves and the pp S-wave with a pion d-wave. A comparison of the results of Ref.²² with the data is given in Fig. 12 as a function of the variable η , which here equals the maximum pion momentum allowed in units of the pion mass. Note that for this reaction a value of $\eta = 0.9$ equals an excess energy $Q = 50.5$ MeV, which is quite large. The dashed line in Fig. 12 is the result of leading and next-to-leading order, namely the nucleon and the Δ direct production terms, the first two diagrams of Fig. 11 (in Ref.²² both counted as leading order), while the solid line contains the result at N^2LO providing an excellent agreement with data. In the calculation of Ref.²² pion d-waves were neglected. This is not necessarily in disagreement with the discussion in Sec. 6, where it is argued that pion d-waves are important for such large excess energy: the observables discussed in that section are defined with the final NN energy limited to very small values at the same time maximizing the pion momentum and therefore the pion d-waves. In contrast to the restricted NN final energy selection presented in Sec. 6, the observable ${}^3\sigma_1$ is fully integrated with respect to the final NN energies and it is therefore expected that the final NN P-waves together with the pion p-wave (Pp final state) become dominant. In order to provide further evidence, we refer to the experimental analysis of $pp \rightarrow pp\pi^0$ in Ref.¹⁰⁵ where in Table 6 it is shown that the Pp final state contribution to the total cross section completely dominates over Sd final state at the energy of interest. We conclude from Fig. 12 that, at least for this spin observable, the perturbative MCS expansion converges nicely and is in agreement with experiment.

In the second part of this section we will demonstrate how the strength of the contact operator d in Fig. 11 could be extracted from experimental data. There are only two reaction channels with NN S-waves in both the final and the initial state where this N^2LO contact interaction can contribute. One corresponds to the

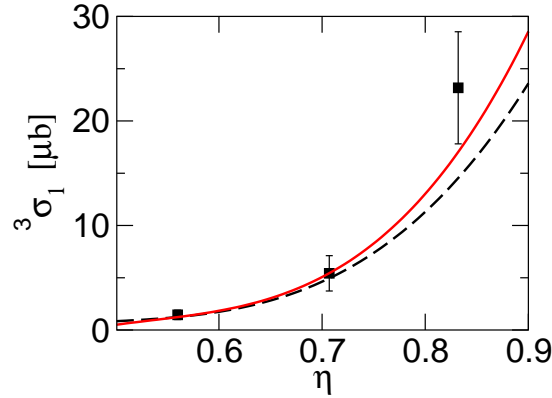


Fig. 12. Results for the double polarization observable ${}^3\sigma_1$ versus η ($\eta = |\vec{q}|/m_\pi$ in the center-of-mass system) as presented in Ref.²² The dashed line denotes the result at leading and next-to-leading order, while the solid line shows the result at N²LO. For this calculation a value of $c_3 = -2.95 \text{ GeV}^{-1}$ was used. The data are from Refs.¹⁰⁴

case with the spin-triplet S-wave NN final state interaction (FSI), which as seen in Table 1 is realized in the $pp \rightarrow pn\pi^+$ and $pp \rightarrow d\pi^+$ reactions, and the other goes with the spin-singlet NN FSI in an S-wave, which appears in $pn \rightarrow pp\pi^-$. In general, when we restrict the final two nucleons to be in S-wave, the relevant partial waves for production of p-wave pions are: ${}^1S_0 \rightarrow {}^3S_1p$ and ${}^1D_2 \rightarrow {}^3S_1p$ for π^+ production and ${}^3S_1 \rightarrow {}^1S_0p$ and ${}^3D_1 \rightarrow {}^1S_0p$ for producing a π^- , as can be read off from Table 1. This imposed limitation reflects recent $NN \rightarrow NN\pi$ experiments, which will be presented in the next section, where the final two nucleons relative energy was below 3 MeV.

The first extraction of the value of LEC d from $NN \rightarrow NN\pi$ was performed in Ref.²² where the EFT calculation was confronted with the results of the partial wave analysis (PWA) of the experimental data in the channel $pp \rightarrow pn\pi^+$.¹⁰⁶ An attempt to connect the primary solar fusion reaction, $pp \rightarrow de^+\nu$, and $pp \rightarrow pn\pi^+$ through the LEC d was done in Ref.¹⁰⁷ with the result that no simultaneous solution is possible. However, the results of Ref.¹⁰⁷ were compared to the results of the PWA of Ref.¹⁰⁶ which turned out to be incorrect, as pointed out in Ref.⁶⁵ Specifically, the PWA needed the contribution of the spin-singlet pn -state and in Ref.¹⁰⁶ this contribution was extracted from $pp \rightarrow pp\pi^0$ data. Unfortunately, in Ref.¹⁰⁶ this contribution was not corrected for the significant difference between the pp and pn final state interactions in S-wave. In Ref.⁶⁵ the LEC d was therefore adjusted to reproduce the differential cross section and analyzing power in $pp \rightarrow pn\pi^+$ directly. Flammang *et al.*¹⁰⁶ parametrized their measured differential cross section for $pp \rightarrow pn\pi^+$ as

$$\frac{d\sigma}{d\Omega} = A_0 + A_1 \cos\theta + A_2 P_2(\cos\theta) \quad (39)$$

where P_2 is the second Legendre polynomial. Assuming only s- and p-wave pions, Ref.¹⁰⁶ determined that $A_1 \simeq 0$. The results of the calculation in Ref.⁶⁵ for the magnitude A_2 are compared with the experimental values in the left panel of Fig. 13. The problem of the PWA of Ref.¹⁰⁶ is illustrated in the right panel of Fig. 13 where we also show the results of the calculation for the relevant partial wave $^1S_0 \rightarrow ^3S_1p$, denoted below by \tilde{a}_0 . Although the red curve representing the best fit is in agreement with the data presented in Ref.¹⁰⁶ (see left panel in Fig. 6 in Ref.⁶⁵ for details), the partial wave amplitude \tilde{a}_0 extracted from the very same data is not described at all. Note that Ref.¹⁰⁷ stressed that a positive value for \tilde{a}_0 is necessary in order to achieve a result for pion production that is consistent with the ones for the solar fusion rate. This is confirmed by the result of Ref.⁶⁵ based on the data for $pp \rightarrow pn\pi^+$ (cf. red curves in Fig.13).

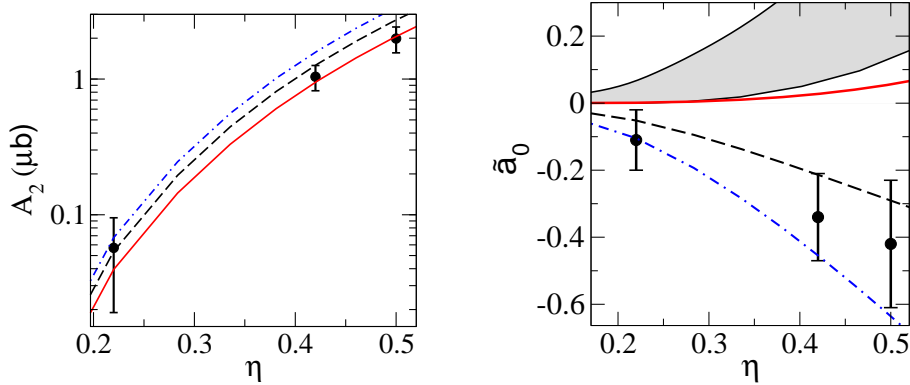


Fig. 13. Results for the magnitude A_2 (left panel) and the partial wave amplitude $\tilde{a}_0(\sqrt{\mu b})$ representing the relevant transition $^1S_0 \rightarrow ^3S_1p$ (right panel) for $pp \rightarrow pn\pi^+$ for different values of the LEC d (in units $1/(f_\pi^2 M_N)$). Shown are $d = 3$ (red solid line), $d = 0$ (black dashed line), and $d = -3$ (blue dot-dashed line). The grey band corresponds to the results of Ref.¹⁰⁷ which incorrectly were interpreted as a failure to connect the solar fusion reaction with pion production, see discussion in the text. The data are from Ref.¹⁰⁶

The purpose of the study in Ref.⁶⁵ was , however, more ambitious than just to reanalyse the data in $pp \rightarrow pn\pi^+$. The idea was to perform a combined analysis of all p-wave pion-production amplitudes contributing to the three different channels, namely $pn \rightarrow pp\pi^-$, $pp \rightarrow d\pi^+$ and $pp \rightarrow pn\pi^+$ [To properly analyze these reactions near threshold the pion s-wave amplitudes are needed. In Ref.⁶⁵ the pion s-wave amplitudes were taken from α , Eq. (26), measured in Ref.⁹⁰ and from the measured $pp \rightarrow pp\pi^0$ total cross section close to threshold¹⁰⁸]. This should provide a non-trivial test of the approach since even in the different channels of the production process, the contact term connects NN wave functions in very different kinematic regimes. For the first channel the p-wave pion is produced along with the slowly

moving protons in the 1S_0 final state whereas for the other two channels the initial 1S_0 pp state is to be evaluated at the relatively large initial momentum. Fig. 14

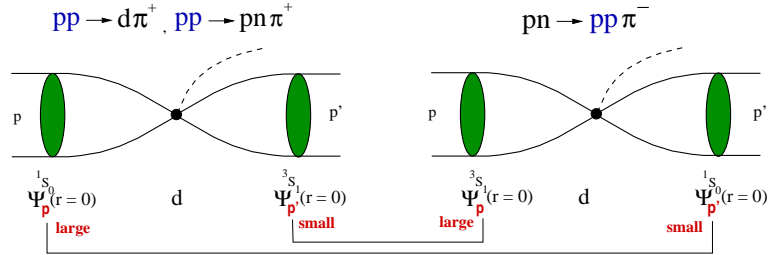


Fig. 14. Illustration of the contribution of the LEC d , which only appears when we have initial and final NN S-wave states, for different $NN \rightarrow NN\pi$ channels. The labels "small" and "large" indicate that the NN wave functions in the same partial wave contribute to different production channels in different kinematic regimes.

illustrates that the contribution of the contact operator gets multiplied with the product of the NN wave functions at the origin. Each of these wave functions, in turn, may be represented by the inverse of the corresponding Jost function,¹⁰⁹ which has an energy dependence that is fixed by the on-shell NN data — up to a polynomial with coefficients known to the required order within MCS.

Since the 3S_1 and 3D_1 partial waves are coupled, a rigorous treatment calls for a coupled channel Jost function. In the reasoning below, however, we will neglect this channel coupling. Note that a recent analysis of data found strong evidence that the channel coupling indeed is weak as will be discussed in Sec. 6. In addition, even if the channel coupling were significant it would not change, the general line of reasoning to be presented. The NN wave functions at the origin can be represented as an integral over the relevant partial wave phase shifts δ_{NN} by means of the so-called Omnès function¹¹⁰ (see also the discussion in Ref.¹¹¹)

$$\begin{aligned} \Psi_p(r=0) &= 1 + m_N \int_0^\infty d^3p' \frac{T(p', p)}{p^2 - p'^2 + i0} \\ &\approx C \exp \left\{ \frac{s}{\pi} \int_{4m_N^2}^\infty \frac{ds'}{s'} \frac{\delta_{NN}(s')}{s' - s(p) + i0} \right\}, \end{aligned} \quad (40)$$

where T is the NN T-matrix, $s(p) \simeq (2m_N + p^2/m_N)^2$ for the nonrelativistic nucleons and C is a model-dependent constant (up to higher order terms in p/m_N). Thus the whole momentum dependence of the contact term contribution is model-independent, since it is fully determined by the product of the two Omnès functions for the 1S_0 and 3S_1 partial waves. The product of the constants C_{1S_0} and C_{3S_1} is absorbed into the strength (the LEC, d) of the contact term for all $NN \rightarrow NN\pi$

channels. In Ref.⁶⁵ the value of the LEC d was varied to achieve qualitatively the

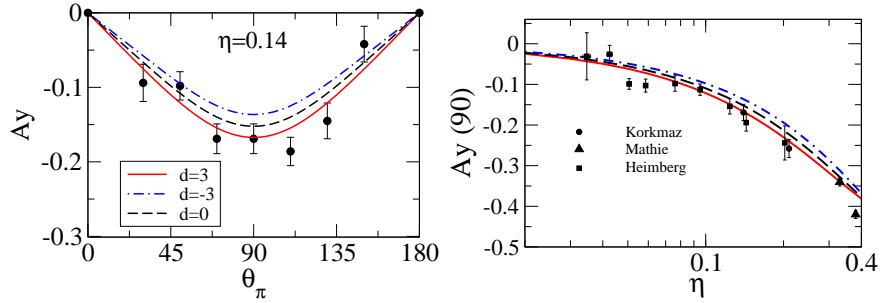


Fig. 15. Results for the analyzing power at $\eta=0.14$ (left panel) and the analyzing power at 90 degrees (right panel) for the reaction $pp \rightarrow d\pi^+$ for different values of the LEC d (in units $1/(f_\pi^2 M_N)$) of the $(NN)^2\pi$ contact operator. Shown are $d = 3$ (red solid line), $d = 0$ (black dashed line), and $d = -3$ (blue dot-dashed line). The data are from Refs.^{87,88,112–114}

best overall description of the differential cross sections and analyzing powers in the different $NN \rightarrow NN\pi$ channels. In particular, Fig.15 shows the results for the analyzing power for the reaction $pp \rightarrow d\pi^+$ ^{vii} for various values of d . It is found that the data prefer a positive value of $d \sim 3/(f_\pi^2 M_N)$ when the CCF model⁷³ of NN interaction is used. A similar pattern can be observed in the reaction $pn \rightarrow pp\pi^-$, as illustrated in Fig. 16. Again the data show a clear preference of the positive value for the LEC d . Thus, the conclusion of Ref.⁶⁵ was that it is possible to qualitatively describe the data available at that time with the same value of the LEC d . However, as discussed in Ref.⁶⁵ in their analysis there are uncertainties which prevent a more definite conclusion. First of all, the relevant $^1S_0 \rightarrow ^3S_1p$ partial wave for p-wave pions is of minor importance to describe the observables in $pp \rightarrow pn\pi^+$ and $pp \rightarrow d\pi^+$. Secondly, at the relevant measured energies the final NN P-waves may already contribute significantly.^{104,105,119} These higher partial waves were ignored in Ref.⁶⁵ Finally, the channel $pn \rightarrow (pp)_S\pi^-$ has been measured at TRIUMF^{116,117} and only those events were selected that correspond to the energy of the proton pair smaller than 1.5 MeV. This guarantees that the pp -system is purely in an S-wave and that no higher NN partial waves in the final state can spoil the analysis. However, the measurement was done with $T_{\text{lab}} = 353$ MeV ($\eta=0.66$), which means that pion d-waves are important. This is confirmed by a very recent measurement at COSY¹²⁰ to be presented in Sec. 6. Note that the pion d-wave production was discarded in the analysis in Ref.⁶⁵

^{vii}Note also that the first data on the transverse correlation coefficient A_{xx} in $pn \rightarrow d\pi^0$ have been measured recently.¹¹⁵

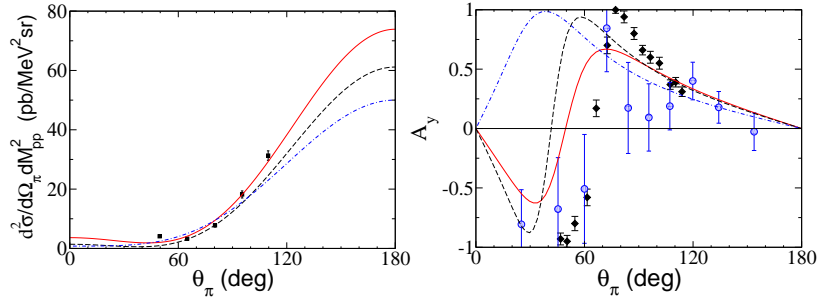


Fig. 16. Results for $d^2\sigma/d\Omega_\pi dM_{pp}^2$ (left panel) and A_y (right panel) for $pn \rightarrow pp(^1S_0)\pi^-$. Shown are the results for $d = 3$ (red solid line), $d = 0$ (black dashed line) and $d = -3$ (blue dot-dashed line). The data are from TRIUMF^{116,117} (black squares) and from PSI¹¹⁸ (blue circles).

6. A combined amplitude analysis of recent measurements of $pn \rightarrow pp\pi^-$ and $pp \rightarrow pp\pi^0$ at COSY

In the framework of the experimental program devoted to the study of pion production at the COSY accelerator in Jülich, the ANKE collaboration has carried out a combined measurement of two reaction channels $pn \rightarrow \{pp\}_s\pi^-$ and $pp \rightarrow \{pp\}_s\pi^0$.^{120,121} Here the $\{pp\}_s$ denotes a proton-proton pair with very low excitation energy, $E_{pp} < 3$ MeV, which is considered to be primarily in the 1S_0 state. The differential cross section and analyzing power for both reactions were measured at $T_{\text{lab}}=353$ MeV, which allows a direct comparison with the earlier TRIUMF data.^{116,117} Whereas the TRIUMF experimental data cover only the pion's central angular region, the ANKE data extend over the whole angular domain and have much higher statistics. In addition, the results of Refs.^{120,121} were extended in Ref.¹²² where the transverse spin-correlation parameters A_{xx} and A_{yy} for the reaction $\vec{n}\vec{p} \rightarrow \{pp\}_s\pi^-$ were extracted from the measurement of $d\vec{p} \rightarrow p_{\text{spec}}\{pp\}_s\pi^-$ at COSY-ANKE at the same energy.

In what follows we summarize the amplitude analysis of these data, further details of these measurements can be found in Refs.^{120–122} In particular, a combined measurement of the differential cross section and analyzing power in $pp \rightarrow \{pp\}_s\pi^0$ allowed the determination of the pion s- and d-wave amplitudes with only minimal theoretical assumptions. Meanwhile, the global partial wave analysis of all data sets yielded several almost equivalent solutions for the p-wave amplitudes with approximately the same value of χ^2 . The only possibility of resolving this ambiguity, as argued in,¹²² would be through an additional measurement of the mixed spin-correlation parameter A_{xz} . In what follows we discuss these issues in some detail.

As long as the final pp -system is purely in an S-wave, the most general structure of the reaction amplitude can be written as

$$M = A \mathbf{S} \cdot \hat{\mathbf{p}} + B \mathbf{S} \cdot \hat{\mathbf{q}}, \quad (41)$$

where $\hat{\mathbf{p}}$ is the unit vector of the initial nucleon momentum in the overall center of

mass system (cms), $\hat{\mathbf{q}}$ is the unit vector of the pion momentum and $\hat{\mathbf{p}} \cdot \hat{\mathbf{q}} = \cos \theta_\pi$. Here $\mathbf{S} = \chi_2^T \frac{\sigma_2}{\sqrt{2}} \sigma \chi_1$ denotes the normalized spin structure corresponding to the initial spin-triplet state and $\chi_{1,2}$ stand for the spinors of the initial nucleons.

It was pointed out in^{120–122} that the data do not support polynomial terms proportional to $\cos^4 \theta_\pi$ and higher. This fact suggests that the partial waves higher than d-waves for the pion can safely be ignored. Thus, up-to-and-including pion d-waves the reaction amplitude for $pn \rightarrow \{pp\}_s \pi^-$ can be written as

$$\begin{aligned}
 M &= M_s^P \mathbf{S} \cdot \hat{\mathbf{p}} + M_p^S \mathbf{S} \cdot \hat{\mathbf{k}} + M_p^D \left((\mathbf{S} \cdot \hat{\mathbf{p}}) (\hat{\mathbf{k}} \cdot \hat{\mathbf{p}}) - \frac{1}{3} \mathbf{S} \cdot \hat{\mathbf{k}} \right) \\
 &+ M_d^P \left((\mathbf{S} \cdot \hat{\mathbf{k}}) (\hat{\mathbf{k}} \cdot \hat{\mathbf{p}}) - \frac{1}{3} \mathbf{S} \cdot \hat{\mathbf{p}} \right) \\
 &+ M_d^F \left((\mathbf{S} \cdot \hat{\mathbf{p}}) (\hat{\mathbf{k}} \cdot \hat{\mathbf{p}})^2 - \frac{2}{5} (\mathbf{S} \cdot \hat{\mathbf{k}}) (\hat{\mathbf{k}} \cdot \hat{\mathbf{p}}) - \frac{1}{5} \mathbf{S} \cdot \hat{\mathbf{p}} \right), \quad (42)
 \end{aligned}$$

where the superscript in the amplitudes M_1^L refers to the partial wave of the initial nucleons and the subscript corresponds to the pion partial wave in the overall cms. Altogether we include in the analysis one s-wave (M_s^P), two p-wave (M_p^S and M_p^D) and two d-wave (M_d^P and M_d^F) amplitudes. These amplitudes correspond to the transitions ${}^3P_0 \rightarrow {}^1S_0s$, ${}^3S_1 \rightarrow {}^1S_0p$, ${}^3D_1 \rightarrow {}^1S_0p$, ${}^3P_2 \rightarrow {}^1S_0d$, and ${}^3F_2 \rightarrow {}^1S_0d$, respectively.

Comparing (42) with (41) one gets the expressions for A and B in terms of the partial wave amplitudes for $pn \rightarrow \{pp\}_s \pi^-$

$$\begin{aligned}
 A &= M_s^P + M_p^D \cos \theta_\pi - \frac{1}{3} M_d^P + M_d^F \left(\cos^2 \theta_\pi - \frac{1}{5} \right), \\
 B &= M_p^S - \frac{1}{3} M_p^D + \left(M_d^P - \frac{2}{5} M_d^F \right) \cos \theta_\pi. \quad (43)
 \end{aligned}$$

For $pp \rightarrow \{pp\}_s \pi^0$ one has to omit the pion p-wave amplitudes in the expression above to arrive at

$$\begin{aligned}
 A &= M_s^P - \frac{1}{3} M_d^P + M_d^F \left(\cos^2 \theta_\pi - \frac{1}{5} \right), \\
 B &= \left(M_d^P - \frac{2}{5} M_d^F \right) \cos \theta_\pi. \quad (44)
 \end{aligned}$$

The observables in terms of these amplitude can be written as

$$\begin{aligned}
 \frac{d\sigma}{d\Omega} &= |A|^2 + |B|^2 + 2\text{Re}[AB^*] \cos \theta_\pi, \\
 A_y \frac{d\sigma}{d\Omega} &= 2\text{Im}[AB^*] \sin \theta_\pi. \quad (45)
 \end{aligned}$$

Omitting the squares of the d-wave amplitudes, one finds the following relation

42 *Vadim Baru, Christoph Hanhart, Fred Myhrer*

between the observables in the $pp \rightarrow \{pp\}_s \pi^0$ channel

$$\begin{aligned} a_0 &= |M_s^P|^2 - \frac{2}{3} \text{Re} [M_s^{P*} (M_d^P + \frac{3}{5} M_d^F)] \\ a_2 &= 2 \text{Re} [M_s^{P*} (M_d^P + \frac{3}{5} M_d^F)] \\ b_2 &= -2 \text{Im} [M_s^{P*} (M_d^P - \frac{2}{5} M_d^F)]. \end{aligned} \quad (46)$$

where a_i and b_i are the coefficients in the expansion in powers of $\cos \theta_\pi$ for the differential cross section and the analyzing power, i.e.

$$\begin{aligned} \frac{d\sigma}{d\Omega} &= \frac{q}{4p} \sum_{n=0} a_n \cos^n \theta_\pi \\ A_y \frac{d\sigma}{d\Omega} &= \frac{q}{4p} \sin \theta_\pi \sum_{n=0} b_{n+1} \cos^{n+1} \theta_\pi \end{aligned} \quad (47)$$

where again p is the incident proton momentum and q is the momentum of the outgoing pion. The analogous expressions connecting the partial wave amplitudes with the observables in the $pn \rightarrow \{pp\}_s \pi^-$ channel are given in.¹²¹ The coefficients a_i and b_i were extracted from the best fits to the data in both reactions $pp \rightarrow \{pp\}_s \pi^0$ and $pn \rightarrow \{pp\}_s \pi^-$.

As seen from Eq.(42), there are five complex partial wave amplitudes, M_1^L , that need to be determined from a global fit to the ten experimentally determined coefficients a_i and b_i in Eq.(47). Fortunately the number of parameters can be reduced if one imposes the Watson theorem to fix the phases of the amplitudes. This theorem states that the phase of the production amplitude in the absence of coupled channels is fully determined by phases of the NN interaction in the initial and final states. Hence, it allows one to fix the phase of the ${}^3P_0 \rightarrow {}^1S_0 s$ transition which removes one parameter. In other partial waves the initial NN interaction appears in coupled channels, and it is known from the phase shift analysis of pp data that the coupling between 3S_1 and 3D_1 partial waves is sizeable for energies around pion-production threshold.^{82,83} Meanwhile, for ${}^3P_2 - {}^3F_2$ transitions the mixing parameter, as well as the inelasticities, are still negligibly small at $T_{\text{lab}} = 353$ MeV.^{82,83} This means that one may neglect the coupled channel effect in ${}^3P_2 - {}^3F_2$ partial waves and use the Watson theorem to remove another two parameters. Under this assumption, the s-wave and two d-wave pion-production amplitudes were extracted in Ref.¹²⁰ based on the partial wave analysis of the $pp \rightarrow \{pp\}_s \pi^0$ data. Simultaneously, the fit to the combined $pp \rightarrow \{pp\}_s \pi^0$ and $pn \rightarrow \{pp\}_s \pi^-$ data sets has been performed in Refs.,¹²¹ with $\chi^2/\text{d.o.f.} = 89/82$ for the best fit. The results for s- and d-waves from the global fit is in good agreement with the values extracted from the analysis of the π^0 data only.

In the recent study¹²² the results of the partial wave analysis for p-waves¹²¹ were questioned. In particular, the important question if the global solution, as shown in Table 2 solution 1, is indeed the true one was raised. In addition to the

Amplitude	Real	Imaginary	Im/Re
Solution 1: $\chi^2/d.o.f. = 101/82$			
M_s^P	53.4 ± 1.0	-14.1 ± 0.3	
M_d^P	-25.9 ± 1.4	-8.4 ± 0.4	
M_d^F	-1.5 ± 2.3	0.0 ± 0.0	
M_p^S	-37.5 ± 1.7	16.5 ± 1.9	-0.44 ± 0.06
M_p^D	-93.1 ± 6.5	122.7 ± 4.4	-1.32 ± 0.11
Solution 2: $\chi^2/d.o.f. = 103/82$			
M_s^P	52.7 ± 1.0	-13.9 ± 0.3	
M_d^P	-28.9 ± 1.6	-9.4 ± 0.5	
M_d^F	3.4 ± 2.6	0.0 ± 0.0	
M_p^S	-63.7 ± 2.5	-1.3 ± 1.6	0.02 ± 0.03
M_p^D	-109.9 ± 4.2	52.9 ± 3.2	-0.48 ± 0.03
Solution 3: $\chi^2/d.o.f. = 106/82$			
M_s^P	50.9 ± 1.1	-13.4 ± 0.3	
M_d^P	-26.3 ± 1.5	-8.5 ± 0.5	
M_d^F	2.0 ± 2.5	0.0 ± 0.0	
M_p^S	-25.4 ± 1.9	-7.3 ± 1.5	0.20 ± 0.07
M_p^D	-172.2 ± 5.6	92.0 ± 6.2	-0.53 ± 0.04

Table 2. Values of the real and imaginary parts of the amplitudes for five lowest partial waves deduced from fits to the ANKE $pp \rightarrow \{pp\}_s \pi^0$ and $np \rightarrow \{pp\}_s \pi^-$ measurements at 353 MeV. Also shown are the ratios of the imaginary to real parts of the p-wave amplitudes that have been freely fitted. The other three ratios for s- and d-wave amplitudes are fixed by the Watson theorem.

global minimum, several local minima with only slightly larger χ^2 were found yielding completely different amplitudes for the p-waves, shown as solutions 2 and 3 in Table 2. The data on the differential cross section and the analysing power only do not allow one to discriminate between the different solutions, see the upper panels in Fig.17. The transverse spin-correlation parameter A_{xx} could resolve this p-wave issue, since the curves for A_{xx} corresponding to the different solutions are, in principle, distinguishable, as shown in the lower left panel of Fig.17, provided the high resolution data existed in the whole angular domain. However, the statistical uncertainty of the recently measured data¹²² did not allow to distinguish between the minima. As argued in,¹²² see also Fig.17 lower right panel, the double polarization measurement of A_{xz} in $pn \rightarrow \{pp\}_s \pi^-$ could be useful in order to lift the ambiguity with the different χ^2 solutions. The different p-waves scenarios could be disentangled either just by determining the sign of A_{xz} or by its magnitude.

It is interesting to note that the phases of the p-wave amplitudes corresponding to different solutions in Table 2 turned out to differ significantly from each other, as can be seen from the last column of this Table. On the other hand, in spite of the sizeable coupling between the 3S_1 and 3D_1 partial waves, one would

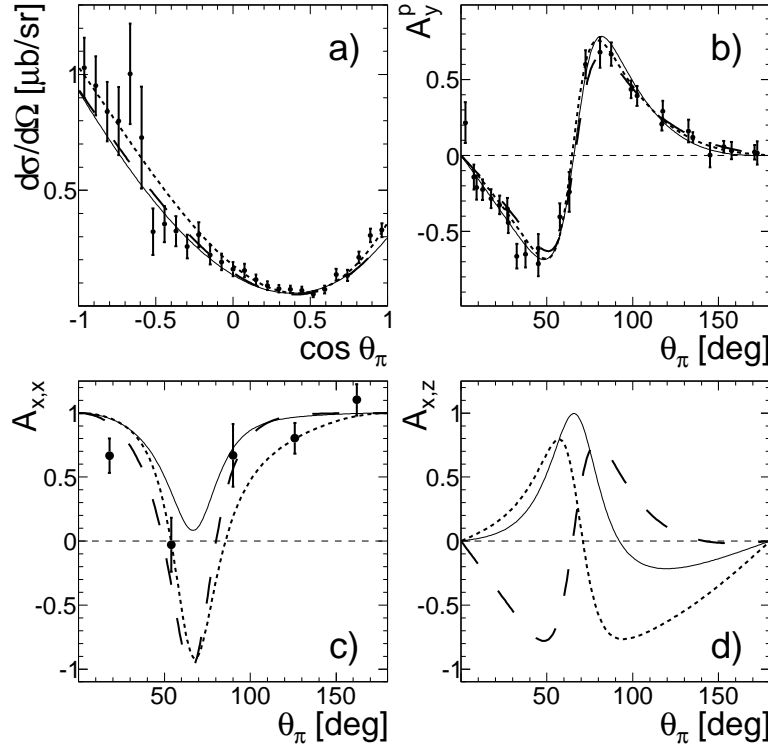


Fig. 17. Predictions of the partial wave analysis for the $pn \rightarrow \{pp\}_s \pi^-$ reaction at 353 MeV with the $E_{pp} < 3$ MeV cut. Also shown are the ANKE experimental data with statistical errors. The full, long-dashed, and short-dashed lines correspond to solutions 1, 2, and 3, as noted in Table 2. a) Differential cross-section taken from Ref.,^{120,121} b) A_y^p data from Ref.,¹²² c) A_{xx} data from Ref.,¹²² d) A_{xz} , for which there are yet no experimental data. The figure is taken from Ref.¹²².

naively assume that the phases of the p-wave pion-production amplitudes should not differ drastically from the elastic NN phases. The values in the last column of Table 2 should be compared with nucleon-nucleon phase-shift analysis values of $(\tan \delta_{3S_1}, \tan \delta_{3D_1}) = (0.03, -0.46)$,^{82,83} and to the values from the theoretical analysis of the p-wave pion production amplitudes of $(0.04, -0.61)$.⁶⁵ This comparison reveals a clear preference against the solution 1 and possibly in favour of solution 2, as pointed out in.¹²²

The experimental measurements^{120,121} are extremely useful to improve our knowledge about pion production: the new high-accuracy measurements of the differential cross section and analyzing power in $pn \rightarrow \{pp\}_s \pi^-$ in the whole angular domain at present constitute a challenge for the theory. The data on $pp \rightarrow \{pp\}_s \pi^0$ clearly demonstrated that the d-wave amplitudes are sizable already at $T_{\text{lab}}=353$ MeV and that neglecting these amplitudes, as was done in Ref.⁶⁵ is not justified. The partial wave analysis of the $pp \rightarrow \{pp\}_s \pi^0$ data led to a successful

extraction of the s- and d-wave pion production amplitudes in the isospin 1 channel and should be confronted soon with the theory calculations within EFT where the complete production operator up to N²LO for s-wave pions has been already derived, cf. Secs. 3 and 4 for details.

7. Charge symmetry breaking in pion-production reactions

Isospin symmetry is normally realized to a few percent accuracy in hadronic reactions. On the QCD level the symmetry is broken only by the different up and down quarks masses (both very small compared to typical hadronic masses) and by their different charges. The largest isospin symmetry breaking effect that emerges is the pion mass difference,

$$2(m_{\pi^+} - m_{\pi^0})/(m_{\pi^+} + m_{\pi^0}) \sim 4\% ,$$

which originate almost completely from electromagnetism. Typical isospin-violating effects are usually dominated by this pion mass difference as seen, e.g., in the spectacular energy dependence in neutral pion photo-production off protons near threshold.^{32,123} Due to this pion mass difference it is therefore difficult to quantify the isospin violations due to the up and down quark mass difference in hadronic observables.

The exceptions are observables that violate charge symmetry (CS). While general isospin symmetry or charge independence implies invariance of interactions under any rotation in isospin space, CS requires invariance only under an isospin rotation by 180° around the "2"-axis. As a consequence, when charge symmetry is broken, isospin invariance is also violated but the converse is not correct. The pion mass difference term is charge symmetric, since the charge symmetry operation transforms a π^+ into a π^- (and they have identical masses as a consequence of CPT invariance). CS is violated by the up and down quark mass difference as well as residual electromagnetic interactions (virtual photons) after effects of the pion mass difference are removed. The impact of virtual photons has been systematically studied in EFT^{33,124-129} and is a well understood and calculable isospin violation.

CSB effects manifest themselves in many different physical phenomena. Some examples of CSB consist in the mass splitting of hadronic isospin multiplets (e.g. $m_n \neq m_p$ and $M_{D^0} \neq M_{D^+}$ ¹³⁰), η -decays (for a recent two-loop calculation, see¹³¹ and references therein), the different scattering lengths of nn and pp systems after removing electromagnetic effects in pp scattering (see, e.g. the review article⁴⁰), neutron-proton elastic scattering at intermediate energies,¹³² hadronic mixing (e.g. $\rho^0 - \omega$ ¹³³ or $\pi^0 - \eta$ ¹³⁴ mixing) and the binding-energy difference of mirror nuclei known as Nolen-Schiffer anomaly.¹³⁵

In this section we will discuss the manifestation of CSB in pion-production reactions. Recently, experimental evidence for CSB was found in reactions involving the production of neutral pions. At IUCF a non-zero value for the $dd \rightarrow \alpha\pi^0$ cross section was established,³⁹ and at TRIUMF a forward-backward asymmetry of the

differential cross section for $pn \rightarrow d\pi^0$ was reported to be $A_{fb} = [17.2 \pm 8(\text{stat.}) \pm 5.5(\text{sys.})] \times 10^{-4}$.³⁸

In what follows we will concentrate our discussion on the reaction $pn \rightarrow d\pi^0$ before we comment on the reaction $dd \rightarrow \alpha\pi^0$ at the end of this section. Following the arguments presented in Ref.,³⁶ we will show that at leading CSB order within the MCS scheme, only the strong (quark-mass induced) contribution to the proton-neutron mass difference enters the CSB pion-production operator in $pn \rightarrow d\pi^0$. This quantity was extracted in Ref.³⁶ based on the $A_{fb}(pn \rightarrow d\pi^0)$ data. It is noteworthy that the effect of $\pi - \eta$ mixing, which was believed to completely dominate this CSB observable, is a sub-leading CSB effect as shown in Ref.¹³⁶

In order to see that $A_{fb}(pn \rightarrow d\pi^0)$ is indeed a CSB observable, note first of all that the final $d\pi$ -state is an isospin-1 state. This means that, in an isospin symmetric world, also the initial states is in isospin-1. Since an isospin-1 pn pair behaves like two identical nucleons pp or nn — the forward and backward asymmetry is absent. However, since CSB distinguishes a proton from a neutron, due to CSB interactions the initial NN state acquires a small isospin-0 admixture, and the interference of this small isospin-0 component combined with the charge symmetry conserving contributions lead to a forward–backward asymmetry.

The forward-backward asymmetry is defined as

$$A_{fb} = \frac{\int_0^{\pi/2} \left[\frac{d\sigma}{d\Omega}(\theta) - \frac{d\sigma}{d\Omega}(\pi - \theta) \right] \sin\theta d\theta}{\int_0^{\pi/2} \left[\frac{d\sigma}{d\Omega}(\theta) + \frac{d\sigma}{d\Omega}(\pi - \theta) \right] \sin\theta d\theta} = \frac{A_1}{2A_0}, \quad (48)$$

where Eq. (39) was used in the last equality. The experiment at TRIUMF was done at $T_{\text{lab}} = 279.5$ MeV, which is very close to threshold and is equivalent to an excess energy of about 2 MeV. At this energy the total cross section $\sigma = 4\pi A_0 = \alpha\eta + \beta\eta^3$, Eq. (26), is largely dominated by the isospin-conserving s-wave pion-production amplitude in the final NN spin-triplet channel, cf. Table 1. In their analysis Ref.³⁶ used the experimental value for α extracted by Ref.⁹⁰ from the extremely precise PSI measurement of the lifetime of the pionic deuterium atom. Note that unlike scattering experiments the measurement at PSI does not suffer from normalization uncertainty. In addition, in the $pn \rightarrow d\pi^0$ experiment close to threshold the contribution from pion p-waves, calculated to N²LO in Ref.⁶⁵ and discussed in Sec. 5, was taken into account in Ref.³⁶ This p-wave contribution to the relevant final NN spin-triplet channel^{viii} determines β and amounts to 10% of the total cross section at the energy of the TRIUMF experiment. Thus the total amplitude is determined to be $A_0 = 10.0_{-0.4}^{+0.2} \cdot \eta + (47.8 \pm 5.7) \cdot \eta^3$ [μb].

^{viii} Note that pion p-waves in the spin-triplet channel relevant here are well under control, cf. Fig. 15 in Sec. 5. On the other hand, the analysis in Sec. 6 discussed the uncertainty regarding the pion p-wave for a final NN spin-singlet channel.

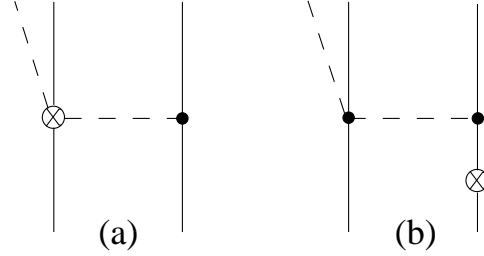


Fig. 18. The leading order CSB diagrams for $pn \rightarrow d\pi^0$. The crosses correspond to isospin-violating vertices.

The coefficient A_1 in Eq. (48) proportional to the interference of the CS and CSB pion-production amplitudes, reads

$$A_1 = \frac{1}{128\pi^2} \frac{\eta m_\pi}{p(m_\pi + m_d)^2} \text{Re} \left[\left(M_1^{\text{CS,p}} + \frac{2}{3} M_2^{\text{CS,p}} \right) M^{\text{CSB,s}\dagger} \right] + \dots, \quad (49)$$

where m_d is the deuteron mass. The amplitudes $M_1^{\text{CS,p}}$ and $M_2^{\text{CS,p}}$ stand for the charge symmetric amplitudes corresponding to production of p-wave pions in the $^1S_0 \rightarrow ^3S_1p$ and $^1D_2 \rightarrow ^3S_1p$ partial waves, while $M^{\text{CSB,s}}$ is the corresponding amplitude for the charge symmetry breaking s-wave production in the $^1P_1 \rightarrow ^3S_1s$ partial wave. Furthermore, the ellipses stand for the other term in which the CSB amplitudes for a p-wave pion interfere with the CS amplitudes for an s-wave pion. Since the other term is suppressed by χ_{MCS}^2 , it was ignored in the leading-order calculation by Ref.³⁶

As the charge symmetry conserving contributions were already discussed in great detail in the previous sections, we will here exclusively focus on the CSB contributions.

At leading-order the isospin-violating (IV) strong and electromagnetic operators have the form

$$\mathcal{L}_{\text{iv}} = \frac{\delta m_N}{2} N^\dagger \tau_3 N - \frac{\delta m_N^{\text{str}}}{4f_\pi^2} N^\dagger \boldsymbol{\tau} \cdot \boldsymbol{\pi} \pi_3 N - \frac{\delta m_N^{\text{em}}}{4f_\pi^2} N^\dagger (\tau_3 \boldsymbol{\pi}^2 - \boldsymbol{\tau} \cdot \boldsymbol{\pi} \pi_3) N + \dots, \quad (50)$$

where the neutron proton mass difference is $\delta m_N = \delta m_N^{\text{str}} + \delta m_N^{\text{em}}$ and the ellipses stand for further terms which are not relevant here. The δm_N^{str} is at this order given by the LEC $c_5 \propto m_d - m_u$, which is part of $\mathcal{L}_{\pi N}^{(2)}$ in Eq. (7), and δm_N^{em} is given by the LEC f_2 . The precise definitions of the LECs c_5 and f_2 can be found in Ref.³³ At leading order in CSB the diagrams that contribute to the transition amplitude from an initial NN isospin-0 state to the final isospin-0 NN state, are shown in Fig. 18. Diagram (a) corresponds to a pion rescattering diagram where the πN scattering vertex breaks charge symmetry. This CSB vertex is due to the last two terms in Eq. (50). Diagram (b) on the other hand includes the πN rescattering

vertex given by the Weinberg-Tomozawa operator [the first term in $\mathcal{L}_{\pi N}^{(1)}$, Eq. (6)]. The isospin-violating term in diagram (b) is, as indicated in Fig. 18, given by the proton-neutron mass difference, which plays a pivotal role in the arguments below.

In the following we will show that due to the interplay of diagram (a) and diagram (b) in Fig. 18, the electromagnetic term cancels, and hence the forward-backward asymmetry of the reaction $pn \rightarrow d\pi^0$ depends only on δm_N^{str} . In order to obtain this result, it is sufficient to focus on the two πN rescattering vertices on nucleon 1 while we only keep the isospin structure from the pion-production vertex on nucleon 2. The other components are identical for both diagrams. The relevant parts of diagram (a), where a charged pion is exchanged between the two nucleons, read

$$\hat{I}_{(a)} = -i \frac{\delta m_N^{\text{str}}}{4f_\pi^2} \left(\boldsymbol{\tau}^{(1)} \cdot \boldsymbol{\tau}^{(2)} + \tau_3^{(1)} \tau_3^{(2)} \right) + i \frac{\delta m_N^{\text{em}}}{4f_\pi^2} \left(\boldsymbol{\tau}^{(1)} \cdot \boldsymbol{\tau}^{(2)} - \tau_3^{(1)} \tau_3^{(2)} \right), \quad (51)$$

where $\boldsymbol{\tau}^{(i)}$ is the isospin operator of the i 'th nucleon. This expression represents the complete rescattering contribution included in Ref.³⁵ Diagram (b) of Fig. 18 requires more scrutiny. First, observe that due to the isospin structure of the Weinberg-Tomozawa πN scattering vertex, only charged pions can be exchanged between the two nucleons to produce a neutral pion. Thus as argued above for CSB reactions in general, the pion mass difference does not enter. However, the proton-neutron mass difference generates an energy difference of the exchanged charge pion in diagram (b), depending on whether a π^+ is produced at the vertex on nucleon 2 via a $p \rightarrow n$ transition, or a π^- , produced via a $n \rightarrow p$ transition. The energy dependence of the Weinberg-Tomozawa vertex in diagram (b) is sensitive to this energy difference and gives rise to the CSB amplitude from diagram (b). On the operator level we obtain analogously to Eq. (51),

$$\begin{aligned} \hat{I}_{(b)} &= \frac{\delta m_N}{2} \frac{1}{4f_\pi^2} \epsilon^{3bc} \tau_c^{(1)} \left(\tau_b^{(2)} \tau_3^{(2)} - \tau_3^{(2)} \tau_b^{(2)} \right) \\ &= -i \frac{\delta m_N}{4f_\pi^2} \left(\boldsymbol{\tau}^{(1)} \cdot \boldsymbol{\tau}^{(2)} - \tau_3^{(1)} \tau_3^{(2)} \right), \end{aligned} \quad (52)$$

where the two terms in the first row include both an insertion of the CSB nucleon mass term before and after the pion emission vertex. It follows that in the sum of the two diagrams, the term from the electromagnetic contributions cancels and the leading isospin-violating transition amplitude is proportional to δm_N^{str} . The relevant transition matrix element for the NN states is³⁶

$$\langle I_f = 0 | \hat{I}_{(a)} + \hat{I}_{(b)} | I_i = 0 \rangle = \frac{i}{4f_\pi^2} 6 \delta m_N^{\text{str}}. \quad (53)$$

Compared to the expression in Eq. (51), which was used in Ref.,³⁵ the rescattering operator in Eq. (53) is enhanced by about 30% when the standard values $\delta m_N^{\text{str}} \approx 2$ MeV and $\delta m_N^{\text{em}} \approx -0.76$ MeV are used.

An alternative method to derive the same result is obtained by redefining the pion and nucleon fields in the Lagrangian as discussed in Refs^{137–139} — see also

Ref.¹⁴⁰ which uses the unitary transformations. The pion and nucleon fields are redefined in order to eliminate the first term in the effective Lagrangian in Eq. (50) and this allows one to work with nucleons as indistinguishable particles. The key point is that the terms in a Lagrangian are invariant under this transformation *except* the ones involving a time derivative. The Weinberg-Tomozawa operator in the πN rescattering vertex in Eq. (6) includes a time derivative of the field which generates an additional isospin-violating $\pi N \rightarrow \pi N$ vertex $\propto \delta m_N$ that cancels exactly the electromagnetic contribution to the πN vertex $\propto \delta m_N^{\text{em}}$, see the last term in Eq. (50).

To summarize, within the leading order CSB calculation the result for the forward-backward asymmetry is calculated to be³⁶

$$A_{\text{fb}}^{\text{LO}} = (11.5 \pm 3.5) \times 10^{-4} \frac{\delta m_N^{\text{str}}}{\text{MeV}}, \quad (54)$$

where the theoretical uncertainty was estimated in³⁶ to be $\chi_{\text{MCS}}^2 \simeq 15\%$ which is doubled in Eq. (54) in order to give a conservative error. This result was confirmed in Ref.³⁷ within error bars. At next order in CSB photon-loop diagrams contribute, and in analogy with the pion s-wave NLO loop amplitudes presented in Sec. 3, the sum of these CSB loop amplitudes is zero,¹⁴¹ i.e. the contribution to the CSB amplitude from the next order diagrams vanishes (see also Ref.³⁷ where some CSB tree-level operators at N²LO were also taken into account). Comparing the experimental result for A_{fb} ³⁸ with Eq. (54) allows an extraction of δm_N^{str} :

$$\delta m_N^{\text{str}} = (1.5 \pm 0.8 \text{ (exp.)} \pm 0.5 \text{ (th.)}) \text{ MeV}. \quad (55)$$

This result is consistent with other evaluations of this contribution to the neutron proton mass difference in Refs^{29,142} based on the Cottingham sum rule¹⁴³ and in Refs.^{144–146} based on lattice simulations, cf. Fig. 19. This consistency is a non-trivial and encouraging test of the applicability of ChPT to $NN \rightarrow NN\pi$ reactions.

As usual in EFT, the next step in the study of $A_{fb}(pn \rightarrow d\pi^0)$ should consist in the extension of the CSB pion-production operator to higher orders. As already said, all CSB operators at NLO vanish. Some examples of CSB operators at N²LO are shown in Fig. 20, see Ref.¹⁴¹ for further details. In particular, the CSB operator at N²LO involves the one-nucleon term with the CSB πNN vertex accompanied by two unknown LECs which were modelled in Ref.¹⁴⁷ by the $\pi - \eta$ mixing mechanism. In addition, at this order, CSB in the pn potential generates a contribution to CSB pion-production. Furthermore, there are many different loop contributions analogous to those discussed in Sec. 3 for CS pion production in an s-wave. It remains to be seen if cancellations which were operative in the CS case, will also take place here. The proper evaluation of $A_{fb}(pn \rightarrow d\pi^0)$ at this order would also require the calculation of CSB pion production in a p-wave at LO, since the interference of the CSB operator for a p-wave pion with the CS s-wave pion-production amplitude starts to contribute at N²LO, as discussed. A valuable help in understanding of

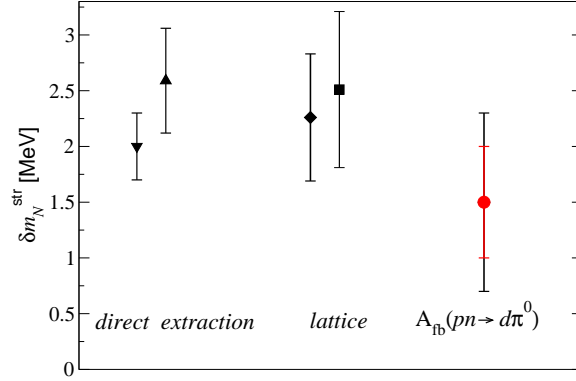


Fig. 19. The proton-neutron mass difference extracted with different methods: a *direct extraction* via the Cottingham sum rule (triangle down,²⁹ triangle up¹⁴²), a determination using *lattice* QCD (diamond,¹⁴⁴ square¹⁴⁵) and an extraction from $pn \rightarrow d\pi^0$.³⁶ For the last value the inner (red) error bar indicates the size of the theoretical uncertainty. Note also that the uncertainties of lattice data are dominated by systematic errors.

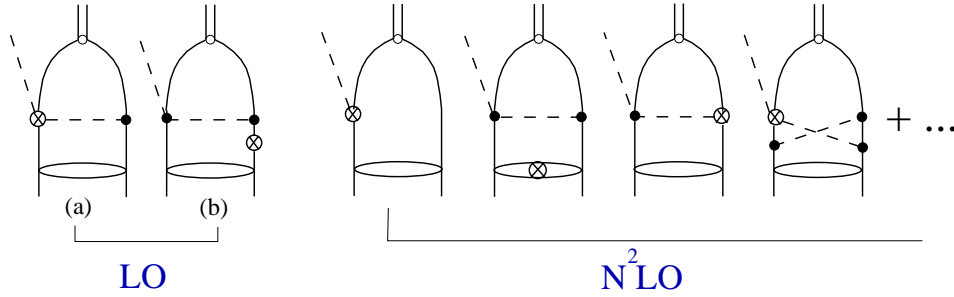


Fig. 20. CSB operators for $pn \rightarrow d\pi^0$ to $N^2\text{LO}$. The double line stands for the deuteron, the crosses correspond to the isospin-violating vertices.

higher order CSB mechanisms in $pn \rightarrow d\pi^0$ could be obtained if this reaction were studied in combination with the $dd \rightarrow \alpha\pi^0$ reaction.

The IUCF measurement³⁹ of the $dd \rightarrow \alpha\pi^0$ reaction inspired the first theoretical evaluation of this process.^{141,148} These studies showed that the relative importance of the various charge symmetry breaking effects are very different for the $pn \rightarrow d\pi^0$ and $dd \rightarrow \alpha\pi^0$ reactions. For example, photon exchange in the dd initial state could significantly enhance the cross sections for $dd \rightarrow \alpha\pi^0$.¹⁴⁹ In addition, the rescattering mechanism with the CSB πN vertices at LO seems to play only a subleading role in $dd \rightarrow \alpha\pi^0$ due to symmetries in the wave functions, as advocated in Refs. ^{141,148} Furthermore, the calculations of Refs. ^{148,150} revealed significant sensitivity to the nuclear interaction model. However, it was demonstrated in Ref. ¹⁵⁰ that a simultaneous analysis of CSB in the two nucleon sector and in $dd \rightarrow \alpha\pi^0$ strongly constraints the calculations of the latter. The main uncertainty in the evaluation

of $dd \rightarrow \alpha\pi^0$ is the treatment of the initial state interactions. At pion threshold energies the $dd \rightarrow \alpha\pi^0$ reaction requires reliable wave functions for $dd \rightarrow 4N$ in low partial waves at relatively high energies around pion-production threshold. A successful theoretical description of the data for the isospin-conserving reaction $dd \rightarrow {}^3\text{He}n\pi^0$,¹⁵¹ which partially shares the same initial state as $dd \rightarrow \alpha\pi^0$, could serve as a valuable test of the theoretical approach to the $dd \rightarrow \alpha\pi^0$ reaction.

There is another important test that could be used to check consistency of the planned combined analysis of the recent CSB experiments. Namely, once the LECs that enter CSB s-wave pion production at N²LO are fixed, the p-waves in $dd \rightarrow \alpha\pi^0$ can be predicted parameter free to leading and next-to-leading order. The IUCF experiment,³⁹ being carried out very close to threshold, was consistent with the contribution of pion s-waves only. Thus, the same experiment at somewhat higher energy (but still well below the Δ region, e.g. at $Q \approx 30 - 60$ MeV) is desirable.

8. Remarks on the reaction $NN \rightarrow NN\pi\pi$

The reaction $NN \rightarrow NN\pi\pi$ provides a contribution to the nucleon-nucleon inelasticity next in importance after one-pion production. The proximity of the Δ resonance mass to the $\pi\pi N$ threshold suggests the dominance of the Δ resonance in the two-pion production mechanism. However, as will be argued below, in the channel where the final isoscalar $\pi\pi$ -pair is in an s-wave, for example in $pn \rightarrow d\pi^0\pi^0$ near threshold, the contribution of the Δ is suppressed due to isospin compared to the other two-pion production channels. The reaction channel $pn \rightarrow d\pi\pi$ is of particular interest due to the so-called ABC effect¹⁵² which has been recently observed by WASA collaboration at COSY.^{153,154} The ABC effect refers to a pronounced low-mass enhancement in the $\pi\pi$ invariant mass spectrum in the reactions where the pion pair is produced together with the final nucleus in, e.g., $pn \rightarrow d\pi\pi$ and $dd \rightarrow \alpha\pi\pi$ (these reactions are often named double-pionic fusion reactions). Furthermore, the data of Ref.¹⁵³ revealed that the ABC effect in $pn \rightarrow d\pi\pi$ is uniquely correlated with a resonance-like energy dependence in the total cross section. We stress that the peak in the total cross section appears at the energy more than 200 MeV above $NN\pi\pi$ threshold, which precludes the use of chiral EFT for understanding this phenomenon. On the other hand, the understanding of the near-threshold behaviour of $pn \rightarrow d\pi\pi$, which provides the background contribution, is possible within chiral EFT.

A complete leading order calculation for the reaction $pn \rightarrow d\pi^0\pi^0$ at threshold within chiral EFT was presented in Ref.¹⁵⁵ The diagrams evaluated in Ref.¹⁵⁵ are displayed in Fig. 21 and at LO there is no free parameter. Previous investigations of this reaction^{156,157} included only the diagrams in the second row whereas Ref.¹⁵⁵ showed that a complete LO evaluation requires all diagrams in Fig. 21 to be considered. The most important findings of Ref.¹⁵⁵ are:

- (1) all diagrams evaluated are of similar magnitude;
- (2) there are important interferences among the diagram contributions;

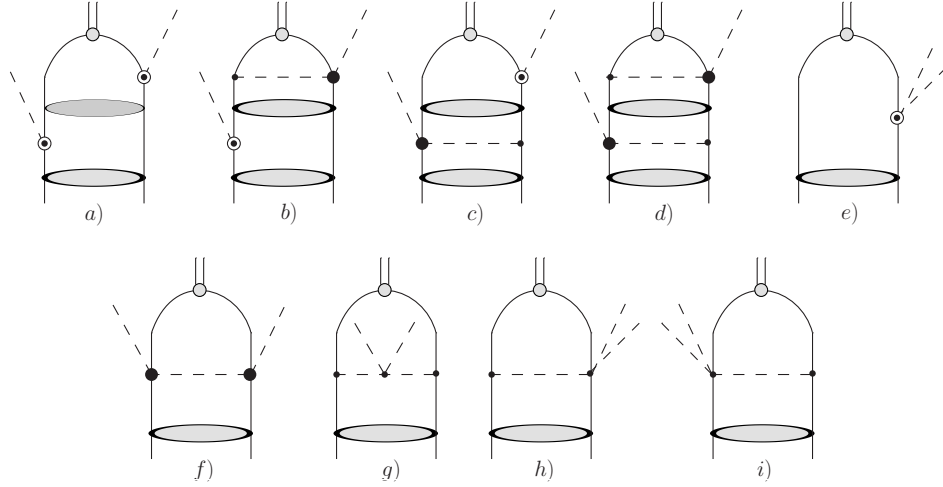


Fig. 21. Leading order diagrams for the reaction $pn \rightarrow d\pi\pi$ at threshold. Solid (dashed) lines denote nucleons (pions), filled ellipses correspond to continuum NN wave functions (including plane wave) in the initial and intermediate state, the outgoing double line denotes the deuteron. Subleading vertices are marked as \odot , while the blob denotes the leading πN WT vertex from Eq.(6) and its recoil correction from Eq.(7).

- (3) an accurate inclusion of the NN interaction in both intermediate as well as initial NN states is very important.

In order to produce two pions at threshold, the initial NN momentum in their center of mass system, $p_{\text{thr}}^{(2)}$, must be larger than that for the single pion production. Consequently, the expansion parameter is

$$\chi = \frac{p_{\text{thr}}^{(2)}}{m_N} \approx 0.5 .$$

An important future task is therefore to calculate higher order contributions in order to check the rate of convergence. As was pointed out, despite the proximity of the $\Delta(1232)$ mass to the $\pi\pi N$ threshold, the potentially most important $N\Delta$ intermediate state is not allowed for the reaction $pn \rightarrow d\pi^0\pi^0$ due to isospin conservation. The reason is that the NN systems in the initial and final states must have isospin zero, while the $N\Delta$ system has isospin one or two. Hence, to fulfil isospin conservation the isospin-1 $N\Delta$ state can only occur after one-pion emission and, thus, the role of the Δ in $pn \rightarrow d\pi\pi$ is expected to be analogous to that in one-pion production, as discussed in the previous sections. In particular, the Δ starts to contribute at NLO due to the fact that the Δ propagator is suppressed by $1/p$ as compared to $1/m_\pi$ in the nucleon case.

It is known from phenomenological studies of $NN \rightarrow NN\pi\pi$ ^{156,157} that the Roper resonance (N^*) can play a significant role already near threshold and that it will become even more important when considering this reaction at higher energies.

This N^* resonance is, however, not included explicitly in the LO evaluation of Ref.¹⁵⁵ The reason is that in chiral EFT its contribution is absorbed into low energy constants that start to matter only at N²LO in the MCS. On the other hand, an interesting question to address would be to understand if its contribution is natural or it is enhanced compared to the dimensional analysis estimate. The contribution of the Roper resonance to the c_i parameters, that scale the strength of the leading isoscalar πN scattering, has been discussed, e.g., in Ref.¹⁵⁸ It seems that it plays only a minor role there. Similar conclusions were drawn from systematic studies within ChPT of the double-pion photoproduction process^{159,160} and the reaction $\pi N \rightarrow \pi\pi N$ ^{161–163} near threshold. In particular, for the reaction $\gamma p \rightarrow \pi^0\pi^0 p$ the contribution of the Roper was found to be rather moderate as compared to the large contribution of chiral loops.¹⁶⁰ A model calculation of $\pi N \rightarrow \pi\pi N$ ¹⁶⁴ suggests also that the Roper resonance plays a rather minor role. On the other hand, the Roper might contribute significantly to the $(NN)^2\pi\pi$ counterterms, which enter at N²LO in a chiral EFT calculation of $NN \rightarrow NN\pi\pi$. Based on the discussions above, one can not expect that a leading order calculation of Ref.¹⁵⁵ for $NN \rightarrow NN\pi\pi$ can describe the experimental data well at higher energies and, hence, to answer the question about the role of the N^* resonance. However, it provides an estimate for the contribution of the non-resonant background near threshold. It therefore forms a basis for future studies and is thus a precondition to extract reliable information on the Roper resonance from future near-threshold experiments.

9. The role of $NN \rightarrow NN\pi$ in πd -atom observables

The isoscalar and isovector pion-nucleon scattering lengths are fundamental quantities of low-energy hadron physics. They serve as tests the QCD symmetries and the chiral symmetry breaking pattern. As stressed by Weinberg a long time ago, chiral symmetry suppresses the isoscalar πN scattering length a^+ compared to its isovector counterpart a^- . These scattering lengths appear as subtraction constants in the Goldberger–Miyazawa–Oehme sum rule,^{165–167} that is used to determine precisely the pion-nucleon coupling constant $g_{\pi NN}$. The scattering lengths are also needed in the dispersive analyses of the pion-nucleon σ term.¹⁶⁸ The most natural choice to determine these quantities is to measure the ground state pionic hydrogen atom level shift and width due to strong πN interaction. It has been known from pioneering work by Deser *et al.*¹⁶⁹ that the hadronic level shift is proportional to the real part of the scattering length of strongly interacting particles, while the lifetime of the atom is related to the imaginary part of the scattering length. Specifically, in isospin limit the atomic level shift in $\pi^- p$ reads $\varepsilon_{1S} \propto a_{\pi^- p} = a^+ + a^-$, while the width is $\Gamma_{1S} \propto a_{\pi^- p \rightarrow \pi^0 n}^2 \sim (a^-)^2$. A systematic inclusion of isospin-violating (IV) electromagnetic corrections to the relation between the energy level shifts and width and the pionic atom scattering lengths is performed in Refs.,^{127,170,171} see also the review article.¹⁷² In addition, taking into account isospin violation in the πN scattering lengths^{127–129,173} is very important. From the PSI measurement¹⁷⁴

the shift ε_{1s} is known with unprecedented accuracy to be $\varepsilon_{1s} = (-7.120 \pm 0.012)$ eV. Meanwhile, the width is known less accurately, $\Gamma_{1s} = (0.823 \pm 0.019)$ eV,¹⁷⁴ yielding a significant uncertainty in the determination of a^+ such that even its sign is unknown. Fortunately, the ground state level shift of the pion-deuteron atom (πd) is experimentally known to a 2% accuracy⁹⁰ and contains complementary information on a^+ and a^- . Schematically, the real part of the pion-deuteron scattering length can be written as

$$\text{Re}(a_{\pi d}) = 2a^+ + (\text{few-body corrections}) + (\text{IV corrections}) . \quad (56)$$

The first term $\sim a^+$ originates from the impulse approximation and is independent of the deuteron structure. Provided one can calculate the few-body corrections accurately the πd scattering is ideally suited to extract a^+ . However, already at threshold the πd scattering length is a complex-valued quantity and it is therefore crucial to obtain a precise understanding of its imaginary part.

A systematic study of the few-body corrections to the πd scattering length has been done within chiral EFT^{ix} in the last two decades.^{10–13,72,175–181} Unlike the pion-production reaction, elastic pion-deuteron scattering is a low-momentum transfer process, and is essentially controlled by the standard ChPT expansion parameter $\chi = m_\pi/m_N$. The other scales, $\sqrt{m_\pi m_N}$ due to pion-absorption, $\delta \sim \sqrt{m_\pi m_N}$ due to the explicit Δ -resonance, the deuteron binding momentum γ and $\sqrt{m_\pi/m_N} m_\pi$ due to the 3-body πNN cut have to be properly accounted for. Ref.¹³ demonstrated that the few-body corrections can be reliably calculated up to $\chi^{3/2} = \chi_{\text{MCS}}^3$, which is smaller than the leading unknown $(NN)^2\pi\pi$ contact term which enters at χ^2 . From a naive dimensional analysis the uncertainty anticipated due to the truncation of the higher-order terms is a few percent. The most important contributions to the transition operator up to $\chi^{3/2}$ can be summarized as follows:

- the double-scattering diagram^{72,175} is the most important contribution in the multiple-scattering series (MSS) as was recognized decades ago
- the triple-scattering diagram is the next correction in the MSS series^{176,177}
- nucleon recoil corrections to the double-scattering process^{178,182}
- dispersive corrections due to $\pi d \rightarrow NN \rightarrow \pi d$ and $\pi d \rightarrow \gamma NN \rightarrow \pi d$ ¹⁰
- explicit Δ -isobar contributions¹¹
- isospin violation in the 3-body sector: few-body corrections caused by the pion mass difference and virtual photons^{12,13}

While the detailed discussion of all these effects can be found in Ref.,¹³ we will here focus on the role of pion production for $a_{\pi d}$, since it controls the strength of the important dispersive corrections.

^{ix} The interested reader can find references to numerous phenomenological studies in, e.g., Ref.¹⁶⁷

^x The characteristic distances in the deuteron are normally estimated by taking the expectation value of $1/r$ between the deuteron wave functions, which gives $\langle 1/r \rangle \simeq 0.5 \text{ fm}^{-1} \sim m_\pi$.

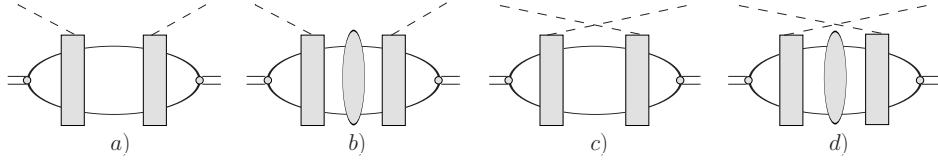


Fig. 22. Dispersive corrections to the πd scattering length. The notation of lines is the same as before. The rectangular blocks refer to the pion-production (or absorption) operator that consists of the direct and rescattering mechanisms including the recoil corrections, as shown in the first row of Fig.3.

The measurement of the πd scattering length shows that its imaginary part is about 1/4 of its real part.⁹⁰ The imaginary part can be expressed in terms of the πd total cross section through the optical theorem,

$$4\pi\text{Im}(a_{\pi d}) = \lim_{q \rightarrow 0} q \{ \sigma(\pi d \rightarrow NN) + \sigma(\pi d \rightarrow \gamma NN) \} , \quad (57)$$

where q denotes the relative momentum of the initial πd pair. Furthermore, the ratio $R = \lim_{q \rightarrow 0} (\sigma(\pi d \rightarrow NN)/\sigma(\pi d \rightarrow \gamma NN))$ was measured to be 2.83 ± 0.04 .¹⁸³ It is expected that diagrams which lead to a sizeable imaginary part of $a_{\pi d}$, will also contribute significantly via dispersive corrections to the real part. In the mid of 70's the dispersive corrections were calculated within the Faddeev formalism,^{184,185} showing that the dispersive and absorptive contributions to the real and imaginary parts of the πd scattering length are indeed of similar size. In Ref.¹⁰ the chiral EFT calculation of the dispersive corrections that emerge from $\pi d \rightarrow NN \rightarrow \pi d$ and $\pi d \rightarrow \gamma NN \rightarrow \pi d$ processes was presented. The hadronic dispersive corrections were defined as contributions from diagrams with an intermediate state that contains only nucleons as well as crossed pion lines. Therefore, all the diagrams shown in Fig. 22 were included in the evaluations in Ref.¹⁰ In other words, in addition to the diagrams a) and b) in Fig. 22, that are present in the Faddeev calculations, the contributions with crossed pions (c) and d)) were part of the EFT study since all diagrams shown in Fig. 22 are of the same EFT order. The rectangular blocks in the diagrams of Fig. 22 refer to the relevant transition operators for the reaction $NN \rightarrow NN\pi$ that consist of the direct and rescattering mechanisms including the recoil corrections, as shown in the first row of Fig.3. It was demonstrated in Sec.3.4 that the same production operator resulted in a good description of the $pp \rightarrow d\pi^+$ total cross section. It is therefore not surprising that the calculation¹⁰ agreed nicely with the imaginary part of the πd -scattering length. Using the CCF potential⁷³ for the NN distortions Ref.¹⁰ found for the dispersive correction from the purely hadronic transition

$$\delta a_{\pi d}^{\text{disp}} = (-6.5 + 1.3 + 2.4 - 0.2) \times 10^{-3} m_{\pi}^{-1} = -3.0 \times 10^{-3} m_{\pi}^{-1} , \quad (58)$$

where the numbers in the first bracket are the results from each diagram in Fig. 22, in order. Note that the diagrams with intermediate NN interactions and the crossed

56 *Vadim Baru, Christoph Hanhart, Fred Myhrer*

ones (diagram (c) and (d)) give significant contributions. None of these diagrams were included in most of the previous calculations. The calculations were done with the four different phenomenological NN potentials: the CCF potential,⁷³ CD Bonn,⁷⁴ Paris,¹⁸⁶ AV18,⁷⁵ and Refs.^{10,11} obtained

$$\delta a_{\pi d}^{\text{disp}} = (-2.9 \pm 1.4) \times 10^{-3} m_{\pi}^{-1}, \quad (59)$$

where the number reflects the theoretical uncertainty of this calculation estimated conservatively — see Ref.^{10,11} for details. In spite of the cancellations between the diagrams (a) and (b) and those with crossed pions ((c) and (d)), the resulting dispersive correction in chiral EFT constitutes an important contribution to the πd scattering length of the order of 10%, which is a factor of two larger than the theoretical uncertainty estimate.

Including the few-body and isospin-violating contributions listed above, the combined analysis of the data on the pionic hydrogen shift and width and deuterium shift yielded^{12,13}

$$\tilde{a}^+ = (1.9 \pm 0.8) \cdot 10^{-3} m_{\pi}^{-1}, \quad a^- = (86.1 \pm 0.9) \cdot 10^{-3} m_{\pi}^{-1}, \quad (60)$$

where \tilde{a}^+ is defined as^{173,187}

$$\tilde{a}^+ \equiv a^+ + \frac{1}{4\pi(1 + m_{\pi}/m_p)} \left\{ \frac{4\Delta_{\pi}}{f_{\pi}^2} c_1 - 2e^2 f_1 \right\}, \quad (61)$$

and Δ_{π} stands for the mass difference between the charged and neutral pions, $\Delta_{\pi} = m_{\pi}^2 - m_{\pi^0}^2$. The isoscalar scattering length a^+ cannot be obtained independent of the LECs c_1 and f_1 . Using the rough estimate of $|f_1| \leq 1.4 \text{ GeV}^{-1}$ by Refs.^{126,127} and $c_1 = (-1.0 \pm 0.3) \text{ GeV}^{-1}$ used in Ref.,¹³ Eqs. (60) and (61) yield a non-zero a^+ at better than the 95% confidence level

$$a^+ = (7.6 \pm 3.1) \cdot 10^{-3} m_{\pi}^{-1}. \quad (62)$$

The results for the scattering lengths were used in Refs.^{12,13} to infer the charged pion-nucleon coupling constant, g_c , from the GMO sum rule, with isospin-violating corrections to the πN scattering lengths fully under control for the first time. The result reads

$$\frac{g_c^2}{4\pi} = 13.69 \pm 0.12 \pm 0.15, \quad (63)$$

where the first error gives the uncertainty due to the scattering lengths and the second that due to evaluation of the cross section integral J^- , see Refs.^{13,166,167} for the definition and further discussion. This value is in agreement with determinations from NN ($g_c^2/4\pi = 13.54 \pm 0.05$ ¹⁸⁸) and πN ($g_c^2/4\pi = 13.75 \pm 0.10$,¹⁸⁹ $g_c^2/4\pi = 13.76 \pm 0.01$ ¹⁹⁰) scattering data where the errors in Refs.^{188–190} mainly reflect the statistical uncertainties.

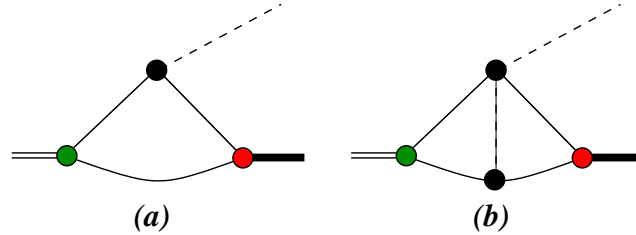


Fig. 23. Loop contributions to transition matrix elements of heavy quarkonia. The double and bold lines denote two different heavy quarkonium states and the red and green filled circles their coupling to heavy open heavy-flavor states, denoted by the internal solid lines. The dashed line denotes a light pseudo scalar that couples to the heavy states via the black solid dots.

10. Implications for EFTs for decays of heavy quarkonia

In this review we have demonstrated that a consistent, convergent effective field theory can be designed for systems controlled by two scales, one of which is a relatively large momentum. This finding has direct implications for the design of effective field theories for heavy quarkonium systems where one needs to control the effect of heavy meson loops on heavy quarkonium decays as stressed in Ref.¹⁹¹

For example the decays of regular quarkonia, like $\psi(2S) \rightarrow J/\psi\pi^0$ and $\psi(2S) \rightarrow J/\psi\eta$, can get sensitive to meson loops, since they are $SU(2)_F$ and $SU(3)_F$ violating, respectively.^{192–195} The reason is that the mass differences of the open charm meson loops induce enhanced violations of the mentioned symmetries, non-analytic in the quark masses. Furthermore, above the open charm thresholds a large number of states were recently found with properties in strong disagreement with well established quark model, see Ref.¹⁹⁶ for a recent review. Several of these new states qualify as candidates for molecular states formed from heavy mesons. For those all transitions and decays are expected to be dominated by loops of heavy mesons.

In an effective field theory formulation the evaluation of observables in the heavy quarkonium systems depends on the non-trivial interplay of several different scales, such as the pion mass, the pion momentum and the heavy meson velocity defined as a ratio of the binding momentum $\sqrt{M_H E}$ (E is the energy of the initial/final quarkonium with respect to the $\bar{H}H$ threshold ($H = D, B, \dots$)) to the heavy meson mass M_H . In order to establish which kind of transitions can be calculated in a controlled way, a power counting was introduced in Refs.^{191,197} that builds on the insights gained from $NN \rightarrow NN\pi$, also outlined in this review. Especially, in order to compare the order estimate for diagrams (a) and (b) of Fig. 23 it was crucial to use the findings of Ref.²⁵ Specifically, similar to Eq. (25) discussed earlier in this review, the $\pi\pi HH$ vertex in diagram (b) was decomposed in several terms in order to properly isolate the leading contribution of the diagram. For more details we refer to the cited references.

11. Summary and outlook

Chiral perturbation theory has been successfully applied in the past decades to describe low-energy dynamics of pions and nucleons as well as electroweak processes. However, the application of this effective field theory to pion production in nucleon-nucleon collisions turned out to be considerably more challenging due to the large three-momentum transfer involved in this reaction. This large momentum called for a modification of the power counting. The resulting slower convergence of the chiral expansion for this reaction [the expansion parameter $\chi_{\text{MCS}} \sim \sqrt{m_\pi/m_N}$ defined in Eq. (15)] provides a strong motivation for extending the calculations to higher orders. In this review we demonstrated that the momentum counting scheme (MCS) properly accounts for the additional scale associated with the large momentum transfer. It is shown to be successful in classify the various contributions to the $NN \rightarrow NN\pi$ transition amplitudes according to their importance. Given the relatively large MCS expansion parameter χ_{MCS} , one may wonder whether the pion-production operator converges sufficiently well to consider the theory predictive. The results of Refs.^{25,65} provide strong indications for the convergence of the s- and p-wave pion-production operators in the final two nucleon spin-triplet channels where no accidental cancellations emerge. Furthermore, good convergence of the results for spin observables in $pp \rightarrow pp\pi^0$, which probe p-wave pion production in this channel, was observed in Ref.²² On the other hand, s-wave pion production in $pp \rightarrow pp\pi^0$ looks exceptional since the experimental cross section in this channel is suppressed by more than an order of magnitude as compared to the charged channels near threshold. The experimental evidence for the smallness of the s-wave operator in the neutral channel is fully in line with the suppression of the Weinberg–Tomozawa (WT) operator for $pp \rightarrow pp\pi^0$, the almost complete cancellation of the pion emission amplitude from the direct diagram at LO and the vanishing of all loop contributions at NLO. Therefore, it is not a surprise that the relative importance of N²LO chiral loops in this channel is significantly enhanced compared to the case where the final NN are in a spin-triplet state. As demonstrated in Ref.,²⁶ the nucleon-pion loops are of a similar size for the spin triplet and singlet channels. In this sense the experimentally measured $pp \rightarrow pp\pi^0$ reaction is unique in that it directly probes the higher order MCS contributions which in the other reaction channels are masked by the dominant lower order WT term.

In this review the evaluation of all loop diagrams with pions, nucleons and Δ degrees of freedom up-to-and-including N²LO has been summarized. It was shown that all diagrams that contribute to NLO cancel exactly — a necessity from field theoretic consistency. As presented, even among the N²LO loop contributions there are significant cancellations as a results of chiral symmetry requirements and its symmetry breaking pattern. In particular, in Ref.²⁶ it is shown that all $1/m_N$ -corrections of the various diagrams cancel at N²LO, and it is also shown that none of the LECs c_i , $i = 1 \dots 4$, of $\mathcal{L}_{\pi N}^{(2)}$ contribute to the pion loops at this order.

In Ref.²⁷ as well as in Sec. 4.6 it was demonstrated that the amplitudes from the

loops which include the Δ , contribute at N²LO to both the NN final state spin-triplet and spin-singlet channels, and interfere destructively with the pure pion-nucleon ones. The isoscalar amplitudes from the loops which include the Δ are significantly smaller than the amplitudes from loops with only pions and nucleons, while the isovector amplitudes from the Δ loops are roughly half the size of the pure pion-nucleon ones. The size of the isovector contributions of the Δ loops is in line with the dimensional analysis estimate, while the suppression of the isoscalar contributions originates from specific numerical factors (spin-isospin coefficients) in this channel.²⁷ What emerges from the resultant loop amplitudes looks very promising in order to quantitatively describe the data for both $pp \rightarrow pp\pi^0$ and $pp \rightarrow d\pi^+$ for near threshold energies. While in the former reaction there persists a huge discrepancy between data and the chiral EFT calculation to NLO, in the latter at NLO the description is already quite good,²⁵ as discussed in Sec.3.4. Therefore, the N²LO chiral loop amplitude is expected to be much more dominating for the isoscalar amplitudes relevant for $pp \rightarrow pp\pi^0$ production than for the isovector ones. In order to be able to compare the amplitudes presented here to experimental data and to make the qualitative arguments given more quantitative, a proper convolution with NN wave functions is necessary.

The loop diagrams at N²LO contributing to the pion-production amplitudes have important phenomenological consequences, as was discussed in Refs.^{26,27} Within various phenomenological meson-exchange approaches,^{7,8,198} the pion production is largely driven by tree-level pion rescattering off a nucleon with the $\pi N \rightarrow \pi N$ amplitude being far off shell. The scalar-isoscalar (σ -exchange) πN interaction is relevant for the isoscalar production amplitude while the isovector (ρ -exchange) πN interaction contributes to the strength of the isovector one. Since the isoscalar πN scattering amplitude essentially vanishes on-shell, see Eq. (62), the production mechanism proposed in Refs.^{7,8,198} relies on the significance of the off-shell properties of the πN scattering amplitude. However, the EFT consideration presented in this review puts this mechanism into question. Pion rescattering via the phenomenological pion-nucleon transition amplitude can in chiral EFT be mapped onto pion rescattering (at tree level) via the low-energy constants c_i plus some contributions from pion loops. The tree-level amplitude contributions $\propto c_i$ are, even in the off-shell (pion production) kinematics, far too small to explain the data for the neutral pion production.^{14,15} As far as the loop contributions are concerned, only the diagrams IV and the mini-football may be regarded as an analog of the corresponding phenomenological mechanism. However, the remaining N²LO contribution of diagrams IV and Δ IV and the mini-football diagram, see Figs. 3 and 10, have a purely isovector structure — all isoscalar contributions cancel exactly. Therefore, none of the pion loop diagrams can be mapped into the particular phenomenological mechanism in the isoscalar case. Thus, Refs.^{26,27} concluded that the rescattering contribution with the isoscalar πN amplitude to $pp \rightarrow pp\pi^0$ that could be modeled phenomenologically by a σ exchange should be very small.

It is noted that none of the previous phenomenological investigations take into account chiral loops which, as found, contribute significantly to the production amplitude. In particular, as presented in Sec. 3.6 the magnitude of the regularization-scheme independent long-range contribution of the pion-nucleon loops to the isoscalar production amplitude turns out to be comparable to the magnitude of the short-range amplitudes in phenomenological models of Refs.³⁻⁶ In some phenomenological models the short-range amplitudes originate from heavy-meson z -diagrams which, in these studies, are advocated as the necessary mechanism to describe experimental data. In chiral EFT these phenomenological heavy meson exchanges contribute via the contact interaction $(NN)^2\pi$ and normally would be used in order to estimate the magnitudes of the low-energy constants (LECs) of Eq. (10) as was done in Sec. 3.6. Thus, the results of the loop diagrams reviewed in Secs. 3 and 4 raise doubts on the role of the short-range physics in pion production as suggested by these phenomenological studies. In order to draw more definite conclusions the complete N²LO operator for s-wave pion production discussed in this review paper should be convoluted with the NN wave functions and confronted with experimental data in order to assess the magnitude of the LECs of Eq. (10). The work in this direction is currently in progress.

As presented in this review, p-wave pion production in $NN \rightarrow NN\pi$ opens an appealing possibility to determine the strength of the $(NN)^2\pi$ contact operator, the LEC d , which can be thought of as the two-nucleon analog of the axial constant g_A . In the introduction we outlined how this LEC contributes to several few-nucleon processes, like the three-nucleon force, the pp fusion and the tritium β -decay, the neutrino deuteron breakup and the muon capture on the deuteron, as well as reactions involving photons $\pi d \rightarrow \gamma NN$ and $\gamma d \rightarrow \pi NN$. A combined analysis of the different channels of $NN \rightarrow NN\pi$ with chiral EFT by Ref.⁶⁵ and presented in Sec. 5 revealed that the reaction $pn \rightarrow pp\pi^-$ appears to be the most interesting channel for the extraction of the LEC d . Unlike s-wave pion production, the p-wave pion-production operator up to N²LO^{22,65} includes only the tree-level diagrams shown in Fig. 11. A large step towards an accurate extraction of the relevant LEC d from data was provided by the recent measurements of $\bar{p}p \rightarrow (pp)_s\pi^0$ and $\bar{p}n \rightarrow (pp)_s\pi^-$ at the COSY accelerator in Jülich.¹²⁰⁻¹²² As outlined in Sec. 6 the latest data from COSY allowed both s-wave and d-wave pion-production amplitudes to be extracted from the amplitude analysis of the data of $pp \rightarrow pp\pi^0$. It should be noted that in these recent measurements at COSY,¹²⁰ the final two nucleons were restricted to have a relative energy less than 3 MeV. This restricted phase space of the final particles enhanced the importance of the pion d-wave. The analysis of these COSY data for $pn \rightarrow pp\pi^-$, while revealing the dominant role of the p-wave pion-production amplitudes, does not yield the unique solution for these amplitudes. In order to pin down the p-wave amplitudes and thereby the LEC d , will require data from the planned double polarisation measurement of A_{xz} at COSY. As advocated in Ref.,¹²² this is the most promising experiment which would lift the ambiguity between different solutions and ultimately allow an extraction of

the p-wave amplitudes from data.

In this review we also presented in some detail a few applications of the two scale expansion underlying the MCS:

- The extraction of the strong part of the proton–neutron mass difference from charge symmetry breaking observables in $pn \rightarrow d\pi^0$ (Sec. 7) — the value extracted is consistent with other, completely different analyses.
- The chiral expansion for $NN \rightarrow NN\pi\pi$ (Sec. 8) which is an important step towards a quantitative understanding of this class of reactions.
- The calculation of dispersive corrections to πd scattering at threshold. This evaluation allowed a high-precision extraction of the isoscalar pion–nucleon scattering length a^+ from pionic atoms data, and a reanalysis of the pion–nucleon coupling constant (Sec. 9).
- The effective field theory outlined and confronted with data in this review is a model case for the design of an effective field theory to investigate certain states in the heavy quarkonium sector (Sec. 10).

These examples show that an understanding of reactions of the type $NN \rightarrow NN\pi$ within effective field theory is not only interesting in its own right, but also provides important new insights into the workings of the strong interaction in different energy regimes.

Acknowledgements

The hospitality of the University of Adelaide, where one of the authors (FM) spent his sabbatical while working on this review, is greatly appreciated. FM is supported in part by the National Science Foundation (US), Grant No. PHY-1068305. This work was supported in part by funds provided by the EU HadronPhysics3 project “Study of strongly interacting matter”, the European Research Council (ERC-2010-StG 259218 NuclearEFT), DFG-RFBR grant (436 RUS 113/991/0-1), and the DFG and NSFC funds to the Sino-German CRC 110 “Symmetries and the Emergence of Structure in QCD”.

Appendix A. Definitions for the various integrals

In this subsection we give the explicit definitions of the common dimensionless loop integrals used in this work. The first integral $J_{\pi\Delta} = \mu^\epsilon J_0(-\delta)$ where the integral

62 *Vadim Baru, Christoph Hanhart, Fred Myhrer*

$J_0(-\delta)$ is defined in Ref.⁶⁰

$$\begin{aligned} \frac{1}{\delta} J_{\pi\Delta}(\delta) &= \frac{\mu^\epsilon}{i\delta} \int \frac{d^{4-\epsilon}l}{(2\pi)^{4-\epsilon}} \frac{1}{(l^2 - m_\pi^2 + i0)(-v \cdot l - \delta + i0)} \\ &= 4L + \frac{(-2)}{(4\pi)^2} \left[-1 + \log\left(\frac{\mu^2}{m_\pi^2}\right) \right] \\ &\quad + \frac{4}{(4\pi)^2} \left[-1 + \frac{\sqrt{1-y-i0}}{\sqrt{y}} \left[-\frac{\pi}{2} + \arctan\left(\frac{\sqrt{y}}{\sqrt{1-y-i0}}\right) \right] \right] \end{aligned} \quad (\text{A.1})$$

$$\begin{aligned} I_{\pi\pi}(k_1^2) &= \frac{\mu^\epsilon}{i} \int \frac{d^{4-\epsilon}l}{(2\pi)^{4-\epsilon}} \frac{1}{(l^2 - m_\pi^2 + i0)((l+k_1)^2 - m_\pi^2 + i0)} \\ &= -2L - \frac{1}{(4\pi)^2} \left[\log\left(\frac{m_\pi^2}{\mu^2}\right) - 1 + 2F_1\left(\frac{k_1^2}{m_\pi^2}\right) \right], \end{aligned} \quad (\text{A.2})$$

where

$$F_1(x) = \frac{\sqrt{4-x-i0}}{\sqrt{x}} \arctan\left(\frac{\sqrt{x}}{\sqrt{4-x-i0}}\right), \quad (\text{A.3})$$

$$L = \frac{1}{(4\pi)^2} \left[-\frac{1}{\epsilon} + \frac{1}{2}(\gamma_E - 1 - \log(4\pi)) \right], \quad (\text{A.4})$$

and the variables x, y are defined via $x = k_1^2/m_\pi^2$, $y = \delta^2/m_\pi^2$.

The integrals with two pion and one Δ propagator and in addition with one nucleon propagator read

$$\Delta J_{\pi\pi\Delta} = \delta \frac{\mu^\epsilon}{i} \int \frac{d^{4-\epsilon}l}{(2\pi)^{4-\epsilon}} \frac{1}{(l^2 - m_\pi^2 + i0)((l+k_1)^2 - m_\pi^2 + i0)(-v \cdot l - \delta + i0)} \quad (\text{A.5})$$

$$\begin{aligned} k_1^2 J_{\pi\pi N\Delta} &= k_1^2 \frac{\mu^\epsilon}{i} \int \frac{d^{4-\epsilon}l}{(2\pi)^{4-\epsilon}} \left[\frac{1}{(l^2 - m_\pi^2 + i0)((l+k_1)^2 - m_\pi^2 + i0)} \right. \\ &\quad \left. \times \frac{1}{(-v \cdot l + i0)(-v \cdot l - \delta + i0)} \right]. \end{aligned} \quad (\text{A.6})$$

The integrals in Eqs. (A.5) and (A.6) can be reduced to simple one-dimensional integrals which can be calculated numerically.

It is also convenient to define finite, scale-independent parts of $J_{\pi\Delta}$ and $I_{\pi\pi}$ in which the divergency L and the $\log(m_\pi/\mu)$ terms are removed.

$$I_{\pi\pi} = -2L - \frac{1}{(4\pi)^2} \log\left(\frac{m_\pi^2}{\mu^2}\right) + I_{\pi\pi}^{\text{finite}}, \quad (\text{A.7})$$

$$I_{\pi\pi}^{\text{finite}} = \frac{1}{(4\pi)^2} \left(1 - 2 \frac{\sqrt{4-x-i0}}{\sqrt{x}} \arctan\left(\frac{\sqrt{x}}{\sqrt{4-x-i0}}\right) \right), \quad (\text{A.8})$$

$$\frac{1}{\delta} J_{\pi\Delta} = 4L + \frac{2}{(4\pi)^2} \log\left(\frac{m_\pi^2}{\mu^2}\right) + \frac{1}{\delta} J_{\pi\Delta}^{\text{finite}}, \quad (\text{A.9})$$

$$\frac{1}{\delta} J_{\pi\Delta}^{\text{finite}} = \frac{4}{(4\pi)^2} \left[-\frac{1}{2} + \frac{\sqrt{1-y-i0}}{\sqrt{y}} \left[-\frac{\pi}{2} + \arctan\left(\frac{\sqrt{y}}{\sqrt{1-y-i0}}\right) \right] \right] \quad (\text{A.10})$$

From the expressions above it is easy to obtain the important relation, which is used in the analysis of the integral combinations in Sec.4, relevant for our study

$$I_{\pi\pi} + \frac{1}{2\delta} J_{\pi\Delta} = I_{\pi\pi}^{\text{finite}} + \frac{1}{2\delta} J_{\pi\Delta}^{\text{finite}}. \quad (\text{A.11})$$

References

1. H. O. Meyer *et al.*, *Nucl. Phys. A* **539** (1992) 633.
2. D. S. Koltun and A. Reitan, *Phys. Rev.* **141** (1966) 1413.
3. T. S. H. Lee and D. O. Riska, *Phys. Rev. Lett.* **70** (1993) 2237.
4. C. J. Horowitz, H. O. Meyer and D. K. Griegel, *Phys. Rev. C* **49** (1994) 1337.
5. C. J. Horowitz, *Phys. Rev. C* **48** (1993) 2920.
6. J. A. Niskanen, *Phys. Rev. C* **53** (1996) 526.
7. E. Hernandez and E. Oset, *Phys. Lett. B* **350** (1995) 158.
8. C. Hanhart, J. Haidenbauer, A. Reuber, C. Schutz and J. Speth, *Phys. Lett. B* **358** (1995) 21.
9. C. Hanhart, J. Haidenbauer, O. Krehl and J. Speth, *Phys. Rev. C* **61** (2000) 064008.
10. V. Lensky, V. Baru, J. Haidenbauer, C. Hanhart, A. E. Kudryavtsev, and U.-G. Meißner, *Phys. Lett. B* **648** (2007) 46.
11. V. Baru, J. Haidenbauer, C. Hanhart, A. E. Kudryavtsev, V. Lensky, and U.-G. Meißner, *Phys. Lett. B* **659** (2008) 184.
12. V. Baru, C. Hanhart, M. Hoferichter, B. Kubis, A. Nogga and D. R. Phillips, *Phys. Lett. B* **694** (2011) 473.
13. V. Baru, C. Hanhart, M. Hoferichter, B. Kubis, A. Nogga and D. R. Phillips, *Nucl. Phys. A* **872** (2011) 69.
14. T. D. Cohen, J. L. Friar, G. A. Miller and U. van Kolck, *Phys. Rev. C* **53** (1996) 2661.
15. B. Y. Park, F. Myhrer, J. R. Morones, T. Meissner and K. Kubodera, *Phys. Rev. C* **53** (1996) 1519.
16. T. Sato, T. S. H. Lee, F. Myhrer and K. Kubodera, *Phys. Rev. C* **56** (1997) 1246.
17. C. da Rocha, G. Miller and U. van Kolck, *Phys. Rev. C* **61** (2000) 034613.
18. C. Hanhart, J. Haidenbauer, M. Hoffmann, U.-G. Meißner and J. Speth, *Phys. Lett. B* **424** (1998) 8.
19. V. Dmitrasinovic, K. Kubodera, F. Myhrer and T. Sato, *Phys. Lett. B* **465** (1999) 43.
20. S. Ando, T. -S. Park and D. -P. Min, *Phys. Lett. B* **509** (2001) 253.
21. V. Bernard, N. Kaiser and U.-G. Meißner, *Eur. Phys. J. A* **4** (1999) 259.
22. C. Hanhart, U. van Kolck and G. A. Miller, *Phys. Rev. Lett.* **85** (2000) 2905.
23. C. Hanhart and N. Kaiser, *Phys. Rev. C* **66** (2002) 054005.
24. C. Hanhart, *Phys. Rept.* **397** (2004) 155.
25. V. Lensky, V. Baru, J. Haidenbauer, C. Hanhart, A. E. Kudryavtsev and U.-G. Meißner, *Eur. Phys. J. A* **27** (2006) 37.
26. A. A. Filin, V. Baru, E. Epelbaum, H. Krebs, C. Hanhart, A. E. Kudryavtsev and F. Myhrer, *Phys. Rev. C* **85** (2012) 054001.
27. A.A. Filin, V. Baru, E. Epelbaum, H. Krebs, C. Hanhart and F. Myhrer, arXiv:1307.6187 [nucl-th] (2013).
28. S. Weinberg. *Trans. New York Acad. Sci.*, **38** (1977) 185.
29. J. Gasser and H. Leutwyler, *Phys. Rept.* **87** (1982) 77.
30. G. A. Miller, B. M. Nefkens, and I. Šlaus. *Phys. Rept.* **194** (1990) 1.
31. H. Leutwyler. *Phys. Lett.*, B **378** (1996) 313.
32. V. Bernard, *Prog. Part. Nucl. Phys.* **60** (2008) 82.
33. U.-G. Meißner and S. Steininger. *Phys. Lett.*, B **419** (1998) 403.

64. Vadim Baru, Christoph Hanhart, Fred Myhrer
34. A.M. Bernstein. *Phys. Lett. B* **442** (1998) 20.
 35. U. van Kolck, J. A. Niskanen, and G. A. Miller. *Phys. Lett. B* **493** (2000) 65.
 36. A. Filin et al., *Phys. Lett. B* **681** (2009) 423.
 37. D. R. Bolton and G. A. Miller, *Phys. Rev. C* **81** (2010) 014001.
 38. A. K. Opper et al. *Phys. Rev. Lett.* **91** (2003) 212302.
 39. E. J. Stephenson et al. *Phys. Rev. Lett.*, **91** (2003) 142302.
 40. G. A. Miller, A. K. Opper and E. J. Stephenson, *Ann. Rev. Nucl. Part. Sci.* **56** (2006) 253.
 41. E. Epelbaum, A. Nogga, W. Gloeckle, H. Kamada, U.-G. Meißner and H. Witala, *Phys. Rev. C* **66** (2002) 064001.
 42. E. Epelbaum, H. -W. Hammer and U.-G. Meißner, *Rev. Mod. Phys.* **81** (2009) 1773.
 43. R. Machleidt and D. R. Entem, *Phys. Rept.* **503** (2011) 1.
 44. D. Gazit, S. Quaglioni and P. Navratil, *Phys. Rev. Lett.* **103** (2009) 102502.
 45. T. S. Park et al., *Phys. Rev. C* **67** (2003) 055206.
 46. S. Nakamura, T. Sato, S. Ando, T. S. Park, F. Myhrer, V. P. Gudkov and K. Kubodera, *Nucl. Phys. A* **707** (2002) 561.
 47. S. Ando, Y. H. Song, T. S. Park, H. W. Fearing and K. Kubodera, *Phys. Lett. B* **555** (2003) 49.
 48. Q.R. Ahmad et al. [SNO Collaboration], *Phys. Rev. Lett.* **87** (2001) 071301; *ibid* **89** (2002) 011301.
 49. V. Lensky, V. Baru, J. Haidenbauer, C. Hanhart, A. E. Kudryavtsev and U. G. Meißner, *Eur. Phys. J. A* **26** (2005) 107.
 50. V. Lensky, V. Baru, E. Epelbaum, C. Hanhart, J. Haidenbauer, A. E. Kudryavtsev and U. G. Meißner, *Eur. Phys. J. A* **33** (2007) 339.
 51. A. Gardestig, *Phys. Rev. C* **74** (2006) 017001.
 52. A. Gardestig and D. R. Phillips, *Phys. Rev. Lett.* **96** (2006) 232301.
 53. A. Gardestig and D. R. Phillips, *Phys. Rev. C* **73** (2006) 014002.
 54. A. Gardestig, *J. Phys. G* **36** (2009) 053001.
 55. S. Ando, T. S. Park, K. Kubodera and F. Myhrer, *Phys. Lett. B* **533** (2002) 25.
 56. V. A. Andreev et al. [MuSun Collaboration], arXiv:1004.1754 [nucl-ex].
 57. L. E. Marcucci, A. Kievsky, S. Rosati, R. Schiavilla and M. Viviani, *Phys. Rev. Lett.* **108** (2012) 052502.
 58. L. E. Marcucci, *Int. J. Mod. Phys. A* **27** (2012) 1230006.
 59. J. Adam, Jr., M. Tater, E. Truhlik, E. Epelbaum, R. Machleidt and P. Ricci, *Phys. Lett. B* **709** (2012) 93.
 60. V. Bernard, N. Kaiser and U.-G. Meißner, *Int. J. Mod. Phys. E* **4** (1995) 193.
 61. Y. Kim, T. Sato, F. Myhrer and K. Kubodera, *Phys. Rev. C* **80** (2009) 015206.
 62. J. A. Niskanen, *Nucl. Phys. A* **298** (1978) 417.
 63. C. Hanhart, J. Haidenbauer, O. Krehl and J. Speth, *Phys. Lett. B* **444** (1998) 25.
 64. V. Baru, J. Haidenbauer, C. Hanhart, A. E. Kudryavtsev, V. Lensky and U.-G. Meißner, eConfC **070910** (2007) 128.
 65. V. Baru, E. Epelbaum, J. Haidenbauer, C. Hanhart, A. E. Kudryavtsev, V. Lensky and U.-G. Meißner, *Phys. Rev. C* **80** (2009) 044003.
 66. C. Ordóñez, L. Ray and U. van Kolck, *Phys. Rev. Lett.* **72** (1994) 1982; *Phys. Rev. C* **53** (1996) 2086.
 67. N. Fettes, U.-G. Meißner and S. Steininger, *Nucl. Phys. A* **640** (1998) 199; N. Fettes, Ph.D. thesis, Bonn University, 2000.
 68. N. Fettes, U.-G. Meißner, M. Mojzis and S. Steininger, *Annals Phys.* **283** (2000) 273 [Erratum-*ibid.* **288** (2001) 249].
 69. S. Weinberg, *Phys. Lett. B* **251** (1990) 288.

70. S. Weinberg, *Nucl. Phys. B* **363** (1991) 3.
71. E. Epelbaum, *Prog. Part. Nucl. Phys.* **57** (2006) 654.
72. S. Weinberg, *Phys. Lett. B* **295** (1992) 114.
73. J. Haidenbauer, K. Holinde and M. B. Johnson, *Phys. Rev. C* **48** (1993) 2190.
74. R. Machleidt, *Phys. Rev. C* **63** (2001) 024001.
75. R. B. Wiringa, V. G. J. Stoks and R. Schiavilla, *Phys. Rev. C* **51** (1995) 38.
76. C. Hanhart, G. A. Miller, F. Myhrer, T. Sato and U. van Kolck, *Phys. Rev. C* **63** (2001) 044002.
77. H. Krebs, V. Bernard and U.-G. Meißner, *Annals Phys.* **316** (2005) 160.
78. J. A. Eden and M. F. Gari, *Phys. Rev. C* **53** (1996) 1102.
79. D. R. Bolton and G. A. Miller, *Phys. Rev. C* **83** (2011) 064003.
80. C. Hanhart and A. Wirzba, *Phys. Lett. B* **650** (2007) 354.
81. T. Nogi, Ph.D. dissertation, Osaka University (2002), unpublished; T. Nogi, T. Sato and H. Ohtsubo, arxiv:nucl-th/0409034 (2004).
82. R. A. Arndt, W. J. Briscoe, I. I. Strakovsky and R. L. Workman, *Phys. Rev. C* **76** (2007) 025209.
83. R. A. Arndt, I. I. Strakovsky, and R. L. Workman, *Phys. Rev. C* **62**, (2000) 034005.
<http://gwdac.phys.gwu.edu>.
84. Y. Kim, T. Sato, F. Myhrer and K. Kubodera, *Phys. Lett. B* **657** (2007) 187.
85. A. Gårdestig, D. R. Phillips and C. Elster, *Phys. Rev. C* **73** (2006) 024002.
86. D. A. Hutcheon *et al.*, *Nucl. Phys. A* **535** (1991) 618 .
87. P. Heimberg *et al.*, *Phys. Rev. Lett.* **77**, (1996) 1012.
88. M. Drochner *et al.* [GEM Collaboration], *Nucl. Phys. A* **643**, (1998) 55.
89. P. Hauser *et al.*, *Phys. Rev. C* **58** (1998) 1869.
90. T. Strauch *et al.*, *Phys. Rev. Lett.* **104** (2010) 142503; *Eur. Phys. J. A* **47** (2011) 88.
91. T.-S. Park, D.-P. Min and M. Rho, *Phys. Rept.* **233** (1993) 341.
92. B. Lee, “Chiral Symmetry” (Gordon and Breach Science Publ., N.Y., 1972); S. Kondratyuk, K. Kubodera and F. Myhrer, *Phys. Rev. C* **68** (2003) 044001.
93. J. Gasser, Sainio and A. Svarc, *Nucl. Phys. B* **307** (1988) 779.
94. A. Filin, PhD thesis, Bochum 2013, to be published
95. E. Epelbaum, U. G.-Meißner, W. Glöckle, C. Elster, *Phys. Rev. C* **65** (2002) 044001.
96. Th. Hemmert, PhD-thesis, University of Massachusetts Amherst (1999).
97. T. R. Hemmert, B. R. Holstein and J. Kambor, *J. Phys. G* **24** (1998) 1831.
98. N. Fettes and U. G. Meißner, *Nucl. Phys. A* **679** (2001) 629.
99. N. Kaiser, S. Gerstendorfer, W. Weise, *Nucl. Phys. A* **637** (1998) 395.
100. G. Höhler, in H. Schopper (Ed.) Landolt-Börnstein, vol.9 (Springer, Berlin 1983).
101. C. Hajduk, P. U. Sauer and W. Struve, *Nucl. Phys. A* **405** (1983) 581.
102. V. Bernard, H.W. Fearing, T.R. Hemmert and U.-G. Meißner, *Nucl. Phys. A* **635** (1998) 121 [Erratum-ibid. A **642** (1998) 563].
103. T. Appelquist and J. Carazzone, *Phys. Rev. D* **11** (1975) 2856; Lowell S. Brown, *Phys. Rev. D* **39** (1989) 3084.
104. H.O. Meyer *et al.*, *Phys. Rev. Lett.* **83**, (1999) 5439; *Phys. Rev. C* **63**, (2001) 064002.
105. R. Bilger *et al.*, *Nucl. Phys. A* **693** (2001) 633.
106. R.W. Flammang *et al.*, *Phys. Rev. C* **58**, (1998) 916.
107. S. X. Nakamura, *Phys. Rev. C* **77** (2008) 054001.
108. S. Abdel Samad *et al.* [COSY-TOF Collaboration], *Eur. Phys. J. A* **17** (2003) 595.
109. M. Goldberger and K.M. Watson, *Collision Theory* (Wiley, New York, 1964).
110. R. Omnès, *Nuovo Cim.* **8**, (1958) 316.
111. A. Gasparyan, J. Haidenbauer, C. Hanhart and J. Speth, *Phys. Rev. C* **69**, (2004) 034006; A. Gasparyan, J. Haidenbauer and C. Hanhart, *Phys. Rev. C* **72**, (2005)

66 *Vadim Baru, Christoph Hanhart, Fred Myhrer*

- 034006.
112. B. G. Ritchie *et al.*, *Phys. Rev. C* **47**, (1993) 21.
 113. E. Korkmaz *et al.*, *Nucl. Phys. A* **535**, (1991) 637.
 114. E. L. Mathie *et al.*, *Nucl. Phys. A* **397**, (1983) 469.
 115. V. Shmakova *et al.*, arXiv:1307.4950 [nucl-ex].
 116. H. Hahn, F. A. Duncan, J. Aclander, D. Ashery, E. G. Auld, D. R. Gill, D. A. Hutcheon and G. Jones *et al.*, *Phys. Rev. Lett.* **82** (1999) 2258.
 117. F. Duncan, H. Hahn, C. Aclander, D. Ashery, E. G. Auld, D. R. Gill, D. A. Hutcheon and G. Jones *et al.*, *Phys. Rev. Lett.* **80** (1998) 4390.
 118. M. Daum, M. Finger, M. Finger, Jr., J. Franz, F. H. Heinsius, A. Janata, K. Konigsmann and H. Lacker *et al.*, *Eur. Phys. J. C* **25** (2002) 55.
 119. P. N. Deepak, J. Haidenbauer and C. Hanhart, *Phys. Rev. C* **72**, (2005) 024004.
 120. D. Tsirkov *et al.* [COSY-ANKE Collaboration], *Phys. Lett. B* **712** (2012) 370.
 121. S. Dymov *et al.* [COSY-ANKE Collaboration], *Phys. Lett. B* **712** (2012) 375.
 122. S. Dymov *et al.* [ANKE Collaboration], *Phys. Rev. C* **88** (2013) 014001.
 123. A. Schmidt *et al.*, *Phys. Rev. Lett.* **87** (2001) 232501 [Erratum-ibid. **110** (2013) 039903].
 124. M. Knecht and R. Urech, *Nucl. Phys. B* **519** (1998) 329.
 125. G. Müller and U.-G. Meißner. *Nucl. Phys. B* **556** (1999) 265.
 126. N. Fettes and U.-G. Meißner, *Phys. Rev. C* **63** (2001) 045201.
 127. J. Gasser, M. A. Ivanov, E. Lipartia, M. Mojžiš, and A. Rusetsky, *Eur. Phys. J. C* **26** (2002) 13.
 128. M. Hoferichter, B. Kubis, and U.-G. Meißner, *Phys. Lett. B* **678** (2009) 65.
 129. M. Hoferichter, B. Kubis, and U.-G. Meißner, *Nucl. Phys. A* **833** (2010) 18.
 130. F. K. Guo *et al.*, *Phys. Lett. B* **666** (2008) 251.
 131. J. Bijnens and K. Ghorbani, *JHEP* **0711** (2007) 030.
 132. R. Abegg *et al.*, *Phys. Rev. D* **39** (1989) 2464; *Phys. Rev. C* **57** (1998) 2126; S. E. Vigdor *et al.*, *Phys. Rev. C* **46** (1992) 410.
 133. L. M. Barkov *et al.*, *Nucl. Phys. B* **256** (1985) 365.
 134. S. A. Coon and M. D. Scadron, *Phys. Rev. C* **51** (1995) 2923.
 135. J. A. Nolen and J. P. Schiffer, *Ann. Rev. Nucl. Part. Sci.* **19** (1969) 471.
 136. J.A. Niskanen. *Few Body Syst.* **26** (1999) 241.
 137. J. L. Friar *et al.*, *Phys. Rev. C* **70** (2004) 044001.
 138. J. L. Friar, G. L. Payne and U. van Kolck, *Phys. Rev. C* **71** (2005) 024003.
 139. E. Epelbaum, H. Krebs and U.-G. Meißner, *Nucl. Phys. A* **806** (2008) 65.
 140. E. Epelbaum, U.-G. Meißner and J. E. Palomar, *Phys. Rev. C* **71** (2005) 024001; E. Epelbaum and U.-G. Meißner, *Phys. Rev. C* **72** (2005) 044001.
 141. A. Gardestig *et al.* *Phys. Rev. C* **69** (2004) 044606.
 142. A. Walker-Loud, C. E. Carlson and G. A. Miller, *Phys. Rev. Lett.* **108** (2012) 232301.
 143. W.N. Cottingham, *Ann. Phys.* **25** (1963) 424.
 144. S. R. Beane, K. Orginos and M. J. Savage, *Nucl. Phys. B* **768** (2007) 38.
 145. T. Blum, R. Zhou, T. Doi, M. Hayakawa, T. Izubuchi, S. Uno and N. Yamada, *Phys. Rev. D* **82** (2010) 094508.
 146. G. M. de Divitiis, P. Dimopoulos, R. Frezzotti, V. Lubicz, G. Martinelli, R. Petronzio, G. C. Rossi and F. Sanfilippo *et al.*, *JHEP* **1204** (2012) 124.
 147. U. van Kolck, J. L. Friar and J. T. Goldman, *Phys. Lett. B* **371** (1996) 169.
 148. A. Nogga *et al.*, *Phys. Lett. B* **639** (2006) 465.
 149. T. A. Lahde and G. A. Miller, *Phys. Rev. C* **75** (2007) 055204 [Erratum-ibid. **C 77** (2008) 019904].
 150. A. C. Fonseca, R. Machleidt and G. A. Miller, *Phys. Rev. C* **80** (2009) 027001.

151. P. Adlarson *et al.* [WASA-at-COSY Collaboration], *Phys. Rev. C* **88** (2013) 014004.
152. N. E. Booth, A. Abashian and K. M. Crowe, *Phys. Rev. Lett.* **7** (1961) 35.
153. P. Adlarson *et al.* [WASA-at-COSY Collaboration], *Phys. Rev. Lett.* **106** (2011) 242302.
154. M. Bashkanov, C. Bargholtz, M. Berlowski, D. Bogoslawsky, H. Calen, H. Clement, L. Demiroers and E. Doroshkevich *et al.*, *Phys. Rev. Lett.* **102** (2009) 052301.
155. B. Liu, V. Baru, J. Haidenbauer and C. Hanhart, *Eur. Phys. J. A* **47** (2011) 12.
156. L. Alvarez-Ruso, E. Oset and E. Hernández, *Nucl. Phys. A* **633** (1998) 519.
157. L. Alvarez-Ruso, *Phys. Lett. B* **452** (1999) 207.
158. V. Bernard, N. Kaiser and U.-G. Meißner, *Nucl. Phys. A* **615** (1997) 483.
159. V. Bernard, N. Kaiser, U.-G. Meißner and A. Schmidt, *Nucl. Phys. A* **580** (1994) 474.
160. V. Bernard, N. Kaiser and U.-G. Meißner, *Phys. Lett. B* **382** (1996) 19.
161. V. Bernard, N. Kaiser and U.-G. Meißner, *Nucl. Phys. B* **457** (1995) 147.
162. N. Fettes, V. Bernard and U.-G. Meißner, *Nucl. Phys. A* **669** (2000) 269.
163. N. Mobed, J. Zhang and D. Singh, *Phys. Rev. C* **72** (2005) 045204.
164. S. Schneider, S. Krewald and U.-G. Meißner, *Eur. Phys. J. A* **28** (2006) 107.
165. M. L. Goldberger, H. Miyazawa, and R. Oehme, *Phys. Rev.* **99** (1955) 986.
166. V. V. Abaev, P. Metsä, and M. E. Sainio, *Eur. Phys. J. A* **32** (2007) 321.
167. T. E. O. Ericson, B. Loiseau, and A. W. Thomas, *Phys. Rev. C* **66** (2002) 014005.
168. J. Gasser, H. Leutwyler, and M. E. Sainio, *Phys. Lett. B* **253** (1991) 252.
169. S. Deser, M. L. Goldberger, K. Baumann and W. Thirring, *Phys. Rev.* **96** (1954) 774.
170. V. E. Lyubovitskij and A. Rusetsky, *Phys. Lett. B* **494** (2000) 9.
171. P. Zemp, PhD thesis, University of Bern (2004).
172. J. Gasser, V. E. Lyubovitskij, and A. Rusetsky, *Phys. Rept.* **456** (2008) 167.
173. U.-G. Meißner, U. Raha and A. Rusetsky, *Phys. Lett. B* **639** (2006) 478.
174. D. Gotta *et al.*, *Lect. Notes Phys.* **745** (2008) 165.
175. S. R. Beane, V. Bernard, T. S. H. Lee, and U.-G. Meißner, *Phys. Rev. C* **57** (1998) 424.
176. S. R. Beane, V. Bernard, E. Epelbaum, U.-G. Meißner, and D. R. Phillips, *Nucl. Phys. A* **720** (2003) 399.
177. S. Liebig, V. Baru, F. Ballout, C. Hanhart, and A. Nogga, *Eur. Phys. J. A* **47** (2011) 69.
178. V. Baru, C. Hanhart, A. E. Kudryavtsev, and U.-G. Meißner, *Phys. Lett. B* **589** (2004) 118.
179. A. Nogga and C. Hanhart, *Phys. Lett. B* **634** (2006) 210.
180. U.-G. Meißner, U. Raha and A. Rusetsky, *Eur. Phys. J. C* **41** (2005) 213 [Erratum-*ibid. C* **45** (2006) 545].
181. V. Baru, E. Epelbaum, C. Hanhart, M. Hoferichter, A. E. Kudryavtsev and D. R. Phillips, *Eur. Phys. J. A* **48** (2012) 69.
182. V. Baru, E. Epelbaum, and A. Rusetsky, *Eur. Phys. J. A* **42** (2009) 111.
183. V. C. Highland *et al.*, *Nucl. Phys. A* **365** (1981) 333.
184. I.R. Afnan and A.W. Thomas, *Phys. Rev. C* **10** (1974) 109;
185. D.S. Koltun and T. Mizutani, *Ann. Phys. (N.Y.)* **109** (1978) 1.
186. M. Lacombe *et al.*, *Phys. Rev. C* **21** (1980) 861.
187. V. Baru, J. Haidenbauer, C. Hanhart, A. E. Kudryavtsev, V. Lensky and U.-G. Meissner, *eConf C* **070910** (2007) 127 [arXiv:0711.2743 [nucl-th]].
188. J. J. de Swart, M. C. M. Rentmeester, and R. G. E. Timmermans, *PiN Newslett.* **13** (1997) 96.

68 *Vadim Baru, Christoph Hanhart, Fred Myhrer*

189. R. A. Arndt, W. J. Briscoe, I. I. Strakovsky, R. L. Workman, and M. M. Pavan, *Phys. Rev. C* **69** (2004) 035213.
190. R. A. Arndt, W. J. Briscoe, I. I. Strakovsky, and R. L. Workman, *Phys. Rev. C* **74** (2006) 045205.
191. M. Cleven, F. -K. Guo, C. Hanhart and U.-G. Meißner, *Eur. Phys. J. A* **47** (2011) 120.
192. F. -K. Guo, C. Hanhart and U.-G. Meißner, *Phys. Rev. Lett.* **103** (2009) 082003 [Erratum-ibid. **104** (2010) 109901].
193. Q. Wang, X. -H. Liu and Q. Zhao, *Phys. Rev. D* **84** (2011) 014007.
194. F. -K. Guo, C. Hanhart, G. Li, U.-G. Meißner and Q. Zhao, *Phys. Rev. D* **82** (2010) 034025.
195. F. -K. Guo, C. Hanhart, G. Li, U.-G. Meißner and Q. Zhao, *Phys. Rev. D* **83** (2011) 034013.
196. N. Brambilla et al., *Eur. Phys. J. C* **71** (2011) 1534.
197. M. Cleven, Q. Wang, F. -K. Guo, C. Hanhart, U.-G. Meißner and Q. Zhao, *Phys. Rev. D* **87** (2013) 074006.
198. R. Shyam and U. Mosel, *Phys. Lett. B* **426** (1998) 1.